RELATING TERRESTRIAL GAMMA-RAY FLASH PRODUCTION TO ASSOCIATED LIGHTNING AND THUNDERSTORM CHARACTERISTICS

by

Reyann Kathleen Larkey

A dissertation submitted in partial fulfillment
of the requirements for the degree

of

Doctor of Philosophy

in

Physics

MONTANA STATE UNIVERSITY
Bozeman, Montana

May 2022

DEDICATION

This dissertation is dedicated to husband, Jake, for always remaining patient, loving, and supportive throughout this process. I doubt I will ever be able to fully convey the level of appreciation I have for your sustained encouragement and dedication throughout the last several years. This work is also dedicated to the memory of my late grandfather, Harold Joiner. Every time I felt the urge to walk away, I could hear you yelling “Carry on troops!” to us kids and reminding me to “Get your education!”, so this one’s for you.

ACKNOWLEDGEMENTS

I would to like acknowledge David Smith, PhD, at the University of California, Santa Cruz for his vital input and guidance over the course of my graduate career, without which the work in this dissertation could not have been completed. I would also like to acknowledge all of the people who have been a major support to me over the past several years: my husband, siblings, mother, in-laws, grandparents, and the rest of my family. And a special thank you to Jeffery Larkey for his ruthless editing of the grammar and content throughout this dissertation for which I am very grateful.

TABLE OF CONTENTS

TABLE OF CONTENTS – CONTINUED

LIST OF TABLES

LIST OF FIGURES

LIST OF FIGURES – CONTINUED

LIST OF FIGURES – CONTINUED

LIST OF FIGURES – CONTINUED

LIST OF FIGURES – CONTINUED

Figure Page

LIST OF FIGURES – CONTINUED

Figure Page

LIST OF FIGURES – CONTINUED

Figure Page

ABSTRACT

Terrestrial Gamma-ray Flashes (TGFs) are puzzling, but potentially hazardous bursts of high-energy radiation associated with the everyday phenomena of lightning. Not every lightning flash produces a TGF, however, and the question of what makes a TGF-associated lightning flash different is not well understood. This dissertation investigates this question by examining how TGF production is related to thunderstorm characteristics such as inter-flash intervals, flash rate trends, and flash amplitudes. Additionally, investigation into the precise timing relationship between TGFs and stroke signatures in their associated lightning flash is also presented.

The conclusions of these studies show that TGFs are most likely to occur after longer than usual charge-up times, when the flash rates tend to be declining in storms, and when amplitudes of flashes are stronger than normal. The last study also details the presence of two distinct excess peaks of delayed lightning signals occurring after TGFs compared to other non-TGF flashes. This study examines the amplitudes of these delayed lightning signals and compares those signals to the entire distribution of non-TGF strokes. These findings hint that TGF-production may be the result of unusually complex lightning flashes. However, further research into these peaks requires additional data from other spacecraft and perhaps updated TGF catalogs to examine the context of these lightning flashes. Nonetheless, this initial study may further help explain why TGFs are not produced in association with all lightning flashes.

INTRODUCTION

Lightning is one of the most common severe weather phenomena that most people have seen and experienced in their lives. It is estimated that, on average, roughly 40 lightning flashes occur on earth every second (over 3 million every day) (Christian, 2003). Lightning has been studied since the iconic experiments of Benjamin Franklin in the 1700s, but a substantial amount of uncertainty remains about its exact production mechanisms and related phenomena.

Terrestrial Gamma-Ray Flashes (TGFs) are one specific example of a perplexing event associated with lightning. TGFs are extremely intense bursts of high-energy radiation that can produce upward of 10^{17} high energy photons (on the order of 10s of MeV) in sub-millisecond time frames. These bursts often paralyze the instruments that observe them and pose a high risk to anyone or anything potentially exposed (Dwyer *et al.*, 2010).

TGFs are not produced in association with every lightning flash. Indeed, they are not even produced in every thunderstorm. Because of their rarity, they are relatively poorly understood. Historically, TGFs have been understood in the context of runaway electron avalanches that produce gamma-rays through Bremsstrahlung radiation. Runaway avalanches of this sort were predicted as early as 1925 when C.T.R. Wilson proposed that high electric fields inside thunderstorms could produce high-energy radiation (Wilson, 1925). However, it was not until 1994 that TGFs were first observed by the Burst and Transient Space Explorer (BATSE) onboard the Compton Gamma Ray Observatory (CGRO) (Fishman *et al.*, 1994). Since their discovery, thousands of TGFs have been observed from spacecraft designed to search for gamma-ray bursts and a handful have been observed from specialized ground and aircraft detectors.

The rarity and sporadic nature of TGFs prompts the question of why some lightning flashes create TGFs and others do not. If there is something special about the production of TGFs, then what are the conditions more likely to result in a TGF? This introductory chapter lays a basis on which the following chapters expand. Different lightning processes necessary to understand TGFs are discussed first, followed by the theory and observations of TGFs.

Thunderstorms and Lightning Physics

To understand the physics of high energy radiation associated with lightning, it is necessary to first understand the basics of how thunderstorms and lightning work. Terminology and concepts discussed in this section will be used in the rest of this dissertation consistently.

The source of lightning and other high-energy lightning related phenomena begins in thunderstorms. In the simplest depiction, one can imagine thunderstorms as enormous parallel plate capacitors. Charge inside thunderstorms tends to concentrate in layers, which one can think of as analogous to the plates of a capacitor. Capacitors often contain dielectric material between their plates, and in thunderstorms, the charge layers are often separated by several kilometers of insulating air. Finally, a capacitor can only store so much energy before dielectric breakdown occurs and a spark is created between the plates, discharging the capacitor. For thunderstorms, of course, the similar discharge is lightning.

Thunderstorms were at first idealized in this way as enormous electrical dipoles, consisting of layers of opposite electrical charge (Simpson, 1909; Wilson, 1916). Over time, this model has been replaced by the standard tripole model consisting of three distinct charge layers (Williams, 1989). This, however, is still thought to be an oversimplification of the charge structure inside thunderstorms (Rust & Marshall, 1996) as the electrification of thunderstorms is a complex process that produces differing and complicated charge structures for all thunderstorms.

In a capacitor, charge is supplied to the conducting plates by a battery or some other power source. In thunderstorms, however, the layers of charge are created in a much different process termed 'non-inductive charging'. Charge separation in thunderstorms is believed to be caused by collisions between small ice crystals and larger ice particles (such as graupel[1] or hail) due to convection in storms (Reynolds *et al.*, 1957). When heavy graupel particles collide with ice crystals, a charge transfer takes place leaving the positively (or negatively) charged graupel particles and the oppositely charged ice crystals. The polarity and degree of charge transfered is determined by the meteorological conditions inside the thunderstorm at the time of the collision (He *et al.*, 2018). The ice crystals are light enough to be carried to higher altitudes while the heavier graupel particles either remain in place or fall to lower altitudes, resulting in layers of opposite charge forming at different altitudes in the storm. Another form of charging, inductive charging, or the attraction between oppositely charged particles, also takes place in thunderstorms. This type of charging is most notably responsible for the charge induced on the Earth's surface below a thunderstorm as well as the upper screening layer of charge near the tops of thunderstorms (Krehbiel, 1986; Rakov, 2003; Stolzenburg & Marshall, 2008). Figure 1.1 shows an example of the charge structure in a thunderstorm.

Given the demonstrated similarities between thunderstorms and capacitors, one might be tempted to think that lightning is simply a case of dielectric breakdown of the air. However, measurements of the electric field in thunderstorms have shown that the fields are much weaker than the dielectric strength of air ($3 \times 10^6 V/m$ at sea level) (Winn *et al.*, 1974; Dye *et al.*, 1988; Marshall & Rust, 1991; Marshall *et al.*, 1995), meaning that lightning is not just a case of dielectric breakdown. The actual process that initiates lightning remains

[1]Graupel is characterized as small pellets of ice that form when supercooled water droplets freeze onto snow crystals. Graupel is not large enough to be considered hail, and is often called "soft hail".

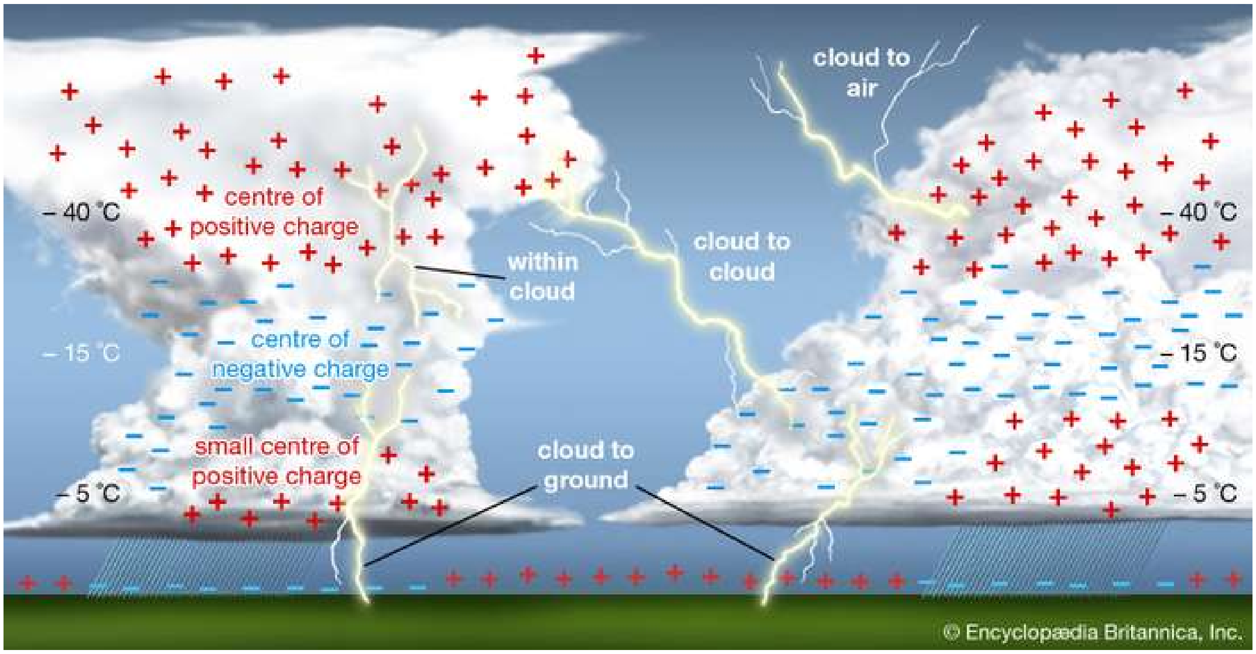

Figure 1.1: Schematic showing an example of a tripole charge structure in two thunderstorms. Shown are examples of storms with a main negative charge layer, an upper positive charge layer, and a smaller lower positive charge layer. Also shown are several different types of lightning processes. Image from Krider (2016).

an important unanswered question in the field of lightning research (Dwyer & Uman, 2014; Petersen *et al.*, 2008).

Lightning is routinely observed to occur at averaged field strengths smaller than the expected breakdown value, as mentioned above. Two main theories have been proposed to explain this fact. The first posits that perhaps locally enhanced electric fields in regions close to hydrometeors (particles of water precipitation, such as raindrops, ice, graupel, etc., that are present in thunderstorms) could allow for the breakdown of the air forming streamers (channels of ionized air) and leading to the eventual production of lightning leader channels, thus starting the lightning flash process (Loeb, 1966; Griffiths & Phelps, 1976). The other leading theory is that runaway electron avalanches, seeded by high energy cosmic rays, could cause the initial breakdown necessary to initiate a lightning leader channel (Gurevich *et al.*, 1992). However, both of these theories have their merits and hybrid theories have been proposed that incorporate both (Petersen *et al.*, 2008).

Shortly after the initial breakdown of air, many streamers can combine to form a larger channel of hot and conductive ionized air. These channels are called lightning "leaders" and are typically tens of meters in length. Because of the conductivity of a leader, free charge from the thunderstorm flows into the channel immediately, causing the enhancement of the electric field and production of even more streamers from the tip. Those streamers can then go on to form another hot channel, and the process repeats. This process produces the step-wise nature of a lightning flash before it attaches to the ground, clouds, or air. Leaders also tend to branch randomly, leading to the tree like nature of a lightning flash. Each time the leader steps, it releases x-rays and other radiation that can be picked up by sensors on the ground.

The whole stepping process takes only a few milliseconds and is not perceivable by the human eye; however, it is well documented using slow motion cameras. When a lightning leader channel attaches with its discharge point, say the ground for example, there is a rush of current from the storm where it initiated to the place where it attached. As the lightning channel acts like a short circuit between the cloud and the ground (in this example) all of the charge in the channel suddenly and violently rushes into the ground. The charge nearer to the ground rushes out first followed by the charge higher up and in the failed branches of the channel. This movement of charge heats the air and brightens every part of the leader channels. The heat also causes the air around the channel to expand and form a shock wave, resulting in thunder that can be heard many miles away. While the charge continues to move down the lightning channel, the bright areas actually appear to move up the channel. This process is known as a "return stroke" and is what the human eye *actually* sees when we observe lightning. Figure 1.2 shows an image of an example lightning strike with these features labeled.

Figure 1.2: Image of a CG lightning flash with stepped leaders and return stroke labeled. Image from Cancalosi (2020).

After the return stroke, there can be several other subsequent strokes that act to discharge more of the built-up charge. These subsequent strokes, referred to as "dart leaders", mainly follow the preexisting channel and so do not exhibit the same degree of branching and stepping as the initial stroke. While return and subsequent strokes are common for cloud-to-ground (CG) lightning (lightning that lowers charge from a cloud to the ground), these strokes are usually not as strong or even present in other types of lightning. Intra-cloud (IC) lightning, or lightning that discharges between one part of the thundercloud and another[2], usually does not exhibit strong return strokes. This is because there is not as vast a difference in electric potential between different parts of the same storm as there is between the storm and the ground (in the case of CG lightning).

Because of the extreme currents and physical extent of lightning flashes, they behave like

[2]IC lightning can also refer to inter-cloud lightning, or lightning that discharges between two different clouds.

antennae and produce electromagnetic radiation in all frequencies. The low frequency (LF) and very low frequency (VLF) radio atmospheric signals or "sferics" that are generated can travel thousands of kilometers due to the wave-guide of the Earth. These signals are easily detected by lightning location networks around the world, which determine the approximate location, time of occurrence, peak current, stroke type, and more about the lightning event. The World Wide Lightning Location Network (WWLLN), the Earth Networks Total Lightning Network (ENTLN), and the Global Lightning Detection Network (GLD360) are a few (but not all) of the most prominent networks used for lightning research and detection today. While these networks are not perfect and do not detect every lightning flash, they are vital to the field of lightning research. More information on these networks is given in the following sections.

The topic of high-energy radiation associated with lightning and thunderstorms is discussed in detail in the following sections. This section has covered the basics of lightning and thunderstorms and, while it only just scratched the surface of lightning and the research around it, it has provided the foundation on which the following chapters rely.

Terrestrial Gamma-Ray Flashes

TGF Observations Terrestrial Gamma-Ray Flashes (TGFs) are extremely intense bursts of high-energy, gamma-ray radiation associated with some lightning strikes. Not all lightning flashes produce TGFs, and the difficulty of in-situ measurements inside thunderstorms necessarily means that there is a fair amount of uncertainty surrounding them.

TGFs were directly associated with lightning a couple of years after their discovery in 1994, when lightning radio sferics were detected within a few milliseconds of an observed TGF (Inan *et al.*, 1996). BATSE eventually detected a total of 78 TGFs over a time period of nine years and remained the main source of TGF observations until the Reuven Ramaty

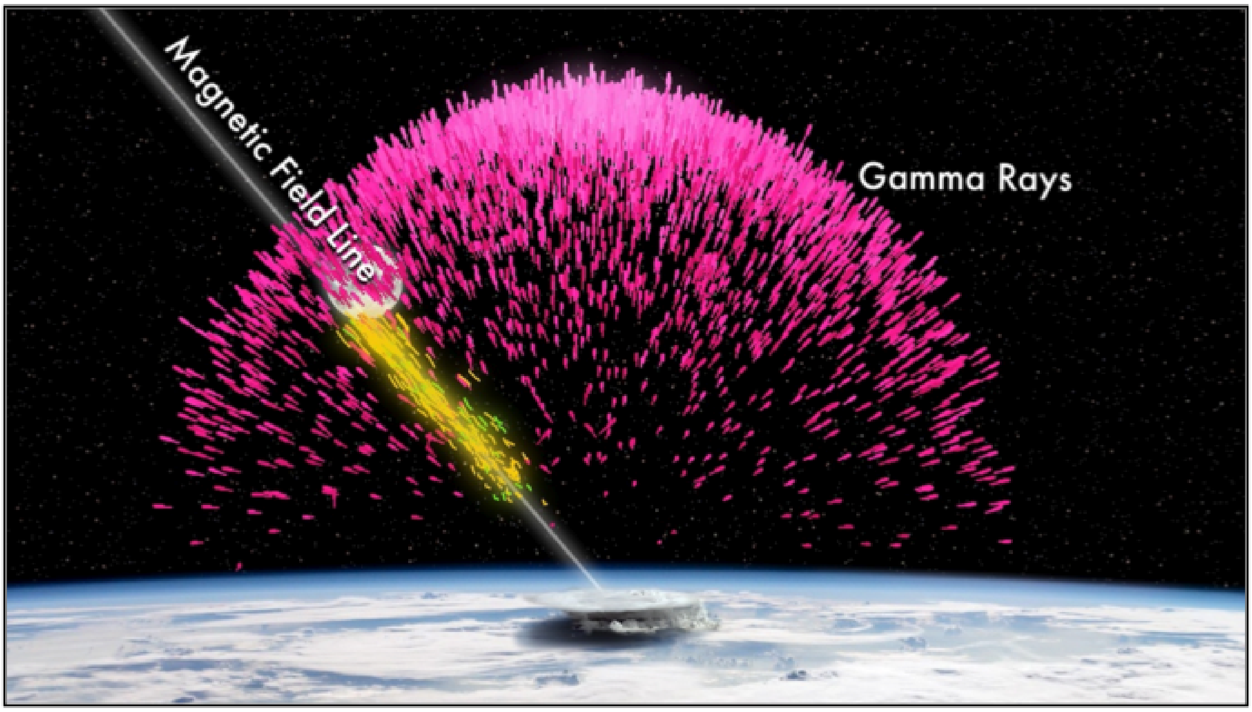

Figure 1.3: A model of what a TGF might look like from the vantage point of space. The magenta particles show the gamma-rays produced from the thunderstorm below, and flying off into space. The yellow particles show charged particles following the magnetic field line. Image credit: NASA Goddard Space Flight Center and J. Dwyer at the Florida Institute of Technology.

High Energy Solar Spectroscopic Imager (RHESSI) satellite began detecting TGFs in 2005. Within the first few years of its commission, RHESSI had observed over 800 TGFs, far surpassing the TGF frequency expected based on the BATSE observations (Smith *et al.*, 2005).

Since the the early 2000s, thousands of TGFs have been observed by RHESSI and other satellites, such as the Astro-Rivelatore Gamma a Immagini Leggero (AGILE), the Fermi Satellite's Gamma-ray Burst Monitor (GBM), and the Atmosphere-Space Interactions Monitor (ASIM) on board the International Space Station. There have also been a handful of TGF observations from ground-based instruments and aircraft (Hare *et al.*, 2016; Wada *et al.*, 2019; Bowers *et al.*, 2018). A timeline showing all the major TGF-observing satellite missions is shown in Figure 1.4.

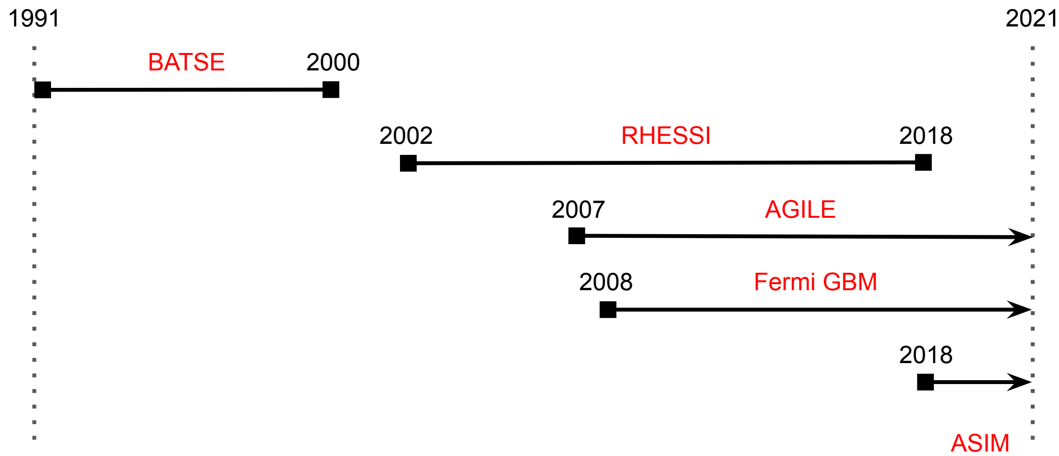

Figure 1.4: A timeline of the major TGF-observing spacecraft missions, showing their launch and decommission years. AGILE, Fermi-GBM, and ASIM are all still observing TGFs at the present time.

In addition to satellite observations of TGFs, ground and aircraft based instruments have also detected TGFs in relatively recent efforts. Dwyer *et al.* (2004) detected a gamma-ray burst at ground level after the initiation of rocket-triggered lightning at the International Center for Lightning Research and Testing (ICLRT). Another downward TGF was produced in association with rocket-triggered lightning at the same site in 2014 (Hare *et al.*, 2016). The ICLRT also detected another downward TGF produced by natural lightning in 2009 (Dwyer *et al.*, 2012a). Smith *et al.* (2011) detected a TGF from an aircraft using the Airborne Detector for Energetic Lightning Emissions (ADELE) instrument. A second, more compact version of this instrument was again used to make another airborne TGF detection, inside the eyewall of Hurricane Patricia in 2015 (Bowers *et al.*, 2018). There have also been several observations of downward TGFs from detectors in Japan, such as the Gamma ray Observations During Overhead Thunderstorms (GODOT) instrument (Bowers *et al.*, 2017) and the Gamma-Ray Observation of Winter Thunderclouds (GROWTH) project (Enoto *et al.*, 2017).

The observations of TGFs from satellites and other instruments have shed light on the important physical characteristics of TGFs. Properties such as estimated flux, photon energies and spectra, frequency, global distribution, and much more have been the topics of intense research for over two decades. However, the exact causes and production mechanisms are still not well understood. The different leading theories as well as any drawbacks are discussed below.

<u>TGF Production</u> While the exact process that produces a TGF is not fully understood, almost all proposed theories of TGF production require an element of Relativistic Runaway Electron Avalanche (RREA). RREA is the exponential growth of a population of relativistic electrons due to an external, ambient electric field. For an electron to be a "runaway" electron, it must gain energy (from the electric field for example) faster than it loses energy (from collisions, radiation, etc.). Figure 1.5 shows the friction curve for an electron in air. The horizontal line represents the driving force of the ambient electric field on the electron.

If the runaway electron collides, via Møller scattering, with other atomic electrons, it can cause those electrons to runaway as well. In the presence of a sufficiently extended background electric field, the process can repeat many times over, resulting in a substantial number of new runaway electrons in each iteration. Those electrons can go on to produce gamma-rays via bremsstrahlung interactions with the air. The number of new runaway electrons can be described by the expression:

$$N_e = N_o exp\left(\int_0^L \frac{dz}{\lambda(z)}\right) \tag{1.1}$$

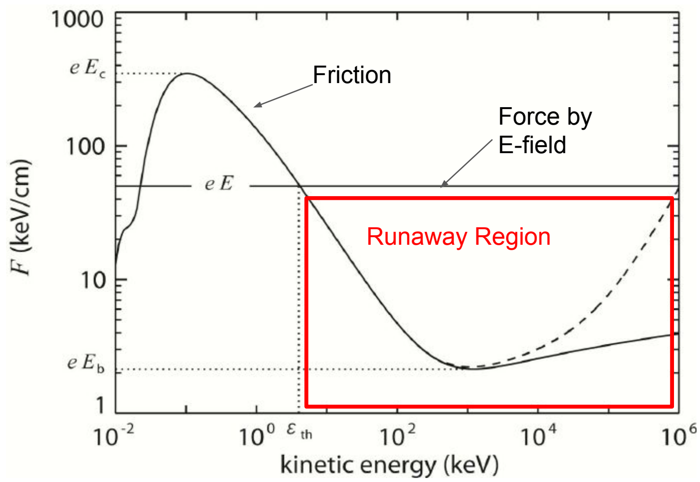

Figure 1.5: The solid curved shows the friction as a function of kinetic energy for a free electron traveling in air. The dashed line shows the effects of bremsstrahlung. The force on the electron by an ambient electric field is shown by the horizontal line. In the region where the force by the electric field is larger than the friction force (i.e. KE $> \epsilon_{th}$), shown in red, runaway electrons will be produced. Figure adapted from Dwyer (2004).

Where N_e and N_o are the number of runaway electrons produced and the number of initial seed electrons, respectively (Dwyer, 2004). L is the length of the electric field region over which the multiplication takes place (which is assumed to span the vertical axis), and λ is the avalanche multiplication length. The avalanche multiplication length is a function of the electric field strength and is given in Gurevich & Zybin (2001):

$$\lambda(z) = \frac{10.8MV}{E(z)} \tag{1.2}$$

More detailed expressions for λ have been calculated using Monte Carlo simulations and can be found in Dwyer (2004). The work done by Dwyer (2004, 2008) showed that RREA acting on its own is incapable of explaining the observed characteristics of TGFs. Prior to this work, RREAs resulting in TGFs were assumed to be seeded by the natural background cosmic radiation in the Earth's atmosphere. However, the number of electrons that would be produced given the measured fluxes of cosmic rays is orders of magnitude lower than what has been observed in TGFs. The other possibility, having a large enough avalanche region to produce the observations, would not be physical based on the inferred sizes of TGF source regions, which are much smaller (Dwyer, 2008).

Even so, the energy spectrum produced by RREA matches well with the observations of TGFs up to at least 20MeV. It does, however, deviate at energies higher than 20MeV (Celestin *et al.*, 2012). Given that photons in TGFs have been observed up to 100MeV, this marks another clear problem with the RREA mechanism. Nonetheless, because of the similarities, it is generally accepted that at least some RREA is occurring in the production of TGFs.

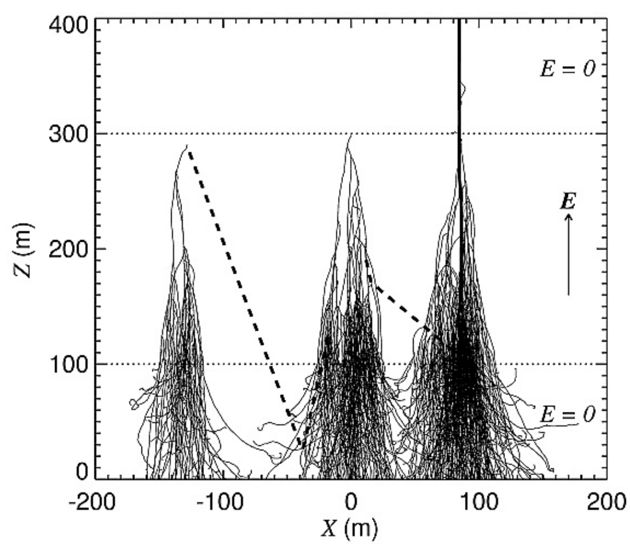

Figure 1.6: A depiction of particle tracks from a simulation including relativistic feedback. The light black lines show the electron paths, the dashed lines show gamma-rays, and the solid black line shows the positrons. A single seed particle was injected in the center of the field at X = 0. The two outer electron avalanches were produced from feedback. Only a small number of the paths were drawn for clarity. Figure from Dwyer (2003).

The main problem in regard to the production of TGFs then is the source of the seed electrons. There are two standard possibilities, the Relativistic Feedback mechanism and the lightning leader tip mechanism. The lightning leader tip model suggests that leaders are responsible for providing the seed particles as well as high electric fields. At the lightning leader tip, where streamers are produced, there exist very high electric field regions. If those fields are higher than the critical electric field (labeled as E_C in Figure 1.5), all electrons in that streamer area are able to runaway (Moss *et al.*, 2006). This is termed “thermal runaway” or “cold runaway”. Because of this, there is no need for an additional source of seed electrons. Simulations of this show that this process could in fact account for TGF observations (Carlson *et al.*, 2010; Celestin & Pasko, 2011).

One other proposed explanation for TGF production is the relativistic feedback (RF) model. As mentioned before, during an RREA process, a small percentage of the relativistic electrons in the avalanche will produce high-energy radiation (such as x-rays and gamma-rays) via interactions with the air. A further small portion of those gamma-rays will undergo pair production, resulting in positrons that travel in the opposite direction as the electron avalanches. Some of the positrons may occasionally travel back to the start of the primary avalanche area where they can trigger yet another avalanche through Bhabha scattering (positron-electron scattering). In addition, gamma-rays can also produce more avalanches via Compton scattering or the photoelectric effect.

As a result of relativistic feedback, the number of runaway electrons grows exponentially and on the timescales of microseconds, effectively and efficiently discharging the background electric field. A simulation of this is shown in Figure 1.6. This method can produce peak fluxes up to 10^9 times larger than RREA alone (Dwyer, 2003). A side effect of this discharge process is a fundamental limit on a stable electric field in air of 2550kV/m. Above that threshold the electric field becomes unstable as the threshold feedback mechanism dominates to discharge the field.

At present, there is no clear observation to suggest cold runaway over relativistic feedback (or vice versa). In all likelihood, the actual production of TGFs involves elements of both mechanisms, or perhaps another process not yet discovered or discussed here.

<u>TGF Lightning Associations</u> To fully understand TGFs and other high energy phenomena associated with lightning, it is necessary to be able to detect lightning with some degree of accuracy. Perhaps the most valuable tool in lightning research is the lightning location network. In general, these are networks made up of many different very low frequency (VLF) sensors (3-30kHz) distributed worldwide, which are capable of detecting lightning flashes with extremely good timing and spatial precision. Because of the extreme currents in lightning flashes (up to hundreds of kiloamperes), lightning flashes act like extremely powerful natural antennae and give off radiation in a broad spectrum. The bulk of that energy is in the VLF range (Cummer *et al.*, 1998); however, some observations employ the very high frequency (VHF) portion of the spectrum. The VLF signals can travel thousands of kilometers from the source due to low attenuation travel within the Earth-Ionosphere waveguide (Rodger *et al.*, 2006). With many sensors, the source location and timing can be located to within tens of kilometers and on the timescale of microseconds. Based on various features of the detected waveforms, these VLF networks can infer even more information about the lightning strokes, such as polarity, peak current, and stroke type (CG or IC).

Lightning locations networks usually employ at least one of three basic methods to locate lightning: (1) Magnetic Direction Finding (MDF); (2) Time of Arrival (TOA); or (3) interferometry (Cummins & Murphy, 2009). MDF uses orthogonal loop antennae to measure the magnetic flux produced by the substantial currents in lightning discharges. The independent directions of these antennae allow for an estimated direction of the lightning source as each one contributes to the location vector. However, with a network of sensors, more precise locations can be determined. The TOA method makes use of a network of sensors designed to measure the arrival time of lightning radio sferics and determines the position of the source based on the relative time differences among sensors (Lewis *et al.*, 1960). Advanced networks use combinations of MDF and TOA to determine lightning locations with a high degree of accuracy (Cummins *et al.*, 1998).

In addition to VLF observations, radio interferometry networks (such as lightning mapping arrays (LMAs) use VHF (60-150MHZ) sensors to make detailed measurements of lightning flashes. While these networks allow for much more detailed and highly resolved observations of lightning strikes, they have smaller maximum ranges (a few hundred kilometers compared with thousands of kilometers for VLF networks) and cannot provide information regarding other important lightning characteristics (peak current, polarity, etc.) (Boccippio *et al.*, 2001; Price, 2008).

The World Wide Lightning Location Network (WWLLN) is probably the most widely used source of lightning location data due to its well-established and longstanding reputation for accuracy and coverage. This network, established and maintained by the University of Washington, today consists of 80 sensors distributed globally for unprecedented detection efficiency on a global scale. Prior to the development of WWLLN, lightning detection was done by satellite or commercial networks with limited coverage in only a few regions. However, these were inadequate for studying lightning on a global scale as they lacked the geographic coverage and ability to observe any specific area over a significant period (Lay *et al.*, 2004).

Prior to WWLLN, there had been a suspected correlation between TGFs and VLF radio signals both for BATSE and RHESSI observations (Inan *et al.*, 1996; Cohen *et al.*, 2006; Cummer *et al.*, 2005; Stanley *et al.*, 2006). Unfortunately, the timing accuracy of both satellite observations and VLF sources left room for ambiguity and the possibility of chance associations. As more WWLLN stations came on line and the number of observations increased, those initial suspicions of TGF-lightning associations were verified as coincident observations were detected in both RHESSI and Fermi-GBM data (Connaughton, 2010; Collier *et al.*, 2011).

In addition to WWLLN, several other VLF lightning location networks are used to study TGFs among other lightning related phenomena. Earth Networks Total Lightning Network (ENTLN), for example, was developed by a private company and has been in operation since 2009. Since its development, Earth Networks has continued to improve the network's measuring capabilities and is now exceptional at detecting lightning and has a much higher detection efficiency (DE) for IC flashes than WWLLN (Rudlosky, 2015; Marchand *et al.*, 2019). ENTLN recently partnered with WWLLN in 2016 to form the Earth Networks Global Lightning Network (ENGLN). With over 1,200 sensors worldwide, ENGLN is the most comprehensive lightning location network in the world. Other notable networks include the Global Lightning Dataset (GLD360) and the National Lightning Detection Network (NLDN), which mainly covers the continental United States.

Scope of Research

Understanding the relationship between lightning generation and TGF production is a necessary step in the advancement of TGF research. Outstanding questions remain about the precise timing relationship between lightning and TGFs, on both sub-second and multi-hour long timescales. For example, there is little understanding about how TGF production is affected by thunderstorm evolution; how storm properties such as lightning flash rates, flash current amplitudes, and charging intervals affect the likelihood of TGF production are not well studied. On shorter timescales, there is evidence that TGF-associated lightning flashes tend to present anomalous sferic time signatures that "typical" lightning flashes do not. Research into these relationships is important for understanding the storm conditions that make TGFs more (or less) likely to occur. Insight into the connection between large scale storm characteristics and TGF production could help to mitigate the risks of accidental exposure to TGFs for both air travel and ground exposure.

This dissertation relates TGF production to the above-mentioned storm characteristics and works to establish the conditions that are most favorable for TGF production. Chapter 2 details observations of longer charging times between lightning flashes immediately prior to TGF production. This study, showing that TGFs tend to be produced after longer than normal charging periods, implies more energetic than usual lightning flashes are more likely to produce TGFs than weaker flashes. Chapter 3 focuses on research that shows how TGFs relate to other storm characteristics on longer timescales, and is a natural, broader continuation of the research in Chapter 2. This later study finds that TGFs are more likely to be produced later in storm cell evolution, when flash rates are falling, and when flash current amplitudes are larger than normal. Lastly, Chapter 4 is a preliminary study into two observed populations of delayed lightning sferics that occur in excess after TGFs but not other flashes. This study examines the TGF-specific lightning flashes that contribute to these excesses in terms of their global distribution, stroke type, and stroke amplitudes. The results indicate that these delayed sferics could be the signatures of an unusual, complex lightning process that is likely to be directly related to TGF-production.

This research provided in this dissertation shows that there is something unique about the thunderstorm environment, and perhaps the lightning process itself, that makes production of a TGF possible, or at least more likely. It is not just the case that *any* lightning flash is capable of producing a TGF, but that the environment plays a critical role.

EVIDENCE FOR EXTENDED CHARGING PERIODS PRIOR TO TERRESTRIAL GAMMA-RAY FLASHES

Contribution of Authors and Co-Authors

Manuscript in Chapter 2

Author: Reyann K. Larkey

Contributions: Defined thunderstorms, applied clustering, and performed statistical analyses.

Co-Author: John G. Sample

Contributions: Mentor who helped organize paper and provided feedback on analysis types.

Co-Author: David M. Smith

Contributions: Mentor who helped guide project and advised next steps in analysis. Helped define motivation and interpret results.

Co-Author: Michael S. Briggs

Contributions: Provided instruction and insight into working with Fermi GBM data.

Co-Author: Jeff L. Lapierre

Contributions: Provided access to and instruction for ENTLN data and helped interpret results.

Co-Author: Robert H. Holzworth

Contributions: Provided feedback and instruction for working with WWLLN data.

Manuscript Information

Reyann K. Larkey, John G. Sample, David M. Smith, Michael S. Briggs, Jeff L. Lapierre, Robert H. Holzworth

Status of Manuscript:
___ Prepared for submission to a peer-reviewed journal
___ Officially submitted to a peer-reviewed journal
___ Accepted by a peer-reviewed journal
_X_ Published in a peer-reviewed journal

Geophysical Research Letters Volume 46, Issue 17-18
DOI: 10.1029/2019GL083827

Key Points

- Inter-flash intervals in 219 Terrestrial Gamma-Ray Flash (TGF) producing thunderstorms are analyzed.
- We typically find a 24% longer than normal interval immediately prior to the TGF.
- These results may indicate that the electric field prior to the TGF is possibly stronger or more spatially extended than for typical flashes.

Abstract

We present an analysis of lightning inter-flash intervals in 219 TGF producing thunderstorms. Clustering was used to identify groups of lightning sferics, interpreted as individual thunderstorms, in combined WWLLN and ENTLN data. In these individual groups of sferics, analysis was done on the lightning flash frequency within within ± 10 minutes of the Fermi recorded TGF. We find that typical inter-flash intervals immediately prior to TGFs are 24% longer than mean inter-flash intervals in their individual producing storms while the inter-flash intervals immediately following the TGFs are typically 8% shorter than normal. The significance of these results, tested using a numerical bootstrap method, was found to be highly significant for the pre-TGF interval. These results could imply that a stronger electric field is necessary for the production of TGFs and may help to explain why some lightning strikes produce TGFs while others do not.

Introduction

Terrestrial Gamma-Ray Flashes (TGFs) are submillisecond, intense bursts of photons with energies often reaching tens of MeV (Smith *et al.*, 2005). TGFs have been associated with thunderstorms since their discovery in 1994 (Cummer *et al.*, 2005; Fishman *et al.*, 1994;

Inan *et al.*, 1996, 2006). Observations of TGFs have been made primarily from spacecraft such as the Burst and Transient Source Experiment (BATSE) on board the Compton Gamma-Ray Observatory (Fishman *et al.*, 1994), the Reuven Ramaty High Energy Solar Spectroscopic Imager (RHESSI) (Smith *et al.*, 2005), the Gamma-ray Burst Monitor (GBM) on the Fermi Gamma-ray Space Telescope (Briggs *et al.*, 2010), and by the Astrorivelatore Gamma a Immagini Leggero (AGILE) satellite (Marisaldi *et al.*, 2010). However, TGFs have also been observed, in a few cases, from the ground (Bowers *et al.*, 2017; Dwyer *et al.*, 2004, 2012a; Enoto *et al.*, 2017; Hare *et al.*, 2016) and by aircraft (Bowers *et al.*, 2018; Smith *et al.*, 2011).

In the past, the Relativistic Runaway Electron Avalanche (RREA) mechanism (Gurevich *et al.*, 1992) acting on cosmic ray seed particles was used to explain TGFs (Lehtinen *et al.*, 1996). However, Dwyer (2008) showed that this mechanism, on its own, was insufficient in explaining the production of TGFs because it would require unrealistic avalanche lateral sizes, unrealistic avalanche multiplication factors, or unrealistic seed fluxes to recreate the observed fluence of TGFs. Other viable explanations include the relativistic feedback (RF) mechanism (Dwyer, 2003) and the lightning leader tip mechanism (Moss *et al.*, 2006; Carlson *et al.*, 2010; Celestin & Pasko, 2011). The RF model accounts for bremsstrahlung x-rays created by initial electron avalanches. These x-rays may create secondary avalanches either through Compton backscattering with other electrons or through pair production, in which backward propagating positrons may interact with other electrons, further seeding RREA (Dwyer *et al.*, 2012a). This model places a fundamental limit on the electric field strength, above which the feedback mechanism dominates and discharges the electric field. The lightning leader tip mechanism allows for low energy electrons to be accelerated to thermal runaway electrons, due to extremely high local electric fields near lightning leader tips. This process is known as "cold runaway" (Gurevich, 1961). These runaway electrons can further act as seed particles for RREA in the ambient electric field, thus eliminating the need for external seeds (Dwyer *et al.*, 2012b).

In this paper we examine the inter-flash intervals between lightning flashes in TGF-producing thunderstorms. We look specifically at how the flash intervals immediately prior to and after the TGF compare to typical inter-flash intervals within the same individual storms. We interpret these results in the context of the ambient electric field charge up time and the idea that longer inter-flash intervals (and thus longer charging times) result in stronger or more extended electric fields before the TGF associated lightning discharge. Higher electric fields may be an important factor in the production of TGFs as suggested by (Smith *et al.*, 2018) who observed two similar upward lightning flashes, one of which produced a TGF, while the other did not. The TGF-producing flash occurred during a gamma ray glow (a state of continuous, low-level RREA, see Tsuchiya *et al.* (2011) which showed that glows exhibit the expected spectra due to RREA), implying that the electric field was higher in that case than for the non-TGF producing flash. This evidence suggests that an enhanced electric field may be required for the production of TGFs. The conclusion of this paper, that TGFs occur after relatively extended charging periods, is important because, to our knowledge, it is the first study to show evidence of an enhanced thunderstorm field driving TGFs in a statistically rigorous way. This is also the first observation that would allow one to guess, in the absence TGF signatures, which flashes in a storm are more likely to produce TGFs.

Data and Methods

In this analysis we use TGFs identified by Fermi GBM. Located Radio atmospheric signal pulses (hereafter referred to as 'sferics'), supplied by the World Wide Lightning Location Network (WWLLN), within ±10 minutes of identified TGFs are available in Fermi's online TGF catalog (Roberts *et al.*, 2018). In addition to data from WWLLN, lightning sferic data have also been provided by the Earth Networks Total Lightning Network (ENTLN).

There are 1339 TGFs for which positive WWLLN associations have been identified. Of this number, 1169 TGFs had both ENTLN and WWLLN data available. This subsample of TGFs was analyzed in this work. A time correction corresponding to a photon propagation time to Fermi (at an altitude of roughly 555 km) from a source altitude of 20 km and a location of the TGF associated sferic, is first applied to all associated ENTLN sferics (Briggs *et al.*, 2010). The WWLLN sferics used have already been time corrected into Fermi's observing frame, so this time correction is necessary to put both WWLLN and ENTLN sferics in the same time frame. This time correction ranges from 1.78 ms to 3.21 ms for the TGFs used in this study. The time corrected ENTLN sferics are then merged with available WWLLN sferics in chronological order. The merged dataset is then spatially clustered using the Hierarchical Density Based Spatial Clustering of Applications with Noise (HDBSCAN) algorithm (McInnes *et al.*, 2017). This is done to identify lightning belonging to individual thunderstorms. The HDBSCAN clustering algorithm requires neither a user specified scale size nor a specified number of clusters. HDBSCAN works by performing the DBSCAN algorithm over a range of varying distance parameters and selecting the most persistent clusters, i.e. the ones that remain stable as the length scale decreases (Campello *et al.*, 2013). Thus HDBSCAN is better suited to this application than typical clustering algorithms such as DBSCAN and k-means (Ester *et al.*, 1996; Wu *et al.*, 2008), as it allows for clusters of varying sizes and arbitrary shapes to be identified and the number of clusters does not have to be known or guessed beforehand.

HDBSCAN assigns a probability score ($0.0 \leq \mathrm{p} \leq 1.0$) to each point in a given cluster. Points with lower scores are not as confidently identified as belonging to their specified cluster, in contrast with points having higher probability scores. For this work, we set this probability score threshold at $\mathrm{p} \geq 0.2$. This threshold was chosen after manually examining cluster assignments over a range of thresholds.Threshold values larger than 0.2 have the effect of including only the inner cores of clusters while excluding the apparent edge points of clusters. Threshold values smaller than 0.2, however, tend to include obvious outlier points which do not appear to be a part of the cluster they are assigned to. A threshold of 0.2 seems to be a good choice as it still excludes obvious outliers, while retaining the inclusion of the main bodies of clusters. As an extra measure, this parameter was varied over a range of 0.0 to 0.99, and the results of this study do not strongly depend on this threshold value. In addition, HDBSCAN classifies some sferics, typically isolated sferics or those which have ambiguous cluster assignments, as 'noise'. Noise classified sferics are excluded from this analysis. Figure 2.1 shows an example of this spatial clustering.

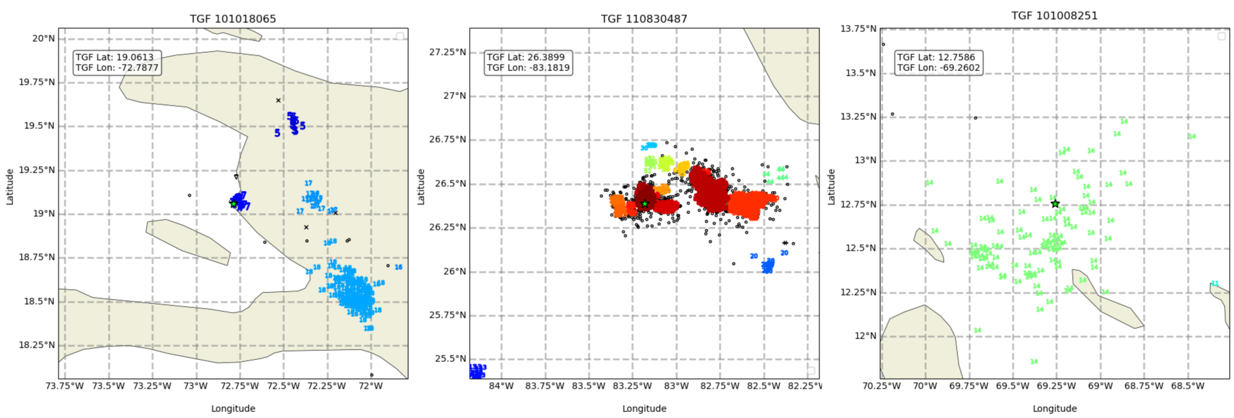

Figure 2.1: Example maps of clustered sferics. Each point on the map represents a single sferic. The different colors and markers represent different clusters. The TGF associated sferic is marked with a green star, and its coordinates are given in the upper left. The unfilled circles represent the "noise" as identified by HDBSCAN, while unfilled markers represent points not included based on the p≥0.2 restriction. Land has been colored beige for reference, while oceans have been left white. (Left) Example of a "good" or useable cluster labeled as cluster "7" (containing the TGF associated sferic). (Middle) Example of a clustering that was unusable for this analysis due to its poor isolation. (Right) Example of rejected cluster, based on its dispersiveness.

In addition to spatial clustering, the sferics associated with the TGF-producing cluster were also temporally grouped using a Gaussian Kernel Density Estimation (KDE) with a bandwidth of 0.25 seconds. This bandwidth parameter controls the width of the gaussian kernel used. Too large of a bandwidth would result in the grouping together of multiple distinct flashes, while too small of a bandwith would result in each sferic being grouped into its own flash. A choice of bandwidth within the range of 0.2 - 0.7 produces consistent results and allows for individual sferics to be grouped into distinct lightning flashes, with total durations typically less than 1 second, a common value for typical lightning flashes (Dwyer & Uman, 2014). This 'flash-grouping' also eliminates any double counting from merging the ENTLN and WWLLN sferics by merging said double counts into the same flash.

After spatially and temporally grouping sferics for all 1,169 events, the full set was then visually reexamined and narrowed down to include only those events with accurate cluster assignments, as determined by two different researchers. The accuracy of cluster assignment was evaluated using the criteria of density, isolation, and distinctiveness. A cluster was considered "good" if it was distinguishable (i.e. not overlapping with other clusters), not clearly made up of several subclusters, and not so close to other clusters that individual sferics might have been included from those nearby clusters (i.e. at least separated by more than the WWLLN location accuracy or distinct, well separated areas of sferic densities are clearly visible). In addition, we required the clusters to have at least 15 distinct lightning flashes and a total extent (farthest distance between any two points in a cluster) of less than 60 km. We required at least 15 distinct lightning flashes to ensure the statistical quality of the mean inter-flash intervals, as this statistic tends to become very imprecise with a small number of samples. This analysis was also performed on clusters with down to 10 flashes and produced similar results. The criterion of 60 km was chosen to exclude the use of clusters which were made up of several obvious subclusters, but which HDBSCAN failed to identify, and to exclude very dispersed clusters which were given questionable cluster assignments by HDBSCAN (see Figure 2.1 (right) for example). Typical thunderstorm diameters can reach up to roughly 100 km with convection regions reaching up to a few tens of kilometers in diameter (Houze, 2004; Klimov *et al.*, 2018). This, considered with WWLLN's location accuracy, makes the 60 km threshold a conservative choice. This process of selecting clusters was entirely blind to the temporal characteristics of the clusters so as to avoid any bias in terms of the parameter being studied (inter-flash intervals). In total, 219 TGF-producing clusters met these standards and were subsequently included in this study. 475 TGF-producing clusters did not have enough recorded flashes to be statistically reliable, 162 clusters were too large or dispersed to identify a single storm, 175 clusters were excluded based on isolation or distinctiveness, 13 clusters were associated with double-pulsed TGFs which were not considered in this study to avoid any systematic differences that may exist between single and double-pulsed TGFs, and in 125 cases the clustering algorithm failed to attribute the TGF strike to any cluster.

In the 219 selected TGF producing clusters, time separations between flashes in the cluster were calculated. Specifically, differences between the terminating sferic in a given flash and the initiating sferic of the next flash were calculated for all flashes. Calculating the time difference in this way results in the minimum possible inter-flash interval, as opposed to calculating the time differences from the start (or end) of every flash, for example. For all 219 events, we kept track of the time differences between the TGF-producing flash and the flashes immediately prior to and immediately after the TGF, referred to here as the "pre-TGF" and "post-TGF flashes, respectively. In addition, we also kept track of the mean inter-flash interval of all flashes in the 20-minute data sample of a given cluster, referred to here as the "typical" inter-flash interval. This analysis has also been done using the median inter-flash intervals, with very similar results. Figure 2.2 shows these inter-flash intervals for an example TGF-producing storm, with all important parameters labeled.

Flash rates in individual thunderstorms can vary dramatically depending on the specific environment in which they develop (Ushiro *et al.*, 2001; Williams *et al.*, 2005). For this reason, we compare the pre and post-TGF intervals to the typical inter-flash interval of their individual producing storms. This is done by dividing the pre and post-TGF intervals by the typical inter-flash interval of their individual storms. The result is a ratio which is then used

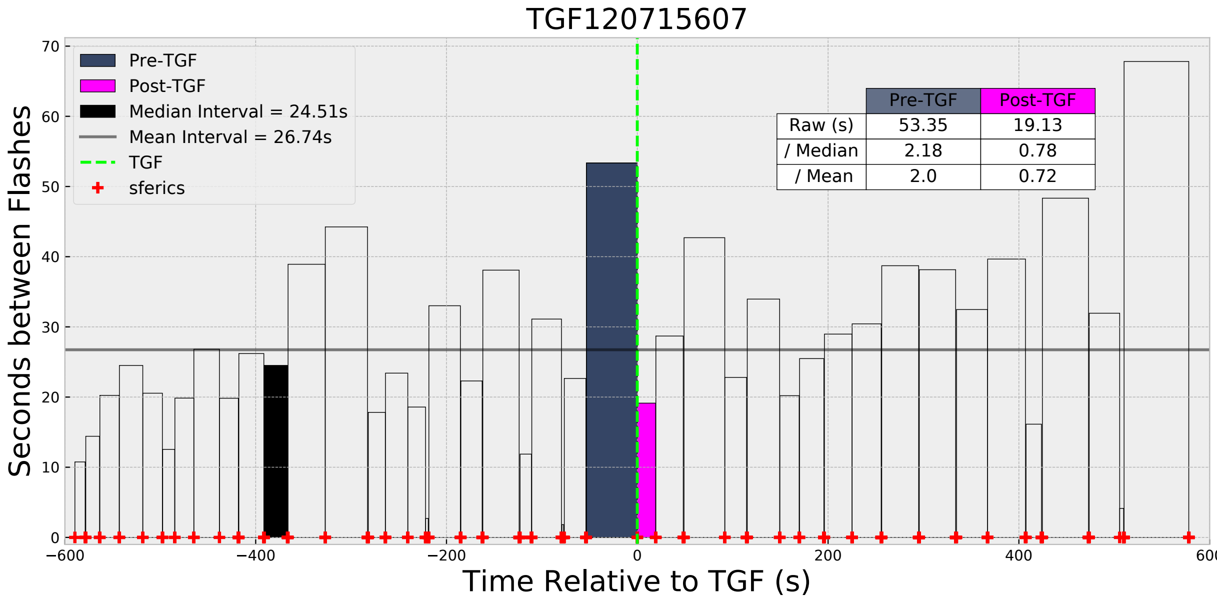

Figure 2.2: Time versus inter-flash intervals for an example TGF-producing storm. The unfilled bars represent general inter-flash intervals, the blue filled bar shows the pre-TGF interval, the magenta filled bar shows the post-TGF interval, and the black filled bar represents the median inter-flash interval. The gray horizontal line shows the value of the mean inter-flash interval, and the vertical green line shows the location of the TGF. The time series of individual sferics are shown as red crosses. Finally, a table showing the raw values for the pre and post-TGF intervals as well as those values divided by the median and mean inter-flash intervals is given.

to characterize the intervals. Comparing the pre, post, and typical interval distributions of all storms directly to each other, without dividing first, would fail to consider this flash rate variation as storms with higher charging rates will necessarily have shorter inter-flash intervals than storms with lower flash rates. It is impossible to determine if the pre or post-TGF intervals are significantly different by comparing storms in this way.

Results

Figure 2.3 shows the results of the above analysis. We find a mean ratio value of 1.24 for pre-TGF intervals and 0.92 for the post-TGF intervals. These results imply that the pre-flash pre-TGF charging period is typically 24% longer than the average charging rate in TGF producing storms, while the post-TGF charging rate is typically 8% shorter than normal. We also note a distinct difference between the pre and post-TGF ratio histograms. In particular, we see an apparent lack of TGFs where the pre-TGF interval is shorter than normal (a ratio of less than 1) as compared to the post-TGF intervals.

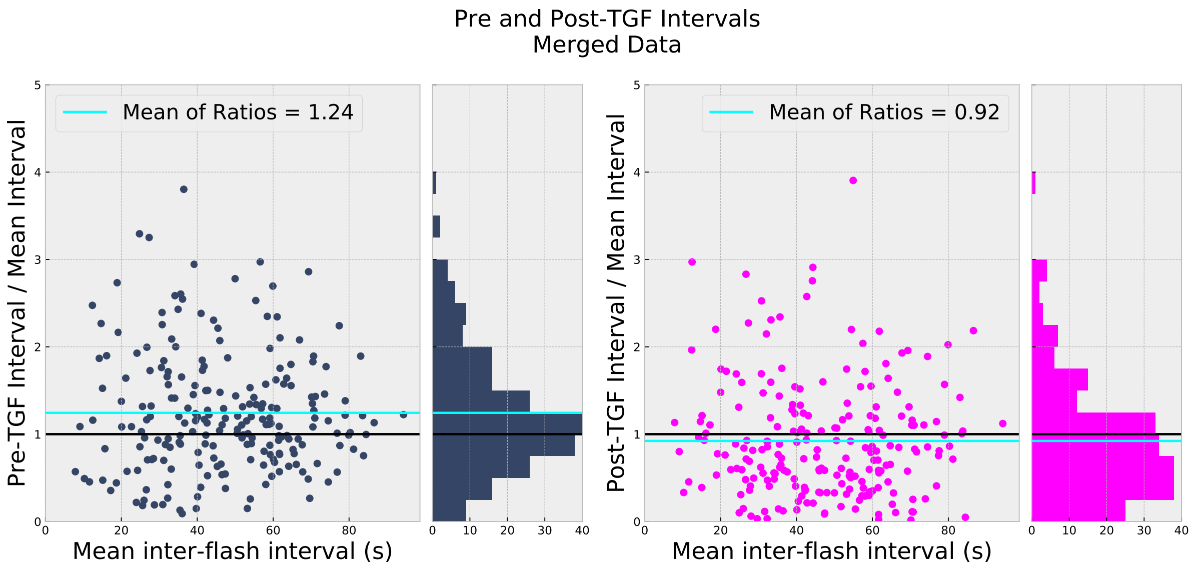

Figure 2.3: Scatter plots of pre-TGF (Left) and post-TGF (Right) inter-flash periods divided by the mean inter-flash period for the same storms. Each point represents a separate TGF producing storm. The black horizontal line is a ratio of 1, for reference, while the cyan horizontal line shows the mean of these ratios for both distributions. Also shown are histograms of the mean ratios.

To test the significance of the 24% and 8% deviations from the typical inter-flash intervals in both the pre and post-TGF distributions, we have used a numerical bootstrap method. For each of the 219 chosen clusters, we randomly select a flash to be the “TGF”. We then calculate the corresponding pre and post-TGF intervals and take the ratio to the typical inter-flash interval for that storm. We then calculate the mean value of these ratios for both the “pre” and “post-TGF” intervals over the entire 219 TGFs. This is then repeated 5 million times for each of the TGFs to get sufficient random sampling. The results of this bootstrapping, shown in Figure 2.4, indicate that the 24% longer than normal interval immediately prior to the TGF seen in Figure 2.3 is extremely unlikely to have occurred by chance, as only twice in 5 million random trials was this statistic larger than 1.24. Conversely, the 8% shorter intervals seen immediately following the TGF are not highly significant, as the random scrambling produced a value lower than 0.92, roughly 6% of the time.

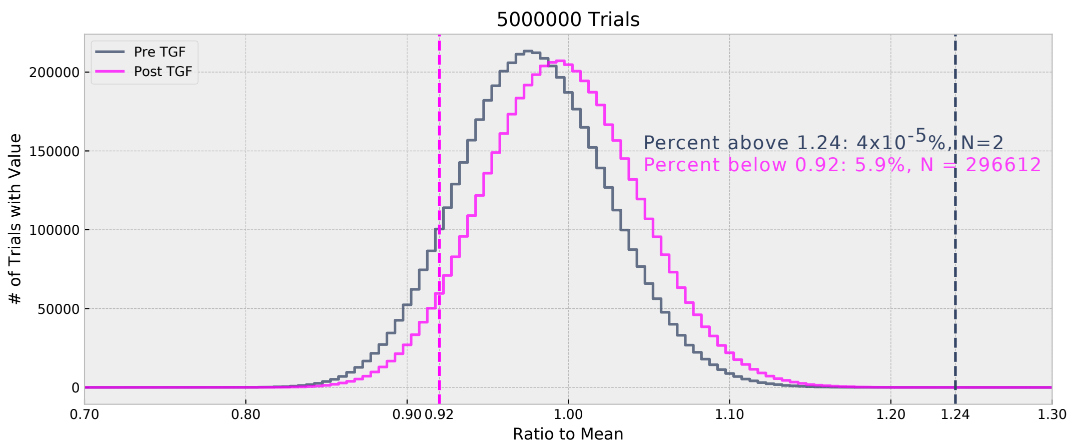

Figure 2.4: Histogram of numerical bootstrap results using 5 million random trials. The solid blue line represents a histogram of the bootstrapped pre-TGF to mean ratios, while the solid magenta line represents the same, but for the post-TGF values (these values correspond to the two horizontal cyan lines in Figure 2.3). The vertical dashed blue line represents the real value of 1.24 (see Figure 2.3) corresponding to the real pre-TGF ratios and the dashed magenta line represents the real post-TGF mean ratio of 0.92.

This significance test was also performed on 317 non-TGF-producing clusters which satisfied the above criteria (and which were within 500 km of the TGF-producing storms to reduce any systematic geographical variations). 219 storms were randomly selected from this sample of 317, and the numerical bootstrap method was performed on that subset of storms in the same manner as above. From each storm, a random "pre" and "post-TGF" interval was selected and divided by the mean inter-flash interval of that storm. After the 219 interval ratios were selected, the mean of that distribution was calculated. This process was repeated 5 million times, producing a distribution similar to that in Figure 2.4. To check the dependence of this statistic on storm selection, this entire process was repeated for 1000 different sets of 219 storms, chosen from the 317 that met the aforementioned criteria. Because each of the 1000 trials were composed of a different set of storms, the number of mean ratios larger than 1.24 varied in each trial. However, of all 1000 different sets of storms, the maximum number of times the 1.24 statistic was exceeded was only 71 out of 5 million random trials (0.001%). For that same set of storms, values lower than 0.92 were found roughly 10% of the time. This bootstrapping represents the worst case scenario, and shows that our finding of a 24% longer charging period prior to TGFs is very significant.

The offset between the two curves in Figure 2.4 is real effect caused by the overall decline of the flash rates in these storms. TGFs are known to occur while the flash rate of a storm is declining (Smith *et al.*, 2010), and so post-TGF intervals in random samples will tend to be slightly longer than pre-TGF intervals.

Conclusions

In this work we have examined lightning inter-flash intervals in 219 TGF producing thunderstorms. We find that the flash interval immediately prior to the TGF is longer than the typical inter-flash interval by an average of 24%. Conversely, we find that the interval immediately after the TGF is shorter than normal by a typical value of 8%. The significance of these results were tested using a numerical bootstrap method. The extended pre-TGF interval was found to be very significant, as only 0.00004% of random trials produced a value larger than 1.24. However, in the case of the post-TGF interval, values with means shorter than the actual value were found, by random, in 6% of the trials. The post-TGF interval is thus consistent with being a “typical” flash.

There are several influences which could produce such extended pre-TGF intervals. For example, lightning flash rates are known to be strongly correlated to factors such as updraft velocity and content, cloud base height, and concentrations of cloud condensation nuclei (CCN) (MacGorman *et al.*, 2010; Williams *et al.*, 2005; Yoshida *et al.*, 2017). It is possible that any of these factors could affect flash rates by affecting charging rates, however, these factors likely all vary on timescales much longer than typical inter-flash intervals. Furthermore, it is difficult to imagine why variations in these factors would influence the production of TGFs.

Longer inter-flash intervals prior to the TGF would imply that the electric field had more time to charge up before a discharge, resulting in stronger or more spatially extended electric fields. As a simple model, if one imagines the charge structure in a thunderstorm to be similar to that of a capacitor, for which the volume remains roughly constant over the span of 10s of seconds, a shorter inter-flash interval would limit the field to a lower value, while a longer interval would allow the field to grow to relatively stronger values before lightning discharges. The assumption of a roughly constant charge structure over 10s of seconds is supported by the results of Pawar & Kamra (2004) who demonstrate the large spatial and temporal scales of the lower positive charge center in a thunderstorm. This mental picture is also supported by the recovery curves of the electric field between lightning flashes as demonstrated in Pawar & Kamra (2002) (see their Figure 2) which show a consistent charging profile between flashes, and that the field at the time of each flash depends on the inter-flash interval.

It is also well established that low-flash rate storms produce more energetic lightning flashes with higher peak currents (Chronis *et al.*, 2015; Hutchins *et al.*, 2013), meaning that the electric field must either be enhanced, or strong over a larger volume than for less energetic flashes. It is also not unexpected that higher flash rates limit the growth of the background electric field (Chronis & Koshak, 2017). An enhanced electric field makes it more likely that a leader channel could push the field well above the feedback threshold over a significant volume (Dwyer, 2008), resulting in more favorable conditions for the production of TGFs. A stronger field could explain why some lightning flashes produce TGFs while similar flashes do not (Smith *et al.*, 2018). Finally, in terms of the electric field, the fact that the post-TGF interval is consistent with typical flashes would imply that the TGF returns the ambient electric field to a “normal” state, as opposed to over or under discharging it.

Acknowledgments

The authors wish to thank the World Wide Lightning Location Network (http://wwlln.net), a collaboration among over 50 universities and institutions, for providing the lightning location data used in this paper. We also acknowledge Earth Networks for providing the ENTLN data used in this study. All code and data pertaining to this work can be accessed at `https://research-archive.scipp.ucsc.edu/intervals`. The authors would also like thank Paul Krehbiel, Ken Cummins, Phil Krider, and Eric Bruning for their valuable insight into the physics of thunderstorms. Finally, the authors wish to thank Will Early and Matthew Thompson for their assistance in helping identify valid clusters. This work was supported by Montana State University.

THE RELATIONSHIP BETWEEN TGF PRODUCTION IN THUNDERSTORMS AND LIGHTNING FLASH RATES AND AMPLITUDES

Contribution of Authors and Co-Authors

Manuscript in Chapter 3

Author: Reyann K. Larkey

Contributions: Defined thunderstorms, clustered data by hand, and performed statistical analyses.

Co-Author: John G. Sample

Contributions: Mentor who helped organize paper and provided feedback on analysis types.

Co-Author: David M. Smith

Contributions: Mentor who helped guide project and advised next steps in analysis. Helped define motivation and interpret results.

Co-Author: Jeff L. Lapierre

Contributions: Provided access to and instruction for ENTLN data and helped interpret results.

Co-Author: Elizabeth DiGangi

Contributions: Provided additional insight into ENTLN data and types of statistical analyses.

Co-Author: Robert H. Holzworth

Contributions: Provided feedback and instruction for working with WWLLN data.

Manuscript Information

Reyann K. Larkey, John G. Sample, David M. Smith, Jeff L. Lapierre, Elizabeth DiGangi, Robert H. Holzworth

Status of Manuscript:
___ Prepared for submission to a peer-reviewed journal
___ Officially submitted to a peer-reviewed journal
___ Accepted by a peer-reviewed journal
_X_ Published in a peer-reviewed journal

Journal of Geophysical Research: Atmospheres Volume 126, Issue 13
DOI: 10.1029/2020JD034401

Key Points

- TGFs tend to occur when the flash rates in thunderstorms are lower and declining.
- TGFs are produced less efficiently during the peak lightning flash rates.
- The flash amplitudes near the TGF tend to be higher than during other times of the same storms.

Abstract

We provide evidence that Terrestrial Gamma-Ray Flashes (TGFs), in well isolated thunderstorms, tend to occur during periods of low and declining flash rates, and when the flash amplitudes are larger than average. This conclusion comes from examining the results of 371 manually tracked TGF-producing thunderstorms. Fermi-GBM identified TGFs are used for this analysis and lightning data come from both WWLLN and ENTLN. The data from these storms suggest that TGFs are likely to occur in almost every phase of storms that last longer than an hour, but tend to occur later on in shorter storms. We also note that, in short storms, TGFs are more likely to accompany a flash when the flash rates of the storm are lower than average, and they are less likely per flash during the peak flash rate periods of the storms. We find that the tendency for TGFs to occur while the flash rate is falling and when the amplitudes of flashes (the sum of the absolute values of peak currents of all constituent sferics in the flash) are larger than average, does not depend strongly on the duration of the storms. This implies that not just any lightning flash can or even will produce a TGF, but that the electrical conditions of the storm play a crucial role in TGF production.

Plain Language Summary

TGFs, which are very intense bursts of high energy radiation that are produced by some lighting, occur in almost every phase of the thunderstorms that produce them. We find that TGFs are more likely to occur when the lightning flash rate in the storm is lower than average. We also find that lightning flashes near the time of the TGFs are usually among the stronger flashes in the storms.

Introduction

Even though Terrestrial Gamma-Ray Flashes (TGFs) were discovered over two decades ago (Fishman *et al.*, 1994), there is still very little known about their production. It is well established that TGFs are associated with lightning flashes, and more specifically positive-polarity intracloud (+IC) discharges (Cummer *et al.*, 2005; Fishman *et al.*, 1994; Inan *et al.*, 1996, 2006; Lu *et al.*, 2010; Shao *et al.*, 2010; Stanley *et al.*, 2006). Observations of TGFs have primarily been made by satellite missions such as the Burst and Transient Source Experiment (BATSE) onboard the Compton Gamma-Ray Observatory (CGRO), the Reuven Ramaty High Energy Solar Spectroscopic Imager (RHESSI), Astro rivelatore Gamma a Immagini Leggero (AGILE), the Gamma-Ray Burst Monitor (GBM) onboard the Fermi Gamma-Ray Space Telescope, and the Atmosphere-Space Interactions Monitor (ASIM) (Briggs *et al.*, 2010; Fishman *et al.*, 1994; Marisaldi *et al.*, 2014; Østgaard *et al.*, 2019; Smith *et al.*, 2005). The bursts of radiation from TGFs can result in gamma-rays with energies up to tens of MeV (Briggs *et al.*, 2010; Smith *et al.*, 2005; Marisaldi *et al.*, 2010, 2019) and can produce enough high energy radiation to deliver hazardous radiation doses to a person exposed to them (Dwyer *et al.*, 2010; Pallu *et al.*, 2021).

The main mechanism thought to produce TGFs is the Relativistic Runaway Electron Avalanche (RREA) process (Gurevich *et al.*, 1992). This mechanism on its own, however, cannot fully explain the observed luminosity of TGFs if one considers cosmic rays as the seed electron providers (Dwyer, 2008). Due to this limitation, modifications have been posited to supplement this theory. For example, the relativistic feedback (RF) model, proposed by Dwyer (2003) allows for secondary electron avalanches to be created by Compton backscattering of bremsstrahlung x-rays and by Bhabha scattering with secondary positrons. This allows for an exponential increase in the number of runaway electrons produced by a single seed particle. Another explanation is that electrons near the high local electric fields at the tips of lightning leaders can gain enough energy to become seed particles for the RREA process (Carlson *et al.*, 2010; Celestin & Pasko, 2011; Moss *et al.*, 2006). This potentially large number of seed particles could explain the observed fluence of TGFs.

Regardless of the model of production, however, there is still no explanation for why some lightning flashes produce TGFs but others do not. Previous studies have looked at the meteorological data of the thunderstorms that produce TGFs (Chronis *et al.*, 2016; Barnes *et al.*, 2015; Fabró *et al.*, 2019; Smith *et al.*, 2010; Splitt *et al.*, 2010, e.g.), but in general, it is found that TGFs can be produced by a wide variety of different types of thunderstorms. Smith *et al.* (2010) found evidence that TGFs occur in the declining stages of flash rate in thunderstorms using 51 storms and RHESSI-identified TGFs. In this paper we examine the relationship between lightning flash rate and TGF production using WWLLN and ENTLN data and Fermi-GBM identified TGFs. The storms used in this study were manually tracked over the course of their lifetime which provides more detail into how these storms evolve, and it also allows for a much larger sample size than previous studies mentioned.

Data and Methods

For this work, we have used lightning data (localized radio atmospheric signals or "sferics") from both the World Wide Lightning Location Network (WWLLN) (Rodger *et al.*, 2006, 2009) as well as the Earth Networks Total Lightning Network (ENTLN) (Marchand *et al.*, 2019; Rudlosky, 2015; Sonnenfeld *et al.*, 2020; Zhu *et al.*, 2017). The motivation for using these two datasets stems from their unprecedented reliability, accuracy, and global coverage. The TGFs used for this study have been observed by Fermi-GBM over a time period ranging from 2008 to 2016. We used only the TGF events for which a positive WWLLN association was found (Roberts *et al.*, 2018) and for which the ENTLN data are available – a sample size of 1,169 events. We have used the locations of the known WWLLN associations to identify the corresponding storms in the ENTLN data (i.e. the storms which would contain the WWLLN associated sferic). The identified storms, which consist entirely of ENTLN data, have then been tracked, by hand, over the course of their evolution. This was done by identifying isolated clusters of lightning sferics and following the clusters over the course of their lifetimes. Of the 1,169 total possible events, 534 were able to be tracked by hand, 231 had too sparse lightning data to pick out an accurate storm, 237 were too irregular to accurately identify a storm, 71 had no clear storm associated with the WWLLN identified sferic, 80 were difficult to track for a variety of other reasons, and 16 had no ENTLN data in the region of the known WWLLN association. Of the 534 events that were tracked by hand, only 418 of them had ENTLN sferics within 5ms of the known TGF time (the same time window used to identify WWLLN associations by Connaughton (2010); Connaughton *et al.* (2013)).We chose to use 5ms as a conservative window for finding associations in the ENTLN data, however, all of the events used in this study had sferics within the stricter, 3.5ms window commonly used for WWLLN associations (Roberts *et al.*, 2018). For each of the different analyses in this work, we used only those storms with at least 15 flashes (N = 371), an arbitrary threshold implemented to ensure the statistical quality of measures like the mean flash rate of the storms for example.

It is likely that our sample contains a variety of storm types, however, we are unable to comment definitively without additional data. It should be noted that the following results of this study can, at this point, only be considered accurate for TGFs produced in well organized, isolated thunderstorms, which is roughly 30% of the total TGFs available for this study. There is necessarily a selection bias introduced by the requirement of the ability to accurately track and identify storms over their lifetimes. There could also be unknown biases due to the changes in lightning network detection efficiency over time. Without additional data, we are unable to say whether these results apply to all TGFs or just TGFs produced in thunderstorms that are "trackable". One could potentially increase the number of "good" storms by incorporating more weather data, expanding the TGF catalog, or developing more sophisticated methods of tracking storms. These endeavours should be considered in future work. More details on the storms used in this study can be found in the Appendix.

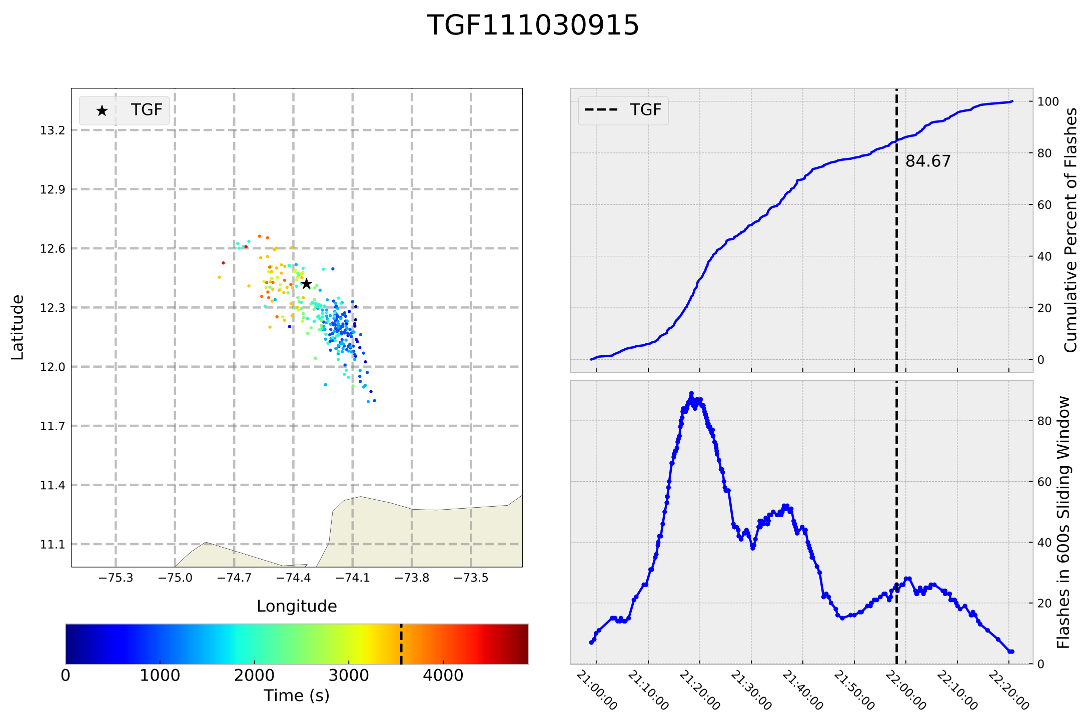

Figure 3.1: (left) Map showing the lightning sferics belonging to this storm. The sferics are colored by time since the start of the storm as indicated in the color bar below. The black star represents the sferic associated with the TGF. (top right) Cumulative percent of flashes over the time of the storm. The dashed vertical line represents the time of the TGF (which occurs after 84.67% of the storm's flashes). (bottom right) 600 second running flash count for the storm, the black dashed line represents the time of the TGF.

TGF Temporal Locations in Storms

For each of the 418 tracked storms, the lightning sferics were then grouped into flashes, using a Kernel Density Estimation (KDE) method and a ten-minute running sum of the distinct flashes was calculated. The KDE method uses a Gaussian kernel with a bandwidth of 0.25s and allows for sferics to be grouped together into distinct lightning flashes with total durations usually less than 1 second. More details can be found in (Larkey *et al.*, 2019). Figure 3.1 shows an example of one of these tracked storms. We used the Z-score, the number of standard deviations away from the mean a data point lies, to perform analysis of when the TGF occurs in the storms. The Z-score, in this case, is therefore analogous to a time measure of when in the storm the TGF occurs. We have used two different versions of this statistic, namely, a Z-score with respect to the mean time of all the flashes in the storm, and a Z-score with respect to the time of the maximum flash rate of the storm. More specifically, we have used the following equations.

$$Z_{Mean} = \frac{(t_{TGF} - \mu)}{\sigma} \tag{3.1}$$

$$Z_{Max} = \frac{(t_{TGF} - argmax(R))}{\sigma} \tag{3.2}$$

Here, t_{TGF} represents the time of the TGF, μ is the mean time of all flashes in the storm, σ is the standard deviation of lightning flash times about that mean, and $argmax(R)$ is the time of the highest flash rate in the storm. Using these statistics, a positive Z-score implies that the TGF occurred after the mean or maximum flash rate, while a negative Z-score implies the opposite. Figure 3.2 shows an example of these statistics for the same storm as in Figure 3.1.

We have performed the analysis on two separate subsets of the storms: those with durations less than 1 hour (N = 129) and storms with durations longer than 1 hour (N =

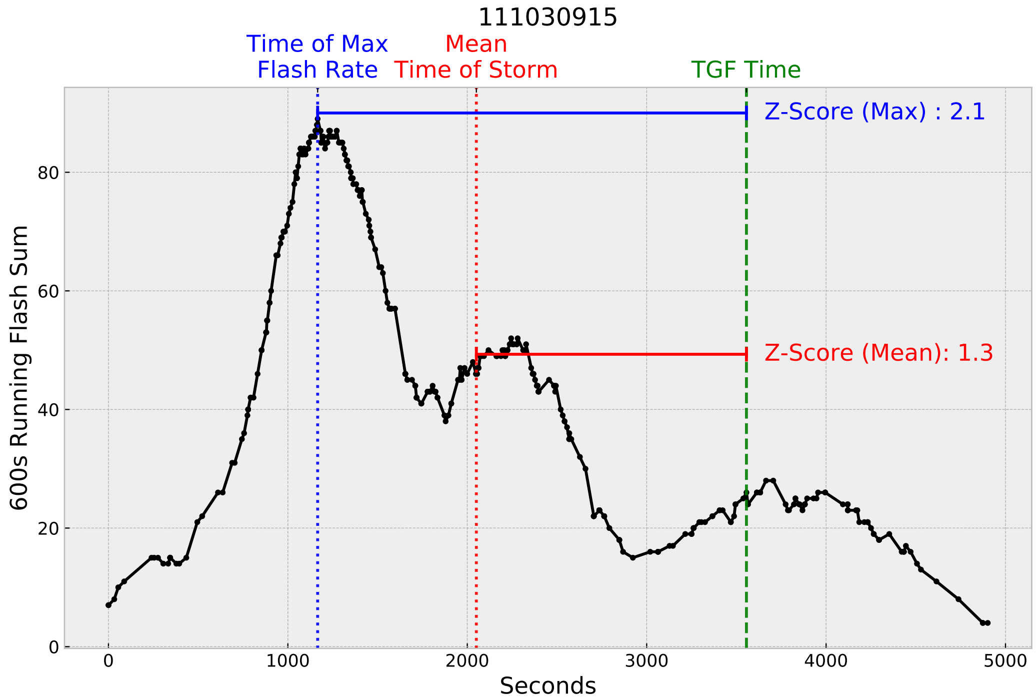

Figure 3.2: Running sum (600s window) of flashes in an example TGF-producing thunderstorm. The vertical, green dashed line represents the time of the TGF. The blue vertical line represents the time of the peak lightning flash rate, while the red vertical line represents the mean time of all flashes. Labeled are the Z-score relative to the mean (red) as well as the Z-score relative to the peak flash rate time (blue).

242). This one hour cut is justifiable as it is generally considered the upper bound on the length of a single-cell storm (Kolzov *et al.*, 2013). It is also the mode of the distribution of storm durations in our sample (see Figure 3.10) and thus emerges as the natural duration to split the datasets into distinct populations.

Flash Rate Change at Time of TGF

We also examined how the flash rate was changing at the time of the TGF. In some cases, the TGF-producing storm might be a multi-cellular storm and, over the course of the evolution of the storm, the lightning flash rate might rise and fall periodically as one cell dies out and another begins to dominate (See Figures 3.2 and 3.3, for example). Because of this it is simply not enough to look at when the TGF occurs in the storm as a whole to determine if it is occurring during a declining phase of the lightning flash rate. It could simply be that while the TGF occurs late in the storm, it occurs early in a cell's increasing stage. Because of this, we wanted to determine if the TGFs are occurring during rising, falling, or plateau stages (i.e. near local peaks in flash rates) of the nearest individual peak of its storm. Note that none of the results of this analysis rely on the definition of a cell or even if these storms are in fact multi-cellular. The reference to multi-cellular storms is meant only as a possible explanation for the flash rate variations seen in Figures 3.2 and 3.3 for example. To examine this, we used a univariate spline (with a degree of 3 and a smoothing factor of 0.2)[1] to interpolate the flash rate data, resulting in a smoother version of the flash rate curve. The derivative of the smoother spline curve gives an idea of whether the flash rate is falling or rising at the time of the TGF. We used a peak finding algorithm to identify peaks and determine their heights relative to zero. We defined a plateau in the flash rate, as those times when the flash rate is greater than or equal to 80% of the height of the closest peak. For each TGF in our sample with at least 15 flashes (N= 371), we use this method to categorize how the lightning flash rate is changing at the time of the TGF. We define four distinct classifications, summarized as follows:

1. Falling: the flash rate at the time of the TGF is less than or equal to 80% the height of the nearest peak and the derivative at the time is negative.

2. Rising: the flash rate at the time of the TGF is less than or equal to 80% the height of the nearest peak and the derivative at the time is positive.

3. Plateau (falling): the flash rate at the time of the TGF is greater than 80% the height of the nearest peak and the derivative at the time is negative.

[1] The number of knots in the spline is chosen to satisfy the condition $\sum(y_i - spl(x_i))^2 <= S$, where y_i is the real data, $spl(x_i)$ is the spline at that point, and S is the smoothing factor (chosen to be 0.2 in this case).

4. Plateau (rising): the flash rate at the time of the TGF is greater than 80% the height of the nearest peak and the derivative at the time is positive.

To determine the significance of our results, we also use a bootstrap method. We pick a random flash from each of the 371 storms and calculate how often the random flashes fall into the above categories. This process is repeated 10,000 times, and the results are compared to the results of using the TGF alone.

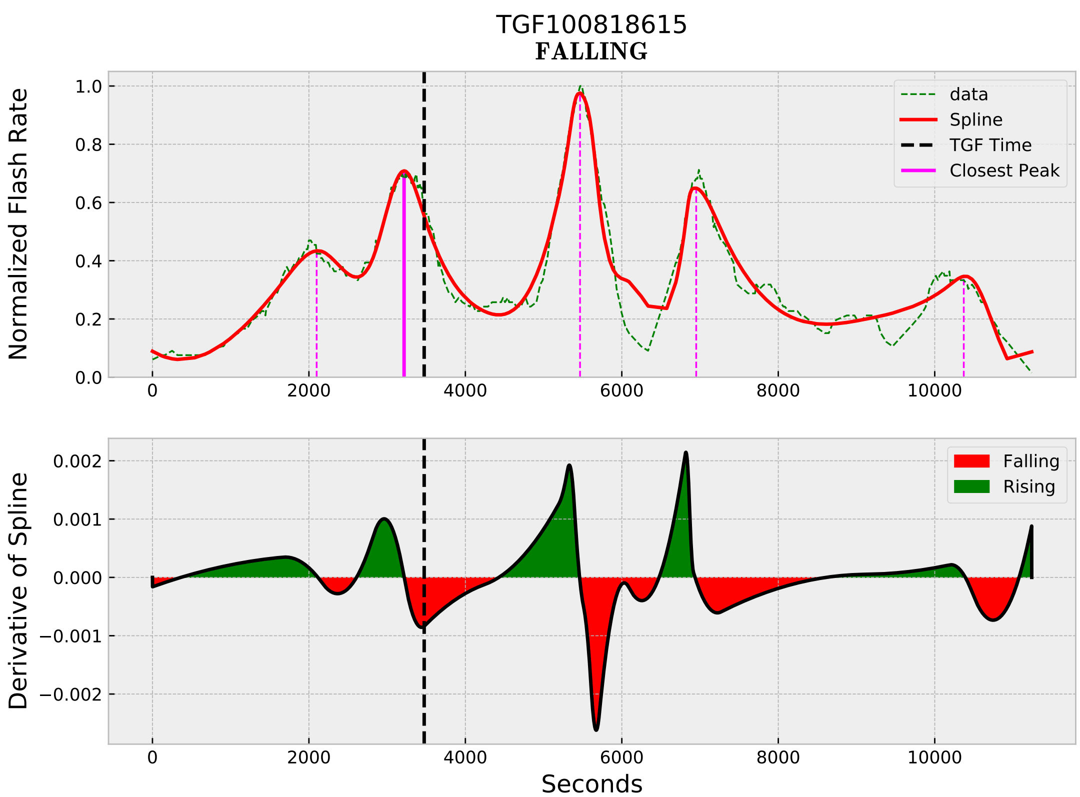

Figure 3.3: Example of a TGF classified as occurring during a falling stage of lightning activity. The top panel shows the raw data (green) and the univariate spline used to fit the data (red). Also shown are the identified peaks (magenta) with their heights being shown by the length of the lines. The solid magenta line shows the closest peak to the TGF (the solid black line). The bottom panel shows the value of the derivative of the spline in the top panel. Falling and rising stages are shown by the color of the shading.

Flash Rate at Time of TGF

In addition to looking at where in the storm phases the TGFs occur, we examined how the flash rate at the time of the TGF compares to the mean and maximum flash rates of the entire storm. We calculated the Z-scores of the flash rate at the time of the TGF relative to the mean and maximum flash rates in the storms. This was also done for randomly selected flashes in the storms to compare random flashes to TGF flashes. The equations used for this analysis (similar to Equations 1 and 2) are as follows:

$$Z_{Mean} = \frac{(FR_{TGF} - \mu_{FR})}{\sigma_{FR}} \tag{3.3}$$

$$Z_{Max} = \frac{(FR_{TGF} - max(FR))}{\sigma_{FR}} \tag{3.4}$$

Here, FR_{TGF} is the flash rate at the time of the TGF, μ_{FR} is the mean flash rate, $max(FR)$ is the maximum flash rate, and σ_{FR} is the standard deviation of the flash rate.

Flash Amplitude at Time of TGF

The final analysis we present here is an examination of how the amplitudes of lightning flashes near the time of the TGF compared to the amplitudes of other lightning flashes in the TGF storms. To start, we defined CG flashes as those which contained one or more return strokes (as specified in the ENTLN data) and IC flashes as those which contained none (Thompson *et al.*, 2014). We assigned each flash an amplitude, designated as the sum of the absolute value of all constituent sferic amplitudes (in kA). For example, if a flash were made up of a 100kA stroke and a -30kA stroke, we assigned the flash an amplitude of 130kA. Figure 3.4 shows an example of how the 10-minute averages of flash rate and flash amplitude vary for a given storm.

We separated the lightning flashes by flash type (IC or CG) to examine the amplitudes

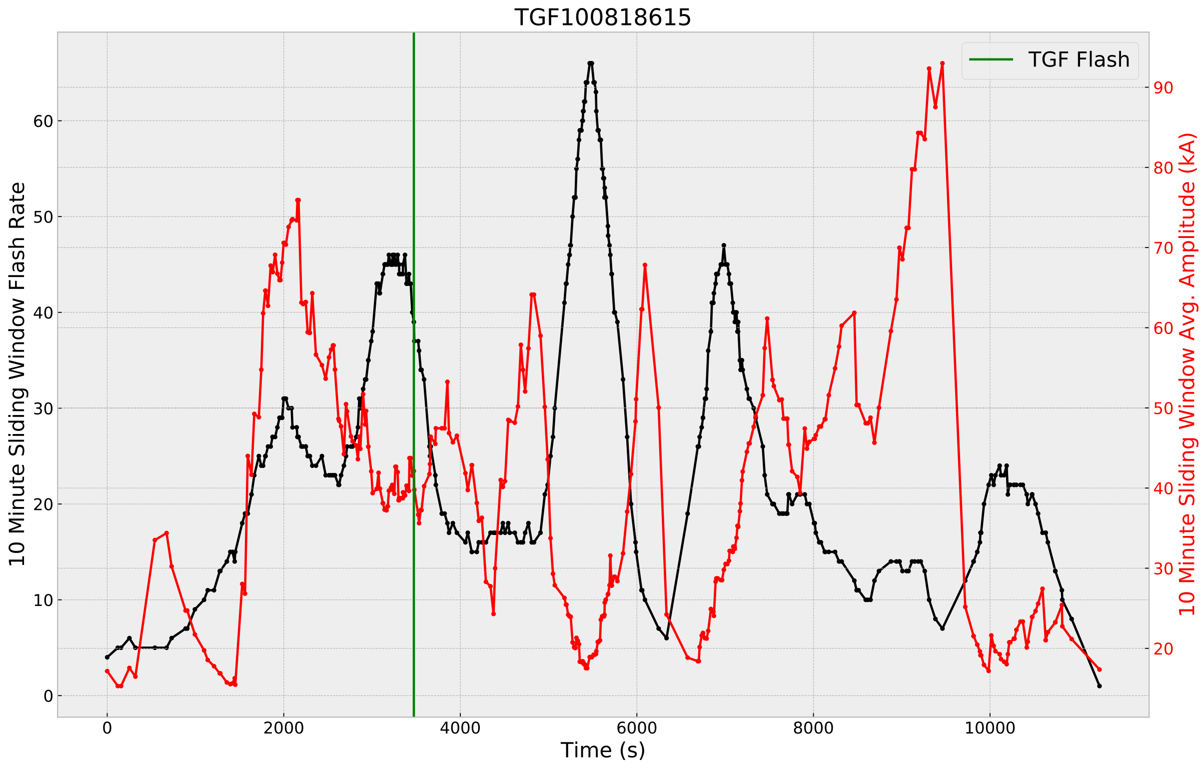

Figure 3.4: Ten-minute running averages of lightning flash rate (black) and flash amplitude (red) over the course of a TGF-producing storm. The vertical green line marks the time of the TGF.

of these types of flashes near the TGF compared to the amplitudes in the rest of the storm. We defined 'near the TGF' to be within a ±300s window of the time of the TGF and took the near-TGF flash amplitude to be the average of the CG (or IC) flashes in that time window – excluding the TGF flash itself. It has been shown that, for some populations of TGFs, the associated radio sferics are stronger than other, typical lightning flashes (Connaughton *et al.*, 2013; Stanley *et al.*, 2006). There is also evidence that some observed sferics are directly associated with the TGF events themselves (Lyu *et al.*, 2016; Mailyan *et al.*, 2018, 2020; Pu *et al.*, 2019). Finally, there is evidence that lightning networks tend to underestimate the peak current associated with TGFs as they assume that peak currents are proportional to the peak radio frequency radiation field, which may not be true for TGFs similar to compact intracloud discharges (CIDs) (Mailyan *et al.*, 2020). Nonetheless, all of the above statements might only be true for a subset of TGFs as there are a large number TGFs without associated sferics, which may be for a variety of reasons, including the possibility that some of the sferics were too weak to be detected by lightning location networks. Regardless, to include the TGF-associated sferic amplitude in this analysis would not be appropriate. For this reason, we used a ten minute average flash amplitude to get a measure of the near TGF flash amplitudes. The results do not change substantially if a different window is used or if one uses just the 5 minutes prior to the TGF or the 5 minutes after the TGF to measure the "near TGF amplitude". This was potentially a concern due to the results of Larkey *et al.* (2019), which showed that the interval immediately before the TGF was usually longer than normal–implying a stronger electric field or potential immediately before the TGF.

We compared the amplitudes of flashes near the TGF to all other flashes in the thunderstorms by calculating the Z-scores of their respective amplitudes using the following equations:

$$Z_{CG} = \frac{(A_{CG(TGF)} - \mu_{A_{CG}})}{\sigma_{A_{CG}}} \tag{3.5}$$

$$Z_{IC} = \frac{(A_{IC(TGF)} - \mu_{A_{IC}})}{\sigma_{A_{IC}}} \tag{3.6}$$

Here, $A_{CG(TGF)}$ and $A_{IC(TGF)}$ represent the amplitude of the CG and IC flashes near the time of the TGF, respectively. $\mu_{A_{CG}}$ and $\mu_{A_{IC}}$ represent the mean CG and IC amplitudes, and $\sigma_{A_{CG}}$ and $\sigma_{A_{IC}}$ are the standard deviations of the respective amplitudes.

This process was done using just IC or CG lightning flashes. In some cases, there were no IC flashes within the 10-minute window of the TGF, and in those cases, we did not use those storms to contribute to this analysis. Furthermore, there were a number of cases where ENTLN did not provide amplitude data for the identified sferics, and therefore those cases could not be used here. Because there are many storms for which this amplitude data is unavailable, it is a possibility that the results of this analysis are not universal to all TGF-producing thunderstorms, and this should considered when applying the results of this section.

Results

TGF Temporal Locations in Storms

For each of the 371 tracked events with at least 15 flashes, we calculated the two Z-score statistics mentioned in section 2.1. The distributions of these two statistics are shown in Figure 3.5. To test if these results are significantly different from "typical" lightning flashes, we have also calculated the statistics for randomly selected flashes in each storm (also shown in Figure 3.5). Using a two sample Kolmogorov-Smirnov (KS) test, we see that for storms with durations shorter than an hour, the two distributions are very significantly different (p-values of <0.01 [a confidence level of 99%] for each), however the p-values for the longer storms are much higher and not statistically significant.

We find that, in the case of the shorter storms, for both measurements (relative to the mean and relative to the max), there is an enhancement for Z-scores greater than zero, and fewer cases of Z-scores less than zero–implying that TGFs occur more often later in those storms than early in their development. For the Z-scores taken relative to the time of the peak flash rates of the storms, we also see a significant departure between the two distributions. The TGF distribution clearly has fewer events around a Z-score of 0 (i.e. near the peak flash rate), and a slight enhancement for Z-scores greater than 0. This implies that TGFs are less likely to occur on a per-flash basis during periods of peak lightning activity in thunderstorms and that they are more likely to occur after the peak flash rate times in shorter storms. This is consistent with Smith *et al.* (2010) which found that TGFs tend to occur when the lightning flash rate of a storm is declining.

The lack of significance in the bottom panels of Figure 3.5 is likely due to the fact that the longer storms are more likely to be multi-cell storms and thus also tend to have more oscillations in the flash rate curve see Figures 3.3 and 3.4 for example). In these storms, the conditions conducive to producing TGFs could potentially be met several times over the lifetime of the entire system as the flash rate rises and falls repeatedly. On the other hand, for shorter, perhaps single-cell, storms they might only be achieved near the end of the storms lifetime.

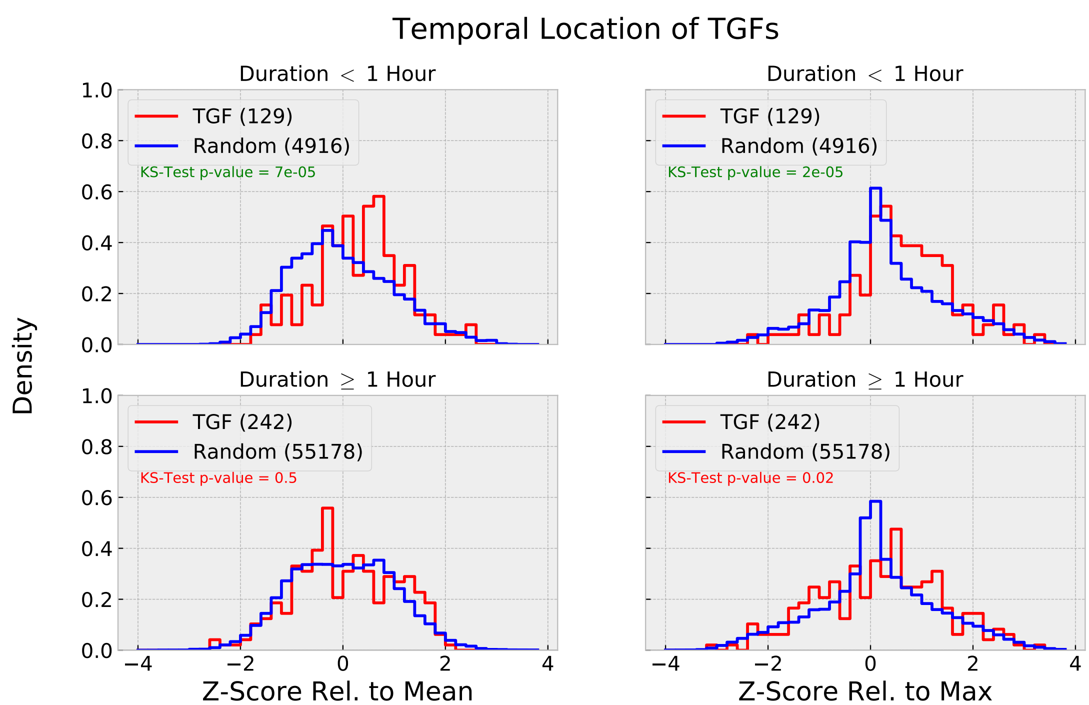

Figure 3.5: Histograms of Z-scores relative to the mean time of the thunderstorms (normalized such that the integral over the range is equal to one). Each panel has a different threshold for the minimum length of the storm. The red curves show the distributions for the TGFs, while the blue curves show the distributions for randomly selected flashes. (right column) Histograms of Z-scores relative to the peak flash rate times. The different colored curves are the same as the left column. Also labeled in each panel is the p-value associated with the 2-sample Kolmogorov-Smirnov Test for the distributions.

Flash Rate Change at Time of TGF

With regards to how the flash rate is changing at the time of the TGF, we found that 139 (37%) of the TGFs in our sample occurred when the flash rate of the storm was falling, 60 (16%) occurred when the flash rate was increasing, 103 (28%) occurred near a plateau and while the flash rate was falling, and 69 (19%) occurred near a plateau and while the flash rate was increasing. To be sure that this was not just a selection bias (i.e. a result of unequal rising and falling rates in the storms) we tested the significance of these results as described in section 2.2. The results of 10,000 random trials are summarized in Table 4.1 and Figure 3.6 (the probabilities given in Table 1 assume a normal distribution). These results show that the large number of TGFs which occur during a falling stage is extremely difficult to reproduce using random flashes and is likely not the result of selection bias. The results remain significant even if a different threshold for the plateau height is chosen and if only shorter (duration less than an hour) storms or longer (durations greater than an hour) storms are used in the analysis.

Flash Rate at Time of TGF

In addition to looking at when in the storm phases the TGFs occur, we examined how the flash rate at the time of the TGF compares to the mean and maximum flash rates of the entire storm. To do so, we calculated the Z-scores of the flash rate at the time of the TGF relative to the mean flash rate and the maximum flash rate in the storms. This was also done for randomly selected flashes in the storms. These distributions are shown in Figure 3.7.

In this case, we see that there is no significant dependence on the flash rate (neither relative to the mean flash rate nor the maximum flash rate) for the shorter storms. However, there is a strong tendency for the TGF to occur at lower flash rates in the longer storms. It is evident from Figure 3.12 that shorter storms tend to have lower overall flash rates when

Classification	Real Values	Random Trials (Mean)	Random Trials (Std. Dev.)	Probability of Result (%)
Falling	139	88.16	8.02	$1.75\text{x}10^{-8}$
Rising	60	68.28	7.38	13.14
Plateau (Falling)	103	111.66	8.67	15.87
Plateau (Rising)	69	102.9	8.54	0.0036

Table 3.1: Results of the bootstrap method described earlier. Given are the values found using just TGF flashes, as well as the mean and standard deviation for each classification found during the random trials. The last column shows the probability of getting the observed results by chance.

compared to the longer storms. This, along with the dependence to occur at the lower flash rates during the long duration storms, indicates that TGFs have a preference to occur during low flash rate periods in general and that the periods of relatively higher flash rates in longer storms makes the production of TGFs less probable.

Flash Amplitude at Time of TGF

Of the 371 storms used for this analysis, 305 of them had at least one CG flash within 10 minutes of the TGF and 102 had at least one IC flash in that time. Figure 3.8 shows the results of the amplitude analysis described in the previous section. We see that for both flash types and storm duration thresholds, the distributions representing the flashes near the TGF are shifted to higher Z-scores which translates to higher amplitudes. The skewed shape of the blue curves in Figure 3.8 is caused by a larger number of relatively low amplitude flashes occurring during high flash rate periods of the storms which acts to shift the distribution

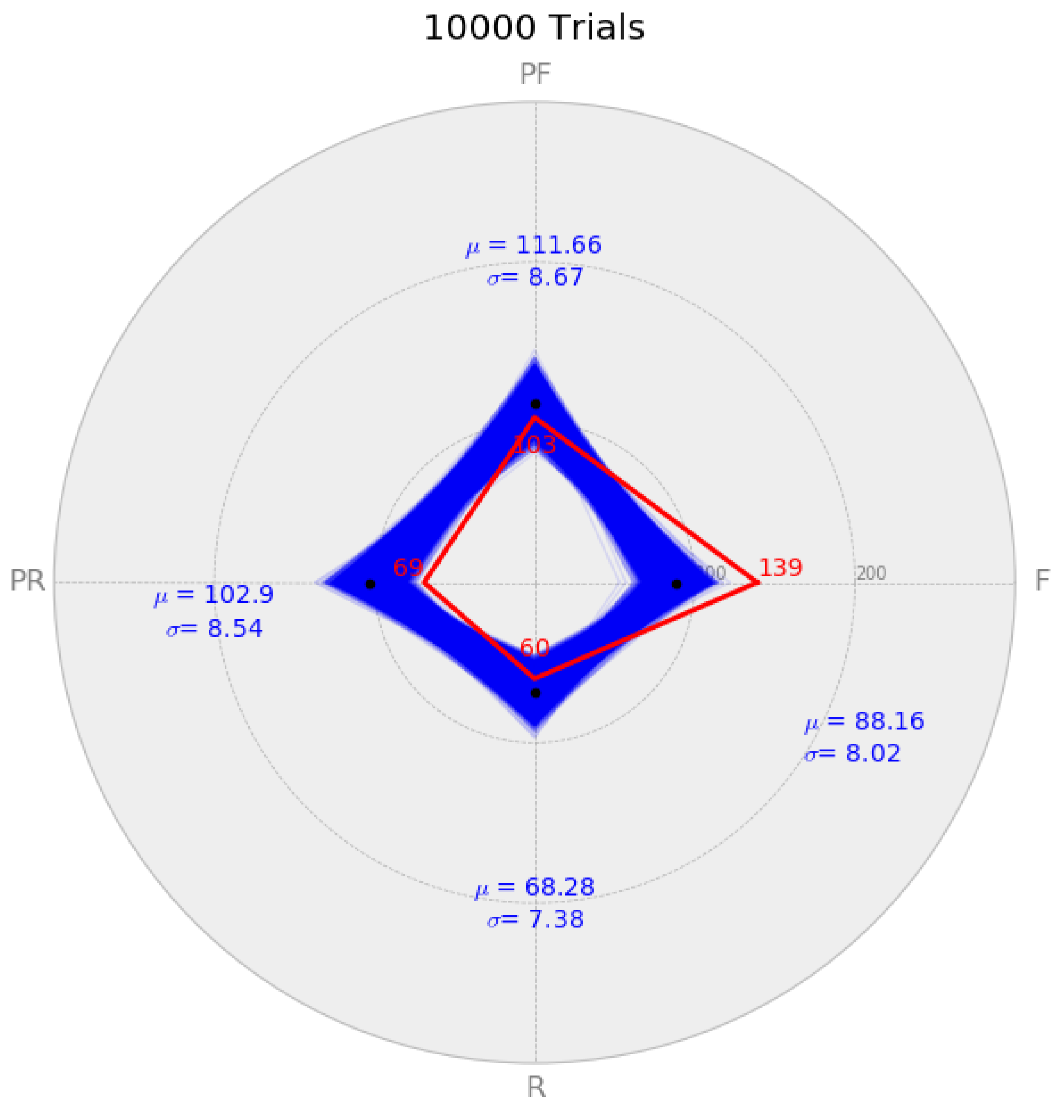

Figure 3.6: Radar plot showing the distribution of TGFs classified as falling ("F"), rising ("R"), plateau (falling) ("PF"), and plateau (rising) ("PR"). The red curve shows the distribution for the actual TGFs, while each blue curve shows one random trial (10,000 trials in total). Also labeled are the means and standard deviations for the random trials. The black dots mark the mean for each different classification.

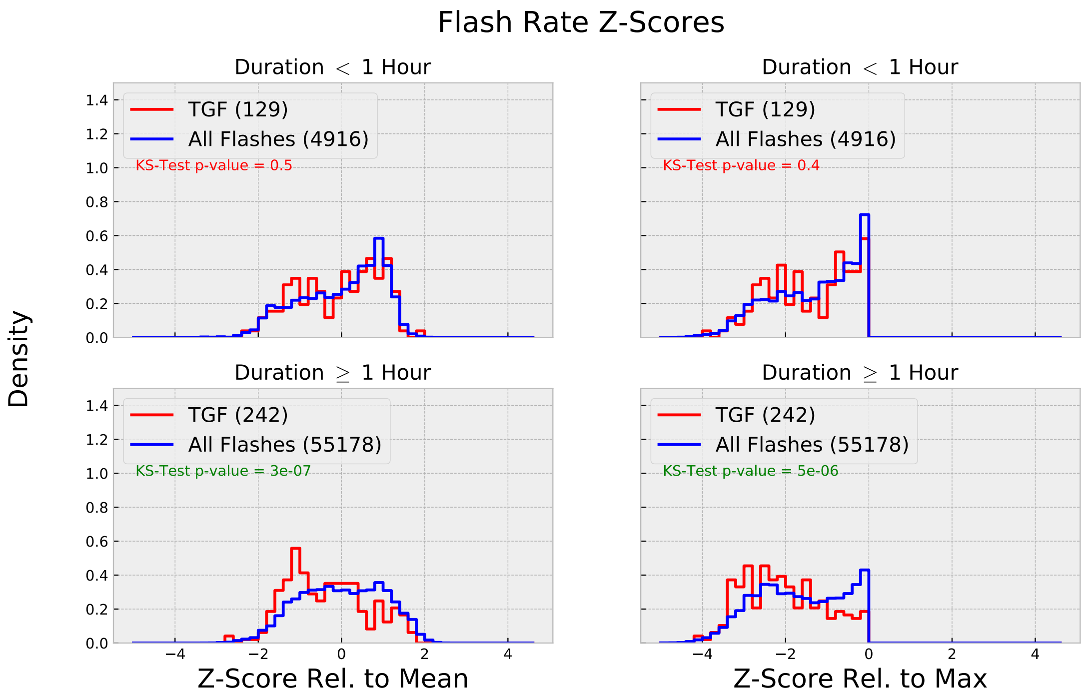

Figure 3.7: Histograms of flash rate Z-scores at the time of the TGF (red) and at randomly selected times (blue) relative to the mean flash rate (left column) and the maximum flash rate (right column) of the storms. The histograms are normalized such that the integral over the range is equal to one. The top row shows the distributions for storms that last less than one hour while the bottom row shows the distributions for longer storms. Also labeled are the p-values from the KS test to test the significance of the differences between the two distributions.

of all flashes to the left as seen. The results here imply that TGFs occur during periods when the amplitude of the flashes tend to be higher than the mean flash amplitude in the storms. This is consistent with the results of the flash rate analysis above, as well as the inverse relationship seen between flash rate and flash amplitude, which is often (but not always) the case (see Figure 3.4). The extremely low p-values produced by performing a KS test on the two distributions, show that the differences between the distributions are statistically significant. This indicates that perhaps the flash amplitude is more important for the production of a TGF than the flash rate of the storm at the time.

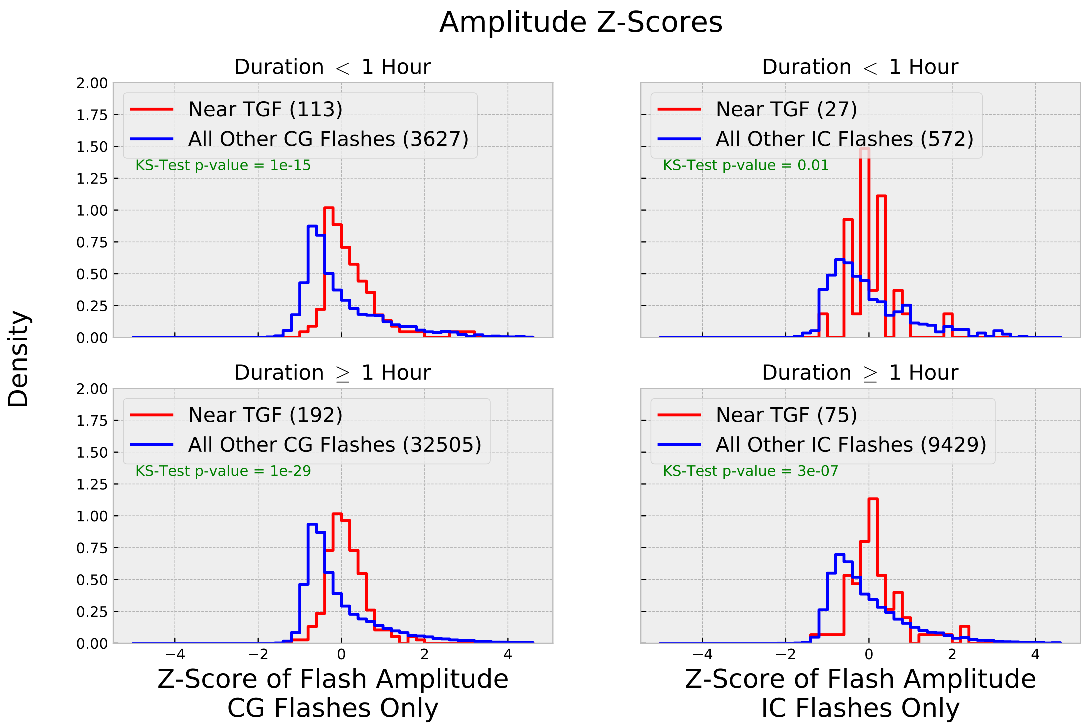

Figure 3.8: Z-score distributions for CG (left column) and IC (right column) flash amplitudes both near the TGF (red) and away from the TGF (blue). Each histogram is normalized such that the integral over the range is equal to one. Labeled are the number of flashes used to make up each of the curves. The top row shows the distributions for storms that last less than one hour while the bottom row shows the distributions for longer storms. Also labeled are the p-values from the KS test to test the significance of the differences between the two distributions.

Discussion

In this study, we have examined the relationship between storm phase and TGF production in 371 tracked thunderstorms. This sample represents a subset of the 1,169 total TGF storms available, and consists of well organized, isolated thunderstorms. The results of this study may not apply to other types of storms. We used 10-minute running sums of lightning flashes to define the lightning flash rates in the storms. We found that while TGFs tend to occur in all phases of storms with durations longer than an hour, they are more likely to occur during later phases and are less efficiently produced during the peak lightning activity of storms with shorter (<1 hour) durations. We further demonstrated that TGFs occur more often during falling stages of local peaks in lightning activity than any other stage. In addition, we demonstrated that TGFs tend to occur at lower flash rates than randomly selected flashes in storms. Finally, we showed that TGFs are more likely to occur when the lightning flash amplitudes are larger than normal. All of these results were tested using a 2-sample Kolmogorov-Smirnov test to quantify the significance.

The distinction between the analysis done in this work and other studies (e.g. Ursi *et al.* (2019) which found that most of the TGFs in their sample occurred within ± 5 minutes of the peak lightning activity) is that we are calculating the probability of the TGF occurring per lightning flash as opposed to the probability per second. During peak lightning flash rate periods, there are obviously many lightning flashes occurring, but the number of TGFs produced is not proportional to the total lightning flashes, meaning that TGFs are produced less efficiently during the peak flash rates than during other phases of the storms.

Several factors may make TGFs less likely during times of peak flash rate. For example, it is well established that lightning activity is strongly tied to updraft speed and content (Baker *et al.*, 1999; MacGorman *et al.*, 2010; Williams *et al.*, 2005; Yoshida *et al.*, 2017). Higher hydrometeor concentration, caused by higher updraft velocities, could make streamer initiation easier and result in lightning initiating repeatedly when large-scale electric fields are too low to support TGFs (Motley, 2006). Stronger convection at these times could also compress the distance between the main negative and upper positive charge centers, resulting in a lower overall potential, and therefore less chance of a TGF even regardless of the lightning initiation field; this scenario was proposed by Fabró *et al.* (2019) as an explanation for why TGFs were surprisingly under-produced in storms in central Africa. In addition, charge structure in storms is also known to become more disorganized as the storms intensify and mature (Marshall *et al.*, 1995; Stolzenburg *et al.*, 1998; Coleman *et al.*, 2003; Marshall *et al.*, 2009). However, there is evidence that the charge structure becomes more horizontally extensive in decay phases (Bruning *et al.*, 2007). This may imply that the environment of the decay phases of storms is more suitable for TGF production.

Our findings that TGFs occur later in shorter storms and the results showing that TGFs occur more often as the flash rate is falling are consistent with the results of Smith *et al.* (2010) which found that TGFs tend to occur when the flash rate is declining. The observation of an excess of TGFs occurring after the peak flash rate in shorter storms is possibly explained in two different manners. First, it is likely that a larger electric potential difference is required for TGF production as reflected in the RF model (Dwyer, 2003, 2008). It might be possible that this electric potential or field is more likely to be reached after the peak flash rate, as the storm has had longer to charge up and also because the flash rates are lower in later stages.

This explanation is contrasted by observations of Stolzenburg & Marshall (2008) in which balloon measurements show that electric potentials tend to be smaller later in thunderstorms. It has also been observed that the energy released per lightning flash tends to increase with time (Maggio *et al.*, 2009). Furthermore, TGFs are observed to occur in winter thunderstorms in Japan (Bowers *et al.*, 2017; Enoto *et al.*, 2017; Wada *et al.*, 2019, 2020) where the thunderstorms are shorter and therefore cannot reach the same electric potentials as taller thunderstorms (Rakov, 2003). Yet, these storms are still known for producing very powerful lightning flashes (Brook *et al.*, 1982; Holzworth *et al.*, 2019; Turman, 1977). It is therefore possible that energy transferred by a lightning flash is the driving factor in determining whether or not a TGF is produced. Namely, the more energy released by a lightning flash, the more likely it is to result in a TGF. This theory also fits well with the other results of this paper, namely the fact that TGFs tend to occur during low flash rate periods which are consequently usually (but not always) periods of high amplitude flashes.

Our other findings, namely that TGFs occur during periods of lower flash rates and that the flashes near the time of the TGF tend to be stronger than other flashes in the storm, is also consistent with the above explanations. TGFs have been shown to be associated with higher energy flashes in prior work (see Inan *et al.*, 1996, 2006; Stanley *et al.*, 2006; Connaughton *et al.*, 2013; Cummer *et al.*, 2014). The results presented here, however, are distinct in the fact that the TGF flash itself is excluded from the calculations. These results show that the non-TGF flashes near the time of the TGF, not just the TGF flash, are stronger than normal. This implies that there is a special relationship between storm phase and TGF production. Properties of the storm such as charge structure, electric field, flash rate, etc. likely play a role in the production of a TGF, and therefore it is ultimately the surroundings or conditions of the storm at the time of a given lightning flash that determine the production of a TGF. It is not just that any lightning flash can or will produce a TGF, but rather that the environment plays a large part in whether or not a TGF will actually be produced.

In summary, the results described in this paper show that TGFs tend to occur later in storms with shorter durations, TGFs tend to occur while the flash rate is lower than average and declining, and that TGFs tend to occur when the flash amplitudes are higher than average. These results apply for a subset of TGFs that occur in isolated, well organized storms (roughly 30% of the total number of observations available).

Acknowledgments

The authors wish to thank Maribeth Stolzenburg and Michael Briggs for their help, advice, and contributions in the interpretation of the results of this study. The authors wish to thank the World Wide Lightning Location Network (http://wwlln.net), a collaboration among over 50 universities and institutions, for providing the lightning location data used in this paper. We also acknowledge Earth Networks for providing the ENTLN data used in this study. Fermi TGF and WWLLN Association data can be found at the location: https://fermi.gsfc.nasa.gov/ssc/data/access/gbm/tgf/. Earth Networks data is freely available upon request (www.earthnetworks.com). This material is based upon work supported by the National Science Foundation under Grant No. 1935986.

Appendix: Additional Storm Information

This appendix provides additional information about the thunderstorms used for the analysis in the above sections. Because we used only lightning signature data to track the thunderstorms in this study, we do not have the ability to comment definitively on the types of thunderstorms in our sample. However, it might be possible to make inferments on a case-by-case judgement. The following information offers context on the storm locations and time of day, the storm durations and size, and the flash rates in the storms.

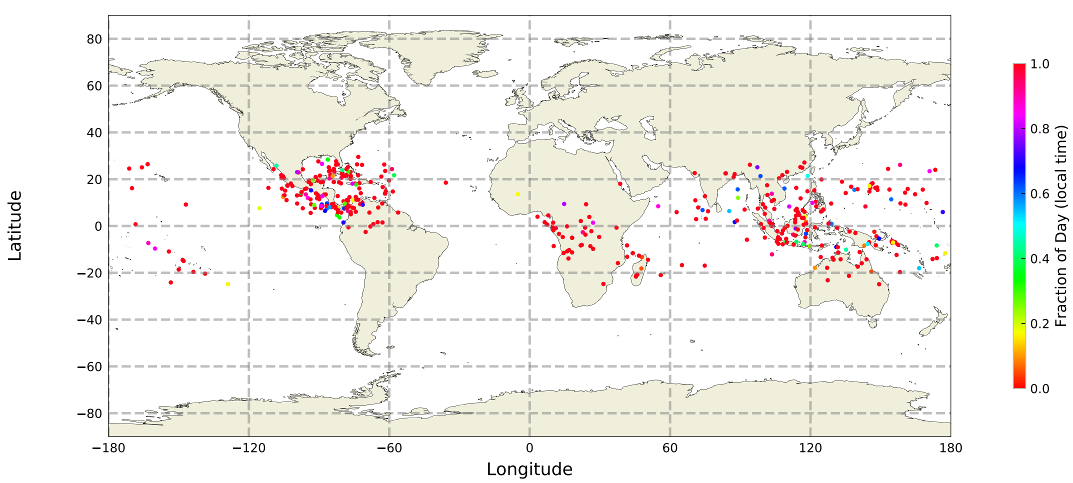

Figure 3.9: Map showing the location of each of the storms used in this study. Each point represents one storm and the color represents the local time of the storm in terms of the fraction of the day.

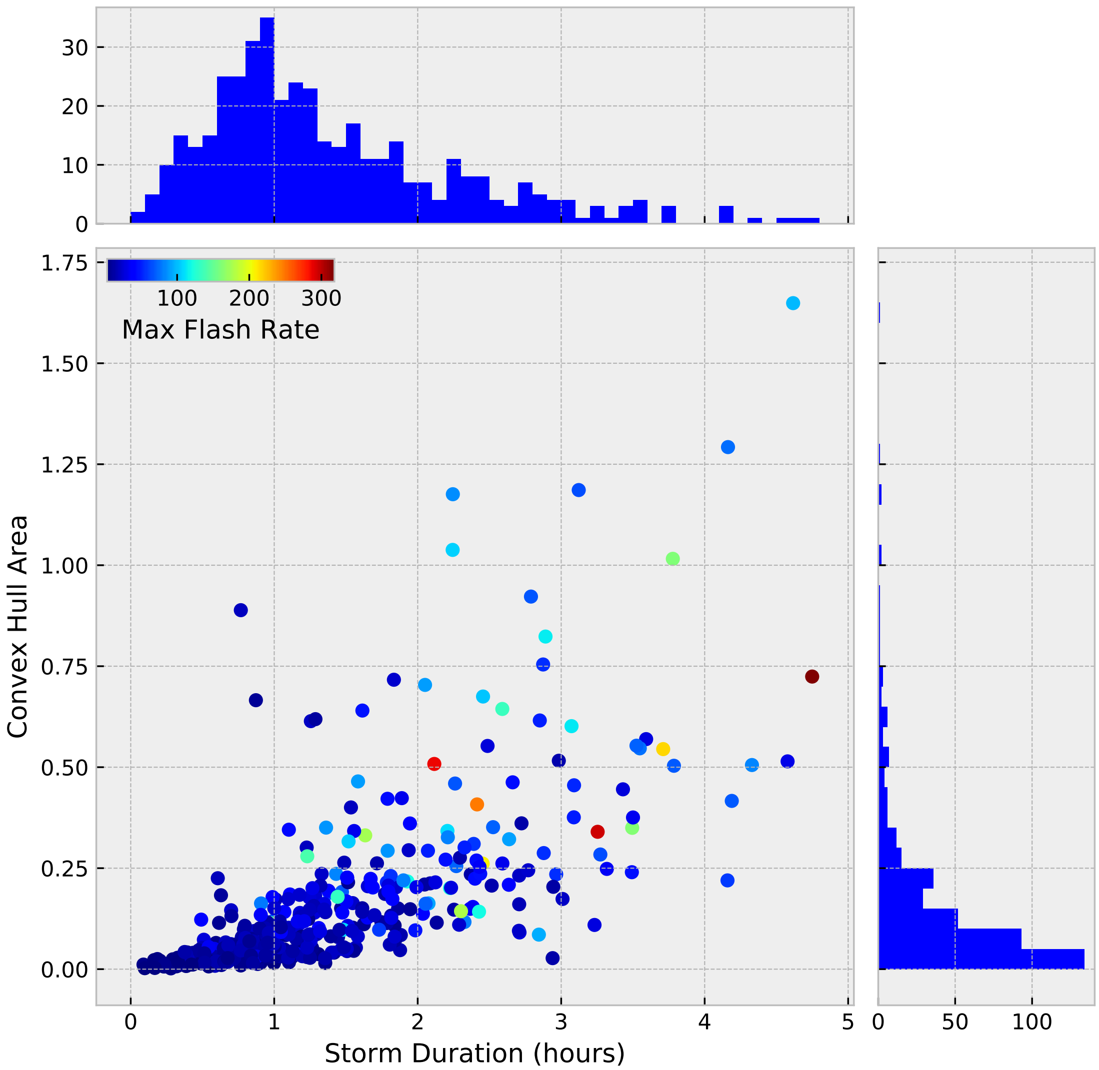

Figure 3.10: Scatter plot showing the relationship between the storm durations (in hours) and the size of the storms. The size of the storms was calculated by measuring the bounding area of the storm using a convex hull of the geolocations of lightning sferics. The individual points are colored based on the maximum flash rate in those storms. Also included are histograms of the size and durations.

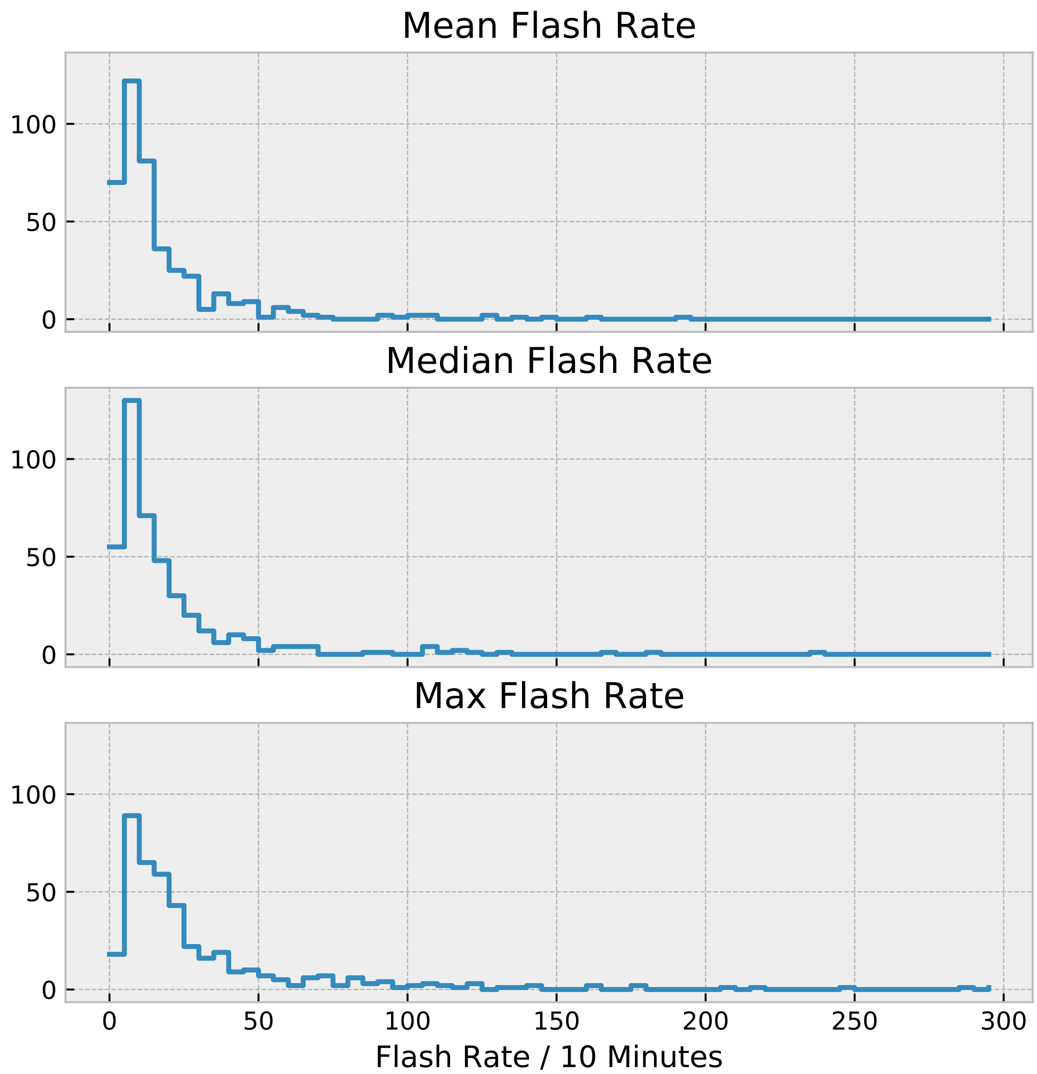

Figure 3.11: Distributions of the mean (top), median (middle), and maximum (bottom) flash rates for all the storms. The x-axis is in flashes per 10 minute window

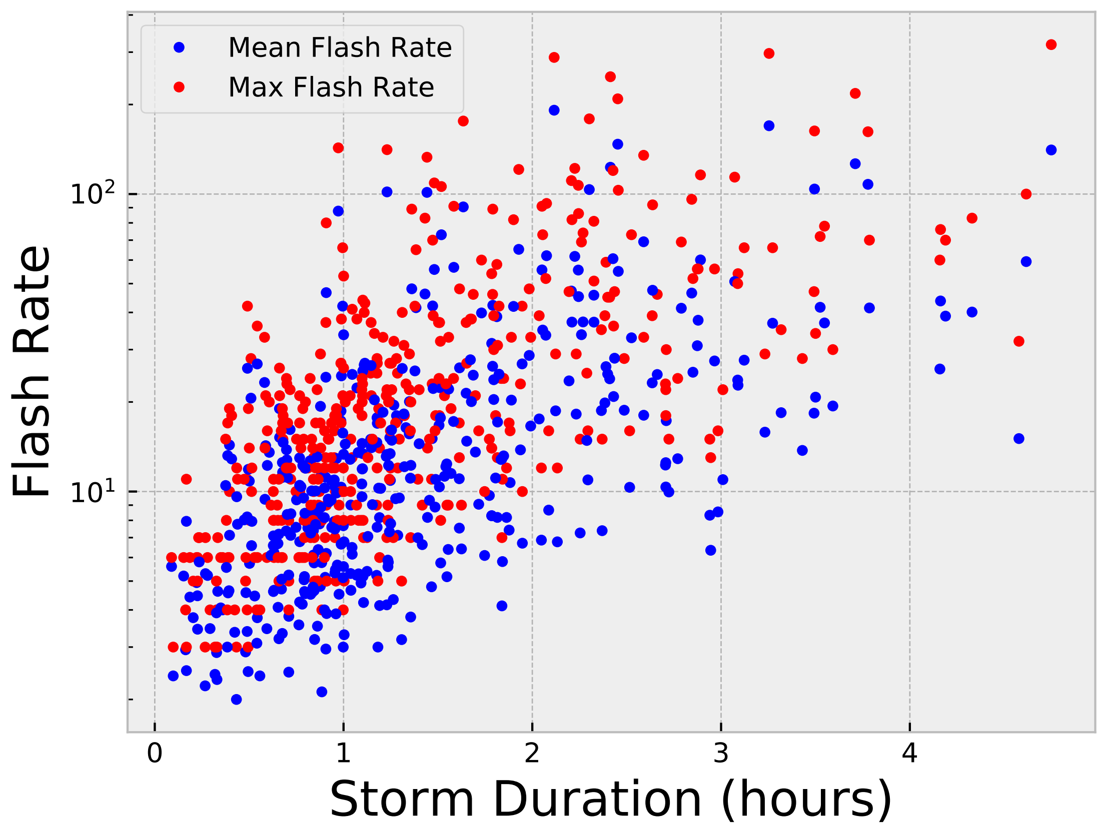

Figure 3.12: Relationship between the storm duration and the mean (blue) and maximum (red) flash rates in the storms.

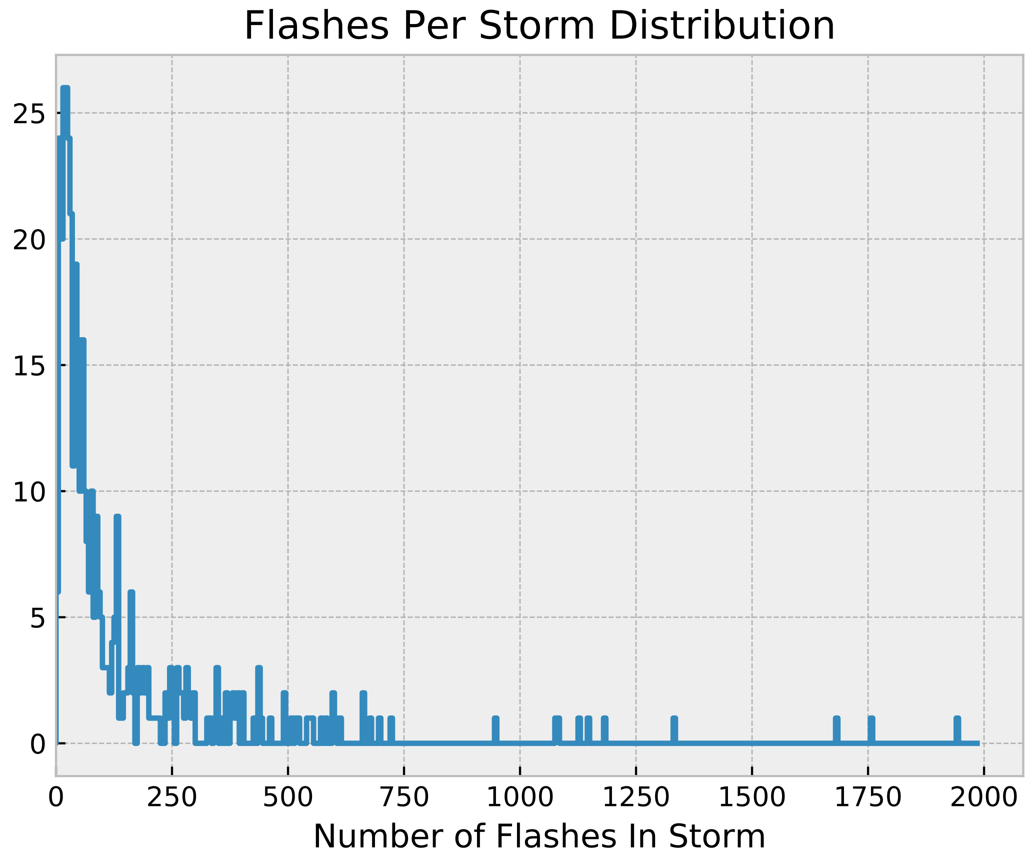

Figure 3.13: Distributions of the total number of flashes in the 418 tracked storms. Only 371 were used for this study.

DESCRIBING THE CHARACTERISTICS OF DELAYED SFERICS FOLLOWING TGFS

Contribution of Authors and Co-Authors

Manuscript in following chapter 4

Author: Reyann K. Larkey

Contributions: Defined TGF-associated flashes, correlated observations with existing datasets, and performed statistical analyses.

Co-Author: John G. Sample

Contributions: Mentor who helped to organize the paper and provided feedback on analysis types.

Co-Author: David M. Smith

Contributions: Made original observation and provided key guidance in analysis. Helped to define motivation and interpret results.

Manuscript Information

Reyann K. Larkey, John G. Sample, David M. Smith

Status of Manuscript:
__X__ Prepared for submission to a peer-reviewed journal
_____ Officially submitted to a peer-reviewed journal
_____ Accepted by a peer-reviewed journal
_____ Published in a peer-reviewed journal

Abstract

We detail observations of excess delayed sferics occurring after TGFs observed by the Fermi Gamma Ray Burst Monitor (GBM). Lightning sferic data from both World Wide Lightning Location Network (WWLLN) and Earth Networks Total Lightning Network (ENTLN) data reveal two anomalous peaks in the distribution of time delays between sferics within TGF-associated flashes and the TGF observations themselves. The first peak, spanning roughly 20-60ms after the TGFs, has not been studied in detail prior to this work. This first peak appears more prominently in the ENTLN data and is likely observable due to ENTLN's higher detection efficiency for intra-cloud strokes. The second peak, spanning approximately 200-700ms after the TGFs, has been observed before when examining TGF data from other spacecraft and is easily seen in stacking analyses (Smith *et al.*, 2016; Lindanger *et al.*, 2021). The present work, however, represents the first analysis of the stroke type and amplitudes of the constituent sferics and shows that the second feature is composed of more powerful strokes than the first. Both are composed of sferics relatively weaker than the full dataset. Further questions remain about the lightning processes that create these delayed sferics, and will require additional data and methods to fully resolve these questions.

Introduction

Extremely intense bursts of gamma-ray radiation originating from lightning in some thunderstorms, known as Terrestrial Gamma-Ray Flashes (TGFs), have been the subject of vigorous research since their discovery in 1994 (Fishman *et al.*, 1994). Since the initial observations of TGFs by the Burst and Transient Source Experiment (BATSE) onboard the Compton Gamma-Ray Observatory (CGRO), there have been thousands of TGF observations by spacecraft such as the Reuven Ramaty High Energy Solar Spectroscopic

Imager (RHESSI), the Astro rivelatore Gamma a Immagini Leggero (AGILE), the Gamma-Ray Burst Monitor (GBM) onboard the Fermi Gamma-Ray Space Telescope, and the Atmosphere-Space Interactions Monitor (ASIM) (Smith *et al.*, 2005; Briggs *et al.*, 2010; Marisaldi *et al.*, 2014; Østgaard *et al.*, 2019). In addition to spacecraft observations, researchers have also recorded ground and aircraft measurements of TGFs (Bowers *et al.*, 2017, 2018; Dwyer *et al.*, 2004, 2012a; Enoto *et al.*, 2017; Hare *et al.*, 2016; Smith *et al.*, 2011). Dwyer *et al.* (2010) showed that TGFs could pose a significant risk to anyone or anything directly exposed (as in an aircraft, for example).

TGF production is thought to be the result of Relativistic Runaway Electron Avalanches (RREAs) (Gurevich *et al.*, 1992). The RREA mechanism allows for a runaway electron (i.e. an electron that is gaining energy faster than it is losing it), under the influence of an external electric field, to collide with other electrons, forcing some of them into the runaway regime as well. Those new runaway electrons can then go on to collide with further electrons, continuing the cycle and resulting in a large number of high-energy electrons. Through Bremsstrahlung interactions with air, these avalanches can produce significant high-energy radiation. However, RREA alone is insufficient for explaining the observed luminosity of TGFs due to avalanche size and seed particle population constraints (Dwyer, 2008). Nonetheless, modifications to the RREA mechanism, such as Relativistic Feedback (Dwyer, 2003) and lightning leader tip models (Carlson *et al.*, 2010; Celestin & Pasko, 2011; Moss *et al.*, 2006) have been proposed to help bridge this gap, and are capable of explaining TGF characteristics.

Even with the considerable number of TGF observations now available, what exactly causes a TGF is relatively poorly understood. TGFs are not produced by every lightning flash (or even every thunderstorm) and circumstances that lead one lightning flash to produce a TGF, but not others, remain obscured. Studies such as Larkey *et al.* (2019, 2021); Fabró *et al.* (2019); Morales Rodriguez *et al.* (2021) have examined the large-scale characteristics of TGF-producing thunderstorms. These studies have found a variety of features regarding TGF-associated storms and flashes. Specifically, TGFs occur after abnormally longer charging times, when flash amplitudes are higher than usual, and in storms that are taller and more intense. However, a full understanding of what makes a TGF-associated lightning flash different from a more "typical" flash remains not well characterized. As mentioned above, TGFs are known to be fluent enough to pose a serious risk to equipment or persons exposed, and given the frequency of air travel and the projected increase in lightning flash rates due to climate change (Romps *et al.*, 2014), understanding the environment most likely to produce TGFs is vitally important.

This work expands upon an observation, originally made by Smith *et al.* (2016), showing an apparent excess of lightning radio atmospherics ("sferics") occurring a few hundred milliseconds after TGF production. The original work observed this excess of delayed sferics using RHESSI TGF observations and lightning data from the World Wide Lightning Location Network (WWLLN). Other researchers have also examined the same excess of delayed sferics using optical data from the ASIM and photon data from the Fermi-GBM spacecraft (Lindanger *et al.*, 2021). Their work finds statistical evidence that the observed TGFs were produced early on in flash development. However, aside from these mentioned works, there has been very little research on the types of lightning flashes that contribute to this excess. To address this uncertainty, this work uses Fermi-GBM along with WWLLN and Earth Networks Total Lightning Location Network (ENTLN) data to examine this observed excess in further detail.

Data And Methods

For this work, we use WWLLN and ENTLN sferic data in conjunction with TGF observations from the Fermi-GBM spacecraft. The Fermi catalog contains 4,139 TGFs, however, only 3,375 have both ENTLN and WWLLN data accompanying them. For each of these TGFs, the lightning sferic data (within 800km of the Fermi footpoint) is merged chronologically and then constrained to a 10-minute window on either side of the TGF occurrence time. The TGF-associated lightning sferic is then identified based on a calculated association probability using a similar method as those in Connaughton *et al.* (2013) and Roberts *et al.* (2018). Specifically, a sferic is said to be associated with the TGF if it occurs within +/- 3.5ms of the TGF. However, in an effort to avoid chance associations, a further association probability is determined by measuring how often sferics fall within 3.5ms of 1,200 control times spaced in 1s intervals for the 10-minute spans both before and after the TGF. Only those events with a sferic association probability greater than or equal to 0.9 are used in this study. A total of 1,663 TGFs meet these criteria and are used for the following analyses. For each TGF, all lightning sferics within +/- 10s of the TGF are then grouped into flashes using a Kernel Density Estimation (KDE) algorithm (see Larkey et al. (2019, 2021) for details) and a 20km distance threshold.

Delayed Sferics Observations

For each TGF associated lightning flash, we measure the time delays between the constituent sferics in the flash and the time reported by the Fermi satellite. We then separate the time delays prior to the TGF from the time delays after the TGF to be taken into account independently. Figure 4.1 depicts how these are measured within a single TGF-associated flash.

The time delays are measured for all 1,663 TGFs in our data sample and the histograms of these are shown in Figure 4.2 below. Note that the histograms presented here are divided by bin width to account for the differences in bin size across the logarithmic range of timescales. Immediately, there are striking differences between the histograms of the post-TGF time delays and the pre-TGF time delays. Most notably there are two apparent excesses in the post-TGF curve: one that spans from approximately 20-60ms after the TGF

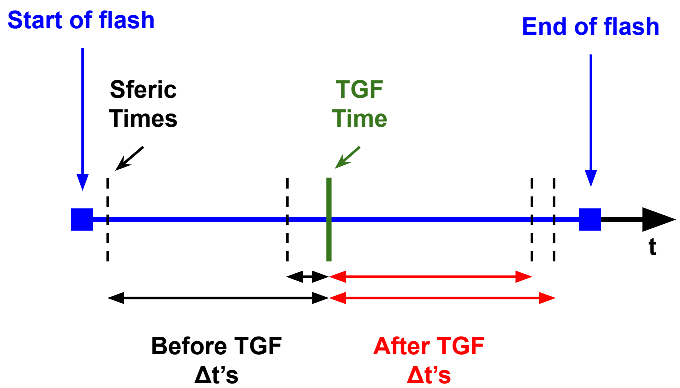

Figure 4.1: Diagram showing how the various time delays are taken relative to the TGF time in a TGF-Associated lightning flash.

and another that spans around 200-700ms afterward. These specific time ranges were selected based on similar time ranges seen in prior studies (Smith *et al.*, 2016). These will be referred to, throughout, as "Feature 1" and "Feature 2", respectively. Of the 1,663 TGFs that contribute to this dataset, 126 of them have at least one accompanying Feature 1 sferic, 445 have at least one accompanying Feature 2 sferic, and 71 have both types of sferics.

To test if these features are significant, or even TGF related, the same process is repeated for randomly selected flashes from the same 20-minute windows (centered on the TGF). From a selected lightning flash (defined the same as above), a random constituent lightning sferic is chosen and its time of occurrence is substituted for the "TGF time" in Figure 4.1. The appropriate time delays can then be measured and a similar histogram to that in Figure 4.2 begins to take shape after many trials. Figure 4.3 shows how those histograms change when using randomly selected flashes. The curves produced using randomly selected flashes show no similar features as those in Figure 4.2, implying that those features are somehow TGF-specific. It is unclear exactly what properties of TGFs or TGF-associated lightning flashes make these delayed sferics more likely in conjunction with TGFs than other lightning flashes. To further investigate these features, however, we have provided analysis on the stroke type and current amplitude of the constituent sferics. These analyses are detailed in the following sections.

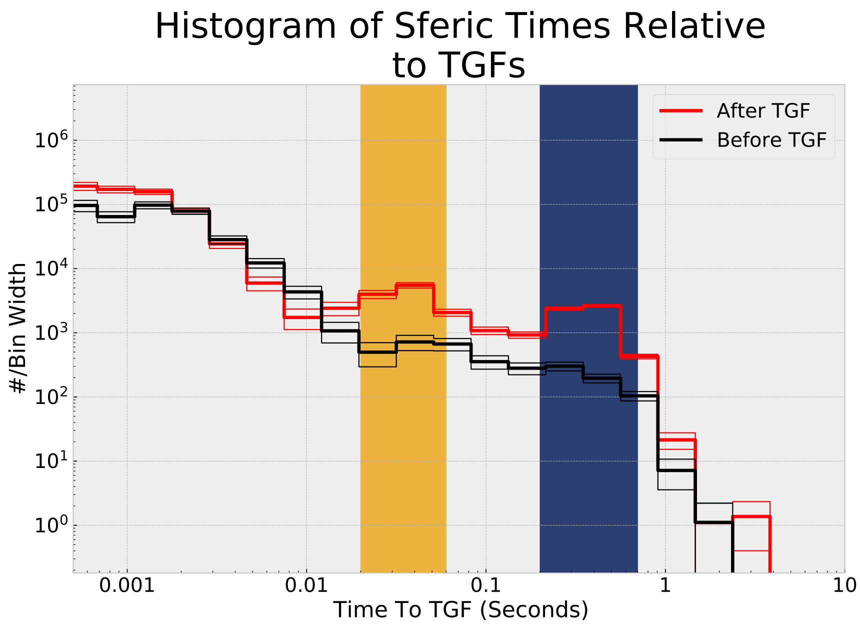

Figure 4.2: Histograms (divided by bin width) showing times relative to the TGF (absolute value) separately for pre-TGF (black) and post-TGF (red) sferics (N=1663 TGFs). The thin red and black lines represent $\sqrt{N}$ error bars. Both the x and y-axes are in log-scale. The yellow region represents 20-60ms relative to the TGF time and highlights "Feature 1", and the blue region spans 200-700ms and captures "Feature 2".

Figure 4.4 shows the global distribution of the events composing Figure 4.2 for reference. The sferics that make up both Features 1 and 2 are present in the same regions as all other lightning flashes associated with the TGFs in the sample. While there are no obvious biases in the global distribution that could indicate a reason for the existence of these two features, closer inspection reveals that there is a preference for both Features 1 and 2 events to occur

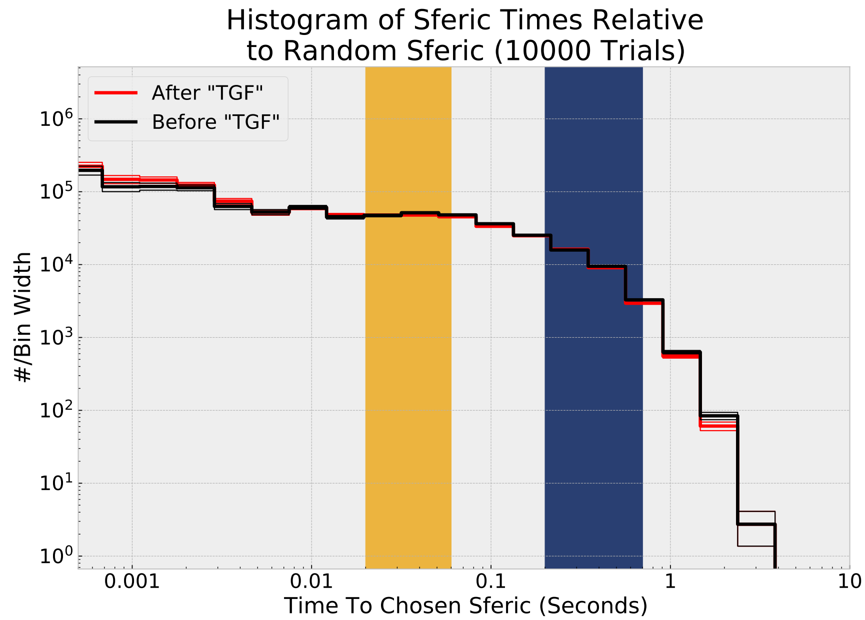

Figure 4.3: Histograms (divided by bin width) showing times relative to randomly chosen lightning sferics (N=10,000). Times before the faux "TGF" are shown in black and the times after are shown in red. The thin red and black lines represent $\sqrt{N}$ error bars. Both the x and y-axes are in log-scale. The yellow and blue regions show the same locations of Features 1 and 2 as seen in Figure 4.2.

near the Americas. Figure 4.5 shows the Cumulative Distribution Functions (CDFs) of the lightning sferics in the three above categories. This figure shows that a higher percentage of Features 1 and 2 events (as compared to the total distribution) occur in the western hemisphere and near the Americas. This, however, could be the result of higher network sensitivity to lower-amplitude sferics in this geographical region (Hutchins *et al.*, 2012; Lapierre *et al.*, 2019; Rudlosky, 2014). Further examination of the sferic amplitudes is detailed in the following section.

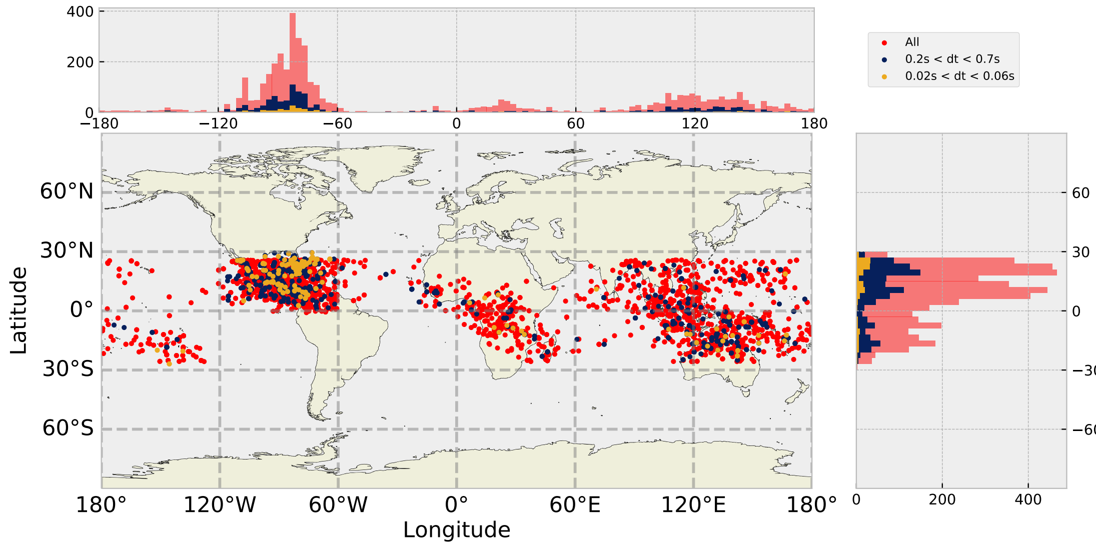

Figure 4.4: Map showing the location of each of the storms used in this study. The red points mark the location of every point in the dataset, while the yellow and blue points represent those sferics that compose Features 1 and 2 respectively. Also shown are histograms of the longitudes and latitudes.

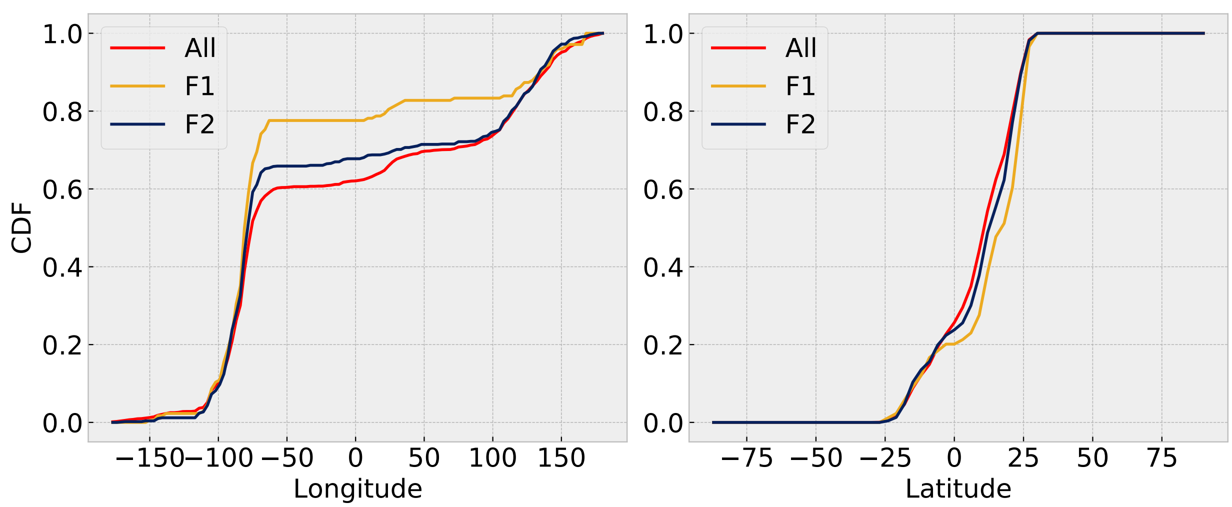

Figure 4.5: (left) CDF of lightning sferics as a function of Longitude. (right) CDF of lightning sferics as a function of Latitude. Features 1 and 2 are represented as "F1" and "F2" respectively. The red curve labeled "All" represents the full dataset of sferics.

Characteristics of Sferics in Features 1 and 2

Stroke Type Analysis

One particular avenue toward understanding the lightning that produces TGFs, and the delayed excesses shown above, is to examine the kind of lightning strokes involved. A specific motivation for this type of analysis is that Feature 1 becomes much less obvious when the dataset is broken into WWLLN or ENTLN data alone. Figure 4.6 shows how the above histograms change when this distinction is made, and Feature 1 is nearly absent in the WWLLN data. Given that this feature did not appear prominently in the Smith *et al.* (2016) work (which used only WWLLN data), this indicates that the additional ENTLN data included in this work is likely the source of this first feature–not any new analysis technique.

The WWLLN data available for this study does not include stroke type or stroke amplitude data. Because of this, all discussions involving these attributes will rely on ENTLN data alone. Figure 4.7 shows the percentage of the sferics in each bin that are identified as IC strokes by ENTLN; it is strongly peaked in the same region as Feature 1, indicating that the addition of Feature 1 is predominately due to ENTLN's higher sensitivity to IC strokes than WWLLN (Bitzer *et al.*, 2016). While this helps to explain why this first feature is not as prominent in the WWLLN data, it still leaves questions about the lightning processes that are producing this excess of sferics in association with TGFs. However, because ENTLN automatically labels all strokes with amplitudes greater than 30kA as CG strokes, further investigation into the stroke amplitude is necessary to better understand the differences between these two features.

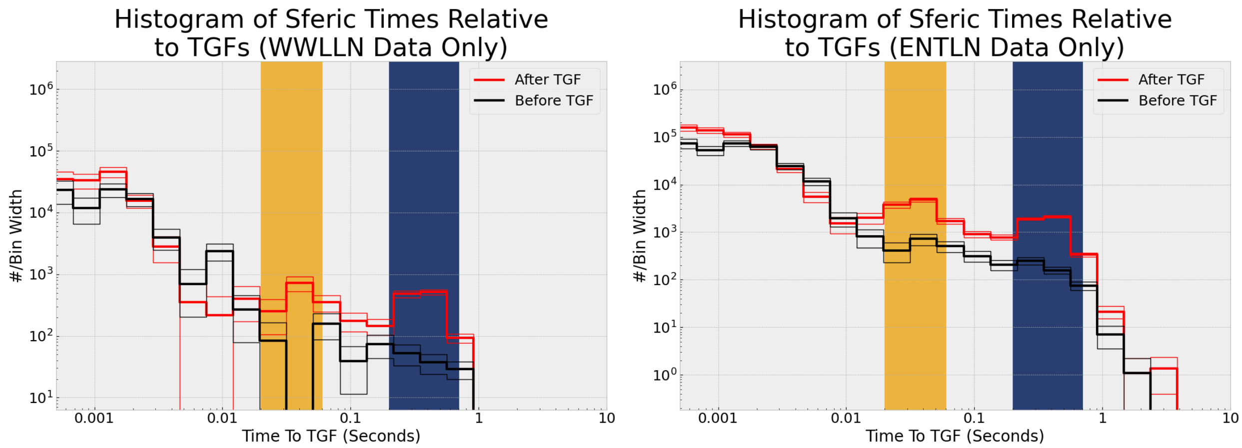

Figure 4.6: (Left) Histogram showing time delays relative to TGF observation using WWLLN sferics only. (Right) Histograms showing time delays using ENTLN data only. The thin red and black lines represent $\sqrt{N}$ error bars in both cases. All histograms are normalized by bin width.

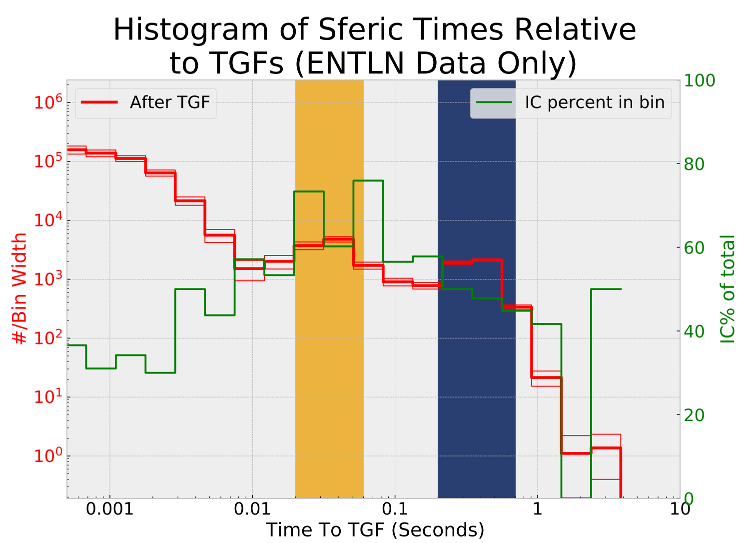

Figure 4.7: (red) Histogram (normalized by bin width) showing sferic delays after the TGFs. (green) The percent of sferics in each bin that are labeled as IC sferics by ENTLN. The thin red lines represent $\sqrt{N}$ error bars. The yellow and blue regions show the same locations of Features 1 and 2 as seen in Figure 4.2.

Stroke Amplitude Analysis

Using ENTLN's amplitude estimates, it is possible to examine how the time delays between sferics and TGFs relate to the sferic currents. Figure 4.8 shows the same histogram as above (just the delays after the TGF), as well as a scatter plot of time delay versus the absolute value of sferic amplitude in kiloamperes. The x-axis only extends down to 3.5ms as sferics occurring before those times are assumed to be associated with the TGF itself. It would be inappropriate to consider the specific TGF-associated sferics in this analysis as they are known to have higher than usual amplitudes as they are likely directly related to the currents produced by the TGF itself (Connaughton *et al.*, 2013; Rodger *et al.*, 2006; Lyu *et al.*, 2016; Mailyan *et al.*, 2018, 2020; Pu *et al.*, 2019).

It is clear from this plot that the sferics spanning the region of Feature 2 have higher amplitudes, in general, than the other regions. These higher-amplitude sferics are predominantly CG strokes as well; however, as mentioned above, ENTLN automatically labels all strokes with amplitudes larger than 30kA as CG strokes, thus some of these *could* be IC strokes. Regardless, there do not appear to be many high amplitude sferics in Feature 1 compared to the sferics in other regions of interest. This is consistent with the results in Figure 4.7, which shows a larger proportion of IC strokes (which are known to be less powerful) in this first feature.

Figure 4.9 further demonstrates the differences in stroke amplitude for the sferics in the two features. The scatter plot on the left shows the same stroke amplitude data as in Figure 4.8 (although zoomed in to more easily see lower amplitude values), while the three histograms to the right show the distributions of stroke amplitude for the two features separately as well as the stroke amplitudes for all sferics within 10s of the TGFs in the dataset. Also, labeled in this figure are the descriptive statistics of mean, median, standard deviation, and skew (the Fisher-Pearson coefficient) of the distributions.

To test the similarity of the distributions, a two-sample Kolmogorov-Smirnov test is

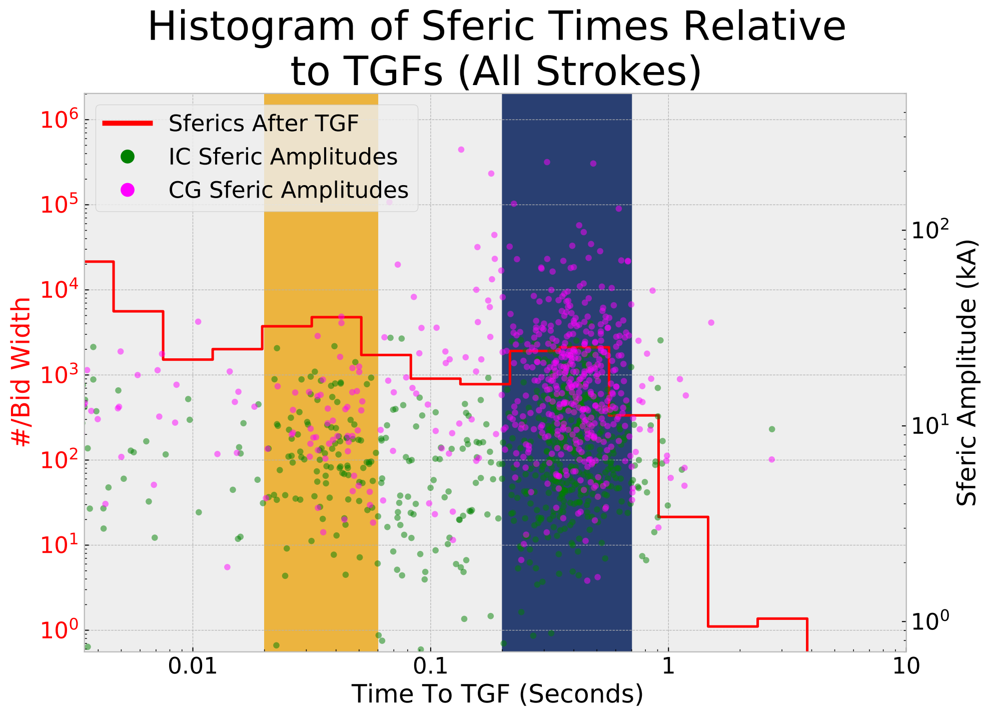

Figure 4.8: (red) Histogram showing stroke times after the TGF in red. The green scatter plot shows how the contributing IC sferics sferics are distributed based on their amplitude. The magenta scatter plot shows how the contributing CG sferics sferics are distributed based on their amplitude. The data in this plot uses ENTLN data only.

performed between the two subset distributions as well as to the distribution of stroke amplitudes of the full dataset ($\pm 10s$ of the TGF). The p-values for these tests are listed in Table 4.1. These tests indicate that the three distributions are statistically, significantly different from each other. Additionally, the p-value for the KS test between F2 and the full distribution shows that these distributions are also significantly different. Figure 4.10 shows the CDFs for the distributions in Figure 4.9 and illustrates how both both F1 and F2 are made up of relatively smaller amplitude strokes, with this effect being more significant for F1.

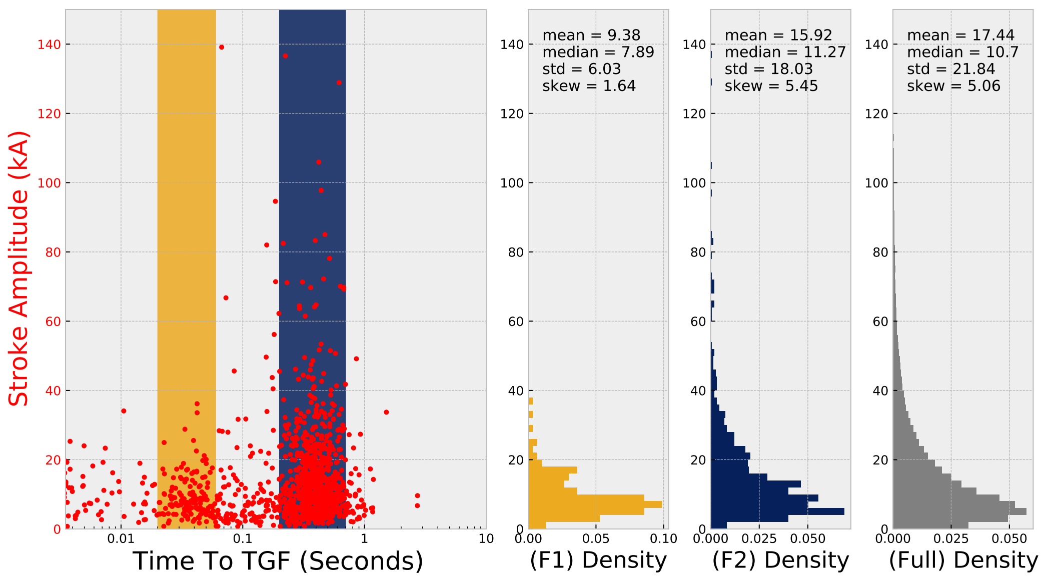

Figure 4.9: (left) Scatter plot showing stroke times after the TGF versus the stroke current amplitude in kiloamperes. (middle-left) histogram showing the distribution of stroke amplitudes in the region of Feature 1. (middle-right) histogram showing the distribution of stroke amplitudes in the region of Feature 2. (right) histogram showing the distribution of stroke amplitudes for all sferics within $\pm 10s$ of the TGFs in the dataset. Labeled are the mean, median, standard deviation, and skew for each distribution.

Distributions	**KS-test p-value**
F1 & F2	1.85×10^{-7}
F1 & Full	7.58×10^{-8}
F2 & Full	5.0×10^{-4}

Table 4.1: KS-test p-values for the different stroke-amplitude distributions shown in Figure 4.9

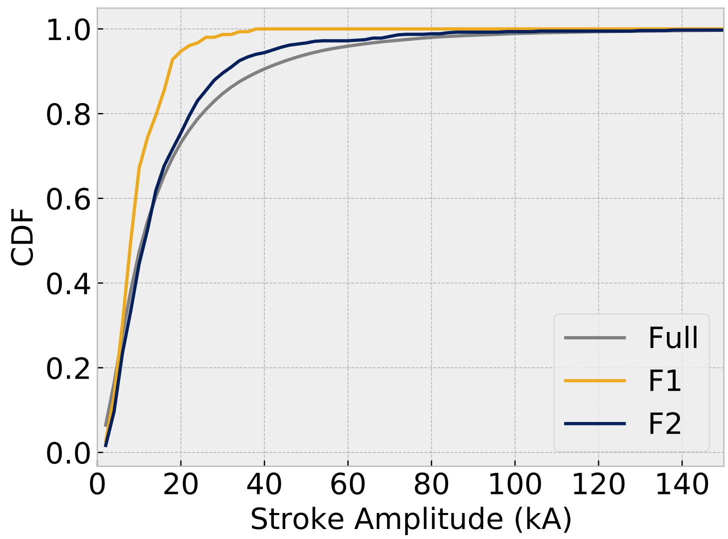

Figure 4.10: CDF of stroke amplitude for the three distributions shown in Figure 4.9

Summary

The work detailed here presents an initial analysis of stroke types and amplitudes of sferics in flashes associated with TGFs. We show that there exist two excesses of sferics occurring 20-60ms and 200-700ms after TGFs, contributing to what we have defined as "Features 1 and 2" respectively. While other studies have examined the sferics in Feature 2, the work here represents the first detailed analysis of the delayed sferics within 20-60ms after observed TGFs. We have also provided evidence that these same excesses do not exist for other non-TGF associated lightning flashes. This implies the existence of something TGF-specific in the development of the lightning flash as a whole.

We provide evidence that the emergence of Feature 1 is likely due to a higher detection efficiency for IC flashes in the ENTLN data, and we see that there are fewer high-amplitude CG flashes contributing to this first excess. The later excess is composed of a higher fraction of labeled CG flashes with higher stroke amplitudes. There is potentially some uncertainty as to the type of strokes that compose these features, however, as ENLTN labels all strokes with amplitudes larger than 30kA as CG strokes (Note some strokes with amplitudes <30kA are still labeled as CG strokes). Regardless, this does not affect the stroke amplitude analysis showing that Feature 1 is composed of smaller amplitude sferics than Feature 2. We have shown that the sferics in Feature 2 are statistically composed of higher-amplitude sferics than those in Feature 1; however, both are composed of lower-amplitude strokes than the whole dataset of strokes within $\pm 10s$ of the TGFs.

Unanswered questions remain about the specific ways these lightning flashes relate to TGF-production and how they may differ from "typical" lightning flashes. For example, are these flashes that begin as IC flashes and develop into CG flashes later with the TGF being produced at some point in that unique development? Do the delayed sferics represent a special kind of discharge that requires a TGF to precondition the cloud? One possible explanation for why both F1 and F2 are composed of relatively smaller amplitude strokes (compared to the full dataset) is that there is less built-up charge being discharged in these strokes after the TGF initiation, which hints toward a complex lightning process taking place. For example, one potential scenario is that after the TGF is initiated along with its associated sferic, it is followed (in some cases) by a weaker intermediate flash (which is most readily detectable in regions where networks are very sensitive), and occasionally this series of events if followed by a somewhat stronger stroke a few hundred milliseconds later. Perhaps these are extended IC discharges that discharge different "pockets" of charge in their clouds. Or maybe these sferic patterns are the result of more complex CG-IC hybrid flashes that occur on the characteristic timescales seen in the data here.

The exact mechanisms that produce these delayed series of sferics are currently unknown, and unfortunately, the data available for this study is not adequate for resolving these mechanisms in a sufficient manner. Future work using simultaneous observations by Fermi-GBM, the Geostationary Lightning Mapper (GLM), ENTLN, and other radio sensors would be able to examine the precise nature of TGFs and their associated lightning flashes and thunderstorms. For example, optical data along with detailed radio waveforms could reveal more about the lightning structure and characteristics, which would provide a much clearer picture of the physical processes taking place.

CONCLUSION

This dissertation details research on the relationships between various properties of thunderstorms and TGF production. Chapter 2 presented observations of longer charging intervals between TGFs and the lightning flashes occurring immediately prior. The results of this study imply that perhaps TGFs require stronger than usual lightning flashes and possibly stronger than normal electric fields. This offers at least one way in which TGF-associated lightning flashes differ from lightning flashes not associated with TGFs.

Chapter 3 focused on how TGF production is dependent on storm electrification characteristics. This study found that TGFs are more likely to be produced later in storm cell evolution, when flash rates are falling, and when flash current amplitudes are larger than average. The conclusions of this study, in addition to those in Chapter 2, imply that there is something about the thunderstorm electrical environment that makes a TGF more probable. These studies have advanced toward answering the question "why do some lightning flashes produce TGFs and other do not?". Namely, that not just *any* lightning flash is capable of producing a TGF, but that environment plays a critical role in determining if a TGF is produced.

Lastly, Chapter 4 is a preliminary study into the observed excesses of delayed lightning sferics that occur following TGFs but not other flashes. This study details the first in-depth examination of the TGF-specific lightning flashes that contribute to these excesses in terms of the stroke type and stroke amplitude. The results of this study show that the observed delayed lightning sferics demonstrate unique characteristics and could be indicative of a more complex lightning process that is not discernible with the data available for this work.

As a whole, the research laid out in this dissertation explores the two main ways in which TGF-producing lightning flashes could be different from typical lightning flashes. Namely, the possibilities that there is either something specific about the thunderstorm environment or that there is something special about the lightning flash itself (or a combination of both) that makes TGF production more likely. The first two studies detail how TGF production is related to the thunderstorm environment, and the last study examines the complex TGF-specific lightning processes taking place during these events. The conclusions of these studies illustrate the definitive differences between "typical" lightning flashes and TGF associated flashes, both in terms of their originating storm characteristics as well as the lightning processes that are associated with them.

Future Work

Continuation of Precise Timing Analysis

There remain unanswered questions about the delayed excess of sferics detailed in Chapter 4. The analyses in that chapter provide descriptive statistics of these sferics, however, it is unclear what the underlying cause of those delayed sferics is. There are multiple paths forward towards understanding the processes occurring within these lightning flashes, and which might provide more insight into TGF production itself.

The first major advancement would be the use of the enhanced Fermi-GBM TGF catalog that is currently being developed by the Fermi team at the University of Alabama Huntsville and the Marshall Space Flight Center. While this updated database is not yet published, it is in progress and an expanded catalog could provide more insight into TGF production and additional data may reveal further features or relationships that are not presently apparent. Additionally, incorporating Fermi photon data to do a summed analysis looking for any delayed features coinciding with the excess sferics will offer more insight into these anomalies. This is something that is most readily achievable using the capabilities of the Fermi satellite instruments.

Another approach for building on these observations would be an examination of waveform data associated with some of these sferics. Both ENTLN and Duke University maintain sferic networks that are able to examine lightning sferic waveforms and a collaboration between our research groups is currently in place to study these. Finally, observing these lightning flashes in the optical band by utilizing data from the Geostationary Lightning Mapper (GLM) on the GOES-R spacecraft may provide definitive evidence into the kinds of lightning flashes that contribute to the features discussed here, that have not been examined before. Lindanger *et al.* (2021) observed different pre and post-TGF behaviour in the optical data than what we expect to see based on our results using radio signals (detailed in Chapter 4). Because of this, closer inspection comparing the radio sferics and optical data is warranted and may yield more information about the associated flashes.

Using these data sources, it would be possible to further understand the lightning/TGF relationship in terms of timing, waveform characteristics, and brightness. These types of statistical analyses on such a broad scale are not something that has been done before, yet could be key to the fundamental understanding of the causal nature of TGFs.

LAFTR

MSU, in collaboration with the University of California, Santa Cruz (UCSC), has developed an instrument called the Light and Fast TGF Recorder (LAFTR), a NASA-Undergraduate Student Instrumentation Project. LAFTR was originally designed as a balloon borne gamma-ray detector with a goal of making up-close, detailed observations of TGFs. Because most observations of TGFs are made from space, they often see only a few tens of photons; however, the goal of these payloads is to be much closer to the TGF source. As such, an up-close measurements would be less affected by atmospheric attenuation and thus provide a more detailed observation of the TGFs.

LAFTR is capable of detecting high-energy gamma rays at a maximum count rate of more than 5 million counts per second and time tagging photons to within 80ns. Observations of TGFs, by the other instruments mentioned throughout this work, do not have high enough

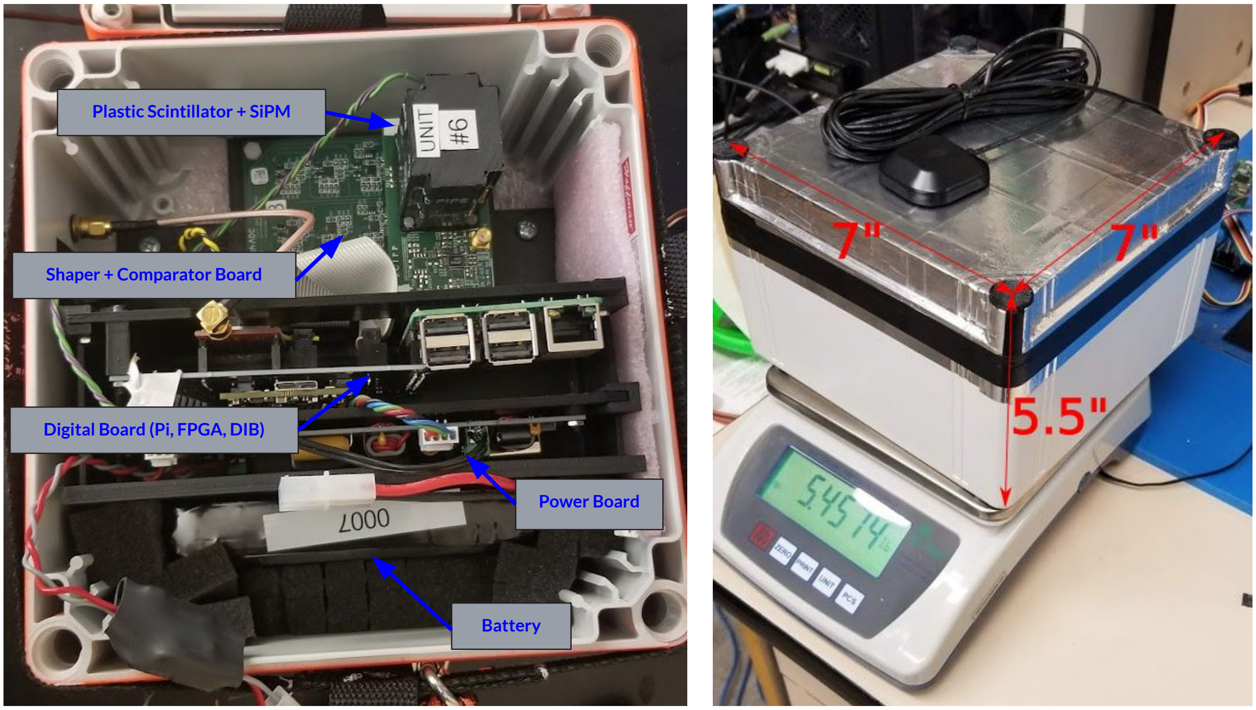

Figure 5.1: (left) Image of inside of one LAFTR unit with all the main components labeled. (right) Image of assembled LAFTR unit, including GPS antenna, with physical dimensions labeled and weight in pounds shown.

time resolutions or enough photon counts to sufficiently study the detailed structure of TGFs. However, LAFTR is designed to be extremely fast and to be in a closer proximity to TGF sources than the spacecraft that most commonly observe them. Measurements of TGFs made by this instrument would have the potential to help discern the exact production mechanisms of TGFs for which a high time resolution is key. Additionally, by deploying the instruments in various geographic locations it may be possible to determine the rarity of TGFs in upper latitudes where satellites often do not have coverage.

LAFTR is light enough (less than 6 pounds) to be deployed on FAA exempt balloons, and it can also be easily deployed for ground observations due to its small size. The instruments contain a plastic scintillator and silicon photomultiplier (SiPM) that produces an electric signal with strength proportional to the number of photons deposited onto its surface. The number of photons deposited onto the SiPM is proportional to the energy of the photon deposited into the plastic scintillator. The electrical signal is then passed through a signal shaper and eight comparators to determine the energy of the original photon based on the pulse height. A field programmable gate array (FPGA) reads and time tags the events and a Raspberry Pi is used to read data from the FPGA where it is stored onboard.

Figure 5.2: Image from 2018 initial test flight of LAFTR in southwest Montana.

Since October of 2018, three LAFTR Units have been deployed to Japan, one has been deployed to the CN Tower in Toronto, Canada, one has been stationed atop Cheyenne Mountain in Colorado, and four have been deployed as balloon payloads. The first balloon payload was flown in November 2018 by the Montana Space Grant Consortium (MSGC) Balloon Outreach, Research, Exploration and Landscape Imaging System (BOREALIS) Program as a test flight. The final three units were flown in the summer of 2019 in Melbourne, Florida, at the Florida Institute of Technology (FIT). These field campaigns were conducted by myself and another MSU student. While these initial balloon flights did not yield any TGF observations, the chances of making such a measurement increases with each new flight and deployment. These FIT campaigns are also well within range of nearby LMAs that are capable of providing excellent concurrent radio data. Additional flights were planned for the summers of 2020 and 2021, however, all balloon campaigns were temporarily halted due to the COVID-19 pandemic. Nonetheless, as the pandemic begins to wane, we expect to be

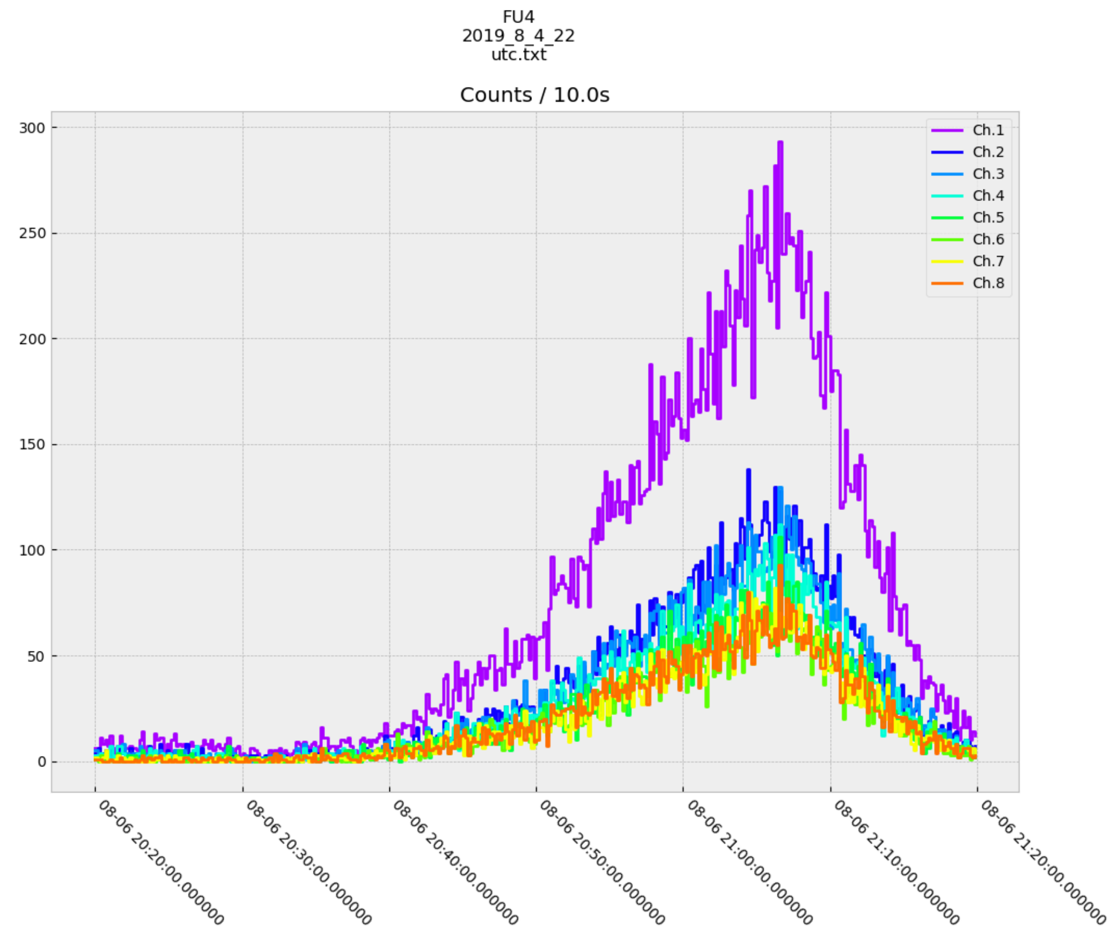

Figure 5.3: Flight data from 2019 Florida Balloon campaign. Units are in counts per 10 second bins over the course of the flight. The trend toward higher count rates is due to the rise in background rates as the altitude of the balloon increased.

able to resume balloon launches in the near future.

These balloon launches and ground deployments offer the potential for unique insights into TGF production mechanisms. A single TGF observation could reveal answers to decades-old questions about the exact TGF production mechanism and in what way TGF associated lightning differs from other lightning flashes.

REFERENCES CITED

Baker, M.B, Blyth, Alan, Christian, Hugh, Latham, J, Miller, K.L, & Gadian, A. 1999. Relationships between lightning activity and various thundercloud parameters: Satellite and modelling studies. *Atmospheric Research*, **51**, 221–236.

Barnes, D. E., Splitt, M. E., Dwyer, J. R., Lazarus, S., Smith, D. M., & Rassoul, H. K. 2015. A study of thunderstorm microphysical properties and lightning flash counts associated with terrestrial gamma-ray flashes. *Journal of Geophysical Research: Atmospheres*, **120**(8), 3453–3464.

Bitzer, Phillip M., Burchfield, Jeffrey C., & Christian, Hugh J. 2016. A Bayesian Approach to Assess the Performance of Lightning Detection Systems. *Journal of Atmospheric and Oceanic Technology*, **33**(3), 563–578.

Boccippio, D. J., Heckman, S., & Goodman, S. J. 2001. A diagnostic analysis of the Kennedy Space Center LDAR network: 1. Data characteristics. *Journal of Geophysical Research: Atmospheres*, **106**(D5), 4769–4786.

Bowers, G. S., Smith, D. M, Martinez-McKinney, G. F., Kamogawa, M., Cummer, S. A., Dwyer, J. R., *et al.* 2017. Gamma Ray Signatures of Neutrons From a Terrestrial Gamma Ray Flash. *Geophysical Research Letters*, **44**, 10063–10070.

Bowers, G. S., Smith, D. M., Kelley, N. A., Martinez-McKinney, G. F., Cummer, S. A., Dwyer, J. R, *et al.* 2018. A Terrestrial Gamma-Ray Flash inside the Eyewall of Hurricane Patricia. *Journal of Geophysical Research: Atmospheres*, **123**, 4977–4987.

Briggs, M. S., Fishman, G. J., Connaughton, V., Bhat, P. N., Paciesas, W. S., Preece, R. D., *et al.* 2010. First Results on Terrestrial Gamma Ray Flashes from the Fermi Gamma-ray Burst Monitor. *Journal of Geophysical Research*, **115**, A07323.

Brook, Marx, Nakano, Minoru, Krehbiel, Paul, & Takeuti, Toshio. 1982. The electrical structure of the hokuriku winter thunderstorms. *Journal of Geophysical Research: Oceans*, **87**(C2), 1207–1215.

Bruning, Eric C., Rust, W. David, Schuur, Terry J., MacGorman, Donald R., Krehbiel, Paul R., & Rison, William. 2007. Electrical and Polarimetric Radar Observations of a Multicell Storm in TELEX. *Monthly Weather Review*, **135**(7), 2525–2544.

Campello, R. J. G. B., Moulavi, D., & Sander, J. 2013. Density-Based Clustering Based on Hierarchical Density Estimates. *Advances in Knowledge Discovery and Data Mining*, **7819**.

Cancalosi, John. 2020. Lightning — meteorology — Encyclopaedia Britannica. (Accessed on 08/20/2020).

Carlson, B. E., Lehtinen, N. G., & Inan, U. S. 2010. Terrestrial Gamma Ray Flash Production By Active Lightning Leader Channels. *Journal of Geophysical Research*, **115**, A10324.

Celestin, S., & Pasko, V. P. 2011. Energy and Fluxes of Thermal Runaway Electrons Produced by Exponential Growth of Streamers During the Stepping of Lightning Leaders and in Transient Luminous Events. *Journal of Geophysical Research*, **116**, A03315.

Celestin, S., Xu, W., & Pasko, V. P. 2012. Terrestrial gamma ray flashes with energies up to 100 MeV produced by nonequilibrium acceleration of electrons in lightning. *Journal of Geophysical Research*, **117**, A05315.

Christian, H. J. 2003. Global frequency and distribution of lightning as observed from space by the Optical Transient Detector. *Journal of Geophysical Research*, **108**(D1).

Chronis, T., & Koshak, W. 2017. Diurnal Variation of TRMM/LIS Lightning Flash Radiances. *Bulletin of the American Meteorological Society*, **98**, 1453–1470.

Chronis, T., Cummins, K., Said, R., Koshak, W., McCaul, E., Williams, E. R., *et al.* 2015. Climatological Diurnal Variation of Negative CG Lightning Peak Current Over the Continental United States. *Journal of Geophysical Research: Atmospheres*, **120**, 582–589.

Chronis, Themistoklis, Briggs, Michael S., Priftis, George, Connaughton, Valerie, Brundell, James, Holzworth, Robert, Heckman, Stan, McBreen, Shelia, Fitzpatrick, Gerard, & Stanbro, Matthew. 2016. Characteristics of Thunderstorms That Produce Terrestrial Gamma Ray Flashes. *Bulletin of the American Meteorological Society*, **97**(4), 639–653.

Cohen, M. B., Inan, U. S., & G., Fishman. 2006. Terrestrial gamma ray flashes observed aboard the Compton Gamma Ray Observatory/Burst and Transient Source Experiment and ELF/VLF radio atmospherics. *Journal of Geophysical Research: Atmospheres*, **111**, D24109.

Coleman, L. M., Marshall, T. C., Stolzenburg, M., Hamlin, T., Krehbiel, P. R., Rison, W., & Thomas, R. J. 2003. Effects of charge and electrostatic potential on lightning propagation. *Journal of Geophysical Research: Atmospheres*, **108**(D9), n/a–n/a.

Collier, A. B., Gjesteland, T., & Ostgaard, N. 2011. Assessing the power law distribution of TGFs. *Journal of Geophysical Research*, **116**, A10320.

Connaughton, V. 2010. Associations between Fermi Gamma-ray Burst Monitor terrestrial gamma ray flashes and sferics from the World Wide Lightning Location Network. *Journal of Geophysical Research*, **115**, A12307.

Connaughton, Valerie, Briggs, Michael S., Xiong, Shaolin, Dwyer, Joseph R., Hutchins, Michael L., Grove, J. Eric, Chekhtman, Alexandre, Tierney, Dave, Fitzpatrick, Gerard, Foley, Suzanne, McBreen, Shelia, Bhat, P. N., Chaplin, Vandiver L., Cramer, Eric, Fishman, Gerald J., Holzworth, Robert H., Gibby, Melissa, von Kienlin, Andreas, Meegan, Charles A., Paciesas, William S., Preece, Robert D., & Wilson-Hodge, Colleen. 2013. Radio signals from electron beams in terrestrial gamma ray flashes. *Journal of Geophysical Research: Space Physics*, **118**(5), 2313–2320.

Cummer, S. A., Inan, U. S., & Bell, T. F. 1998. Ionospheric D region remote sensing using VLF radio atmospherics. *Radio Science*, **33**(6), 1781–1792.

Cummer, S. A., Zhai, Y., Hu, W., Smith, D. M., Lopez, L. I., & Stanley, M. A. 2005. Measurements and implications of the relationship between lightning and terrestrial gamma ray flashes. *Geophysical Research Letters*, **32**, L08811.

Cummer, Steven A., Briggs, Michael S., Dwyer, Joseph R., Xiong, Shaolin, Connaughton, Valerie, Fishman, Gerald J., Lu, Gaopeng, Lyu, Fanchao, & Solanki, Rahulkumar. 2014. The source altitude, electric current, and intrinsic brightness of terrestrial gamma ray flashes. *Geophysical Research Letters*, **41**(23), 8586–8593.

Cummins, K.L., & Murphy, M.J. 2009. An Overview of Lightning Locating Systems: History, Techniques, and Data Uses, With an In-Depth Look at the U.S. NLDN. *IEEE Transactions on Electromagnetic Compatibility*, **51**(3), 499–518.

Cummins, K.L., Murphy, M. J., Bardo, E. A., Hiscox, W. L., Pyle, R. B., & Pifer, A. E. 1998. A Combined TOA/MDF Technology Upgrade of the U.S. National Lightning Detection Network. *Journal of Geophysical Research: Atmospheres*, **103**(D8), 9035–9044.

Dwyer, J. R. 2003. A fundamental limit on electric fields in air. *Geophysical Research Letters*, **30**(20).

Dwyer, J. R. 2004. Implications of x-ray emission from lightning. *Geophysical Research Letters*, **31**(12).

Dwyer, J. R. 2008. Source mechanisms of terrestrial gamma-ray flashes. *Journal of Geophysical Research: Atmospheres*, **113**(D10).

Dwyer, J. R., Rassoul, H. K., Al-Dayeh, M., Caraway, L., Wright, B., Chrest, A., *et al.* 2004. A Ground-Level Gamma-Ray Burst Observed in Association with Rocket-Triggered Lightning. *Geophysical Research Letters*, **31**, L05119.

Dwyer, J. R., Smith, D. M., Uman, M. A., Saleh, Z., Grefenstette, B., Hazelton, B., & Rassoul, H. K. 2010. Estimation of the fluence of high-energy electron bursts produced by thunderclouds and the resulting radiation doses received in aircraft. *Journal of Geophysical Research*, **115**(D9).

Dwyer, J. R., Schaal, M. M., Cramer, E., Arabshahi, S., Liu, N., Rassoul, H. K., *et al.* 2012a. Observation of a Gamma-Ray Flash at Ground Level in Association with a Cloud-to-Ground Lightning Return Stroke. *Journal of Geophysical Research*, **117**, A10303.

Dwyer, J. R., Smith, D. M., & Cummer, S. A. 2012b. High-Energy Atmospheric Physics: Terrestrial Gamma-Ray Flashes and Related Phenomena. *Space Science Reviews*, **173**, 133–196.

Dwyer, Joseph R., & Uman, Martin A. 2014. The physics of lightning. *Physics Reports*, **534**(4), 147–241.

Dye, J. E., Jones, J. J., Weinheimer, A. J., & Winn, W. P. 1988. Observations within two regions of charge during initial thunderstorm electrification. *Quarterly Journal of the Royal Meteorological Society*, **114**(483), 1271–1290.

Enoto, T., Wada, Y., Furuta, Y., Nakazawa, K., Yuasa, T., Okuda, K., *et al.* 2017. Photonuclear Reactions Triggered by Lightning Discharge. *Nature*, **551**, 481–484.

Ester, M., Kriegel, H., Sander, J., & Xu, X. 1996. A Density-Based Algorithm for Discovering Clusters in Large Spatial Databases with Noise. *AAAI Press*, **KDD'96**, 226–231.

Fabró, F., Montanyà, J., Velde, O. A., Pineda, N., & Williams, E. R. 2019. On the TGF/Lightning Ratio Asymmetry. *Journal of Geophysical Research: Atmospheres*, **124**(12), 6518–6531.

Fishman, G. J., Bhat, P. N., Mallozzi, R., Horack, J. M., Koshut, T., Kouveliotou, C., Pendleton, G. N., Meegan, C. A., Wilson, R. B., Paciesas, W. S., Goodman, S. J., & Christian, H. J. 1994. Discovery of Intense Gamma-Ray Flashes of Atmospheric Origin. *Science*, **264**(5163), 1313–1316.

Griffiths, R. F., & Phelps, C. T. 1976. A model for lightning initiation arising from positive corona streamer development. *Journal of Geophysical Research*, **81**(21), 3671–3676.

Gurevich, A. V. 1961. On the Theory of Runaway Electrons. *Soviet Physics JETP*, **12**, 904–912.

Gurevich, A. V., & Zybin, K. P. 2001. Runaway breakdown and electric discharges in thunderstorms. *Physics-Uspekhi*, **44**(11).

Gurevich, A.V., Milikh, G.M., & Roussel-Dupre, R. 1992. Runaway electron mechanism of air breakdown and preconditioning during a thunderstorm. *Physics Letters A*, **165**(5-6), 463–468.

Hare, B. M., Uman, M. A., Dwyer, J. R., Jordan, D. M., Biggerstaff, M. I., Caicedo, J. A., *et al.* 2016. Ground-level observation of a terrestrial gamma ray flash initiated by a triggered lightning. *Journal of Geophysical Research: Atmospheres*, **121**, 6511–6533.

He, Yuanping, Gu, Boyan, Zhang, Daizhou, Lu, Weizhen, Yu, Chuck Wah, & Gu, Zhaolin. 2018. Towards the Understanding of Ice Crystal-graupel Collision Charging in Thunderstorm Electrification. nov.

Holzworth, R. H., McCarthy, M. P., Brundell, J. B., Jacobson, A. R., & Rodger, C. J. 2019. Global Distribution of Superbolts. *Journal of Geophysical Research: Atmospheres*, **124**(17-18), 9996–10005.

Houze, R. A. 2004. Mesoscale Convective Systems. *Reviews of Geophysics*, **42**(4).

Hutchins, M. L., Holzworth, R. H., Brundell, J. B., & Rodger, C. J. 2012. Relative detection efficiency of the World Wide Lightning Location Network. *Radio Science*, **47**, RS6005.

Hutchins, M. L., Holzworth, R. H., Virts, K. S., Wallace, J.M., & Heckman, S. 2013. Radiated VLF Energy Differences of Land and Oceanic Lightning. *Geophysical Research Letters*, **40**, 2390–2394.

Inan, U. S., Cohen, M. B., Said, R. K., Smith, D. M., & Lopez, L. I. 2006. Terrestrial Gamma Ray Flashes and Lightning Discharges. *Geophysical Research Letters*, **33**, L18802.

Inan, Umran S., Reising, Steven C., Fishman, Gerald J., & Horack, John M. 1996. On the association of terrestrial gamma-ray bursts with lightning and implications for sprites. *Geophysical Research Letters*, **23**(9), 1017–1020.

Klimov, P. A., Kaznacheeva, M. A., Khrenov, B. A., Garipov, G. K., Bogomolov, V. V., Panasyuk, M. I., *et al.* 2018. UV Transient Atmospheric Events Observed Far From Thunderstorm by the Vernov Satellite. *IEEE Geoscience and Reomote Sensing Letters*, **15**(8), 1139–1143.

Kolzov, V. I., Mullayarov, V. A., & Shabaganova, S.N. 2013. Characteristics of Thunderstorm Cores from Observations in Yakitia. *Russian Physics Journal*, **56**, 398–404.

Krehbiel, P. R. 1986. *The Earth's Electrical Environment.* Washington, DC: National Academy Press.

Krider, E. Philip. 2016. Thunderstorm. *Encyclopædia Britannica*, Sep.

Lapierre, Jeff, Hoekzema, Mark, Stock, Michael, Merrill, Chad, & Thangaraj, Saiadithya Cumbulam. 2019. Earth Networks Lightning Network and Dangerous Thunderstorm Alerts. *Pages 1–5 of: 2019 11th Asia-Pacific International Conference on Lightning (APL)*.

Larkey, R. K., Sample, J. G., Smith, D. M., Briggs, M. S., Lapierre, J. L., & Holzworth, R. H. 2019. Evidence for Extended Charging Periods Prior to Terrestrial Gamma Ray Flashes. *Geophysical Research Letters*, **46**(17-18), 10619–10626.

Larkey, R. K., Sample, J. G., Smith, D. M., Lapierre, J. L., DiGangi, E., & Holzworth, R. H. 2021. The Relationship Between TGF Production in Thunderstorms and Lightning Flash Rates and Amplitudes. *Journal of Geophysical Research: Atmospheres*, **126**(13), e2020JD034401.

Lay, E. H., Holzworth, R. H., Rodger, J. C., Thomas, J. N., Pinto, O., & Dowden, R. L. 2004. WWLL global lightning detection system: Regional validation study in Brazil. *Geophysical Research Letters*, **31**(3), L03102.

Lehtinen, N. G., Walt, M., Inan, U. S., Bell, T. F., & Pasko, V. P. 1996. Gamma-Ray Emission Produced by a Relativistic Beam of Runaway Electrons Accelerated by Quasi-Electrostatic Thundercloud Fields. *Geophysical Research Letters*, **23**(19), 2645–2648.

Lewis, E. A., Harvey, R. B., & Rasmussen, J. E. 1960. Hyperbolic direction finding with sferics of transatlantic origin. *Journal of Geophysical Research*, **65**(7), 1879–1905.

Lindanger, A., Skeie, C. A., Marisaldi, M., Bjørge-Engeland, I., Østgaard, N., Mezentsev, A., *et al.* 2021. Statistical Evidence of Terrestrial Gamma-Ray Flashes Production During the Early Stages of Lightning Flashes. Presented at AGU Fall Meeting 2021, New Orleans, LA, AE15A-1892.

Loeb, Leonard B. 1966. The mechanisms of stepped and dart leaders in cloud-to-ground lightning strokes. *Journal of Geophysical Research*, **71**(20), 4711–4721.

Lu, Gaopeng, Blakeslee, Richard J., Li, Jingbo, Smith, David M., Shao, Xuan-Min, McCaul, Eugene W., Buechler, Dennis E., Christian, Hugh J., Hall, John M., & Cummer, Steven A. 2010. Lightning mapping observation of a terrestrial gamma-ray flash. *Geophysical Research Letters*, **37**(11), n/a–n/a.

Lyu, F., Cummer, S. A., Briggs, M., Marisaldi, M., Blakeslee, R. J., Bruning, E., *et al.* 2016. Ground detection of terrestrial gamma ray flashes from distant radio signals. *Geophysical Research Letters*, **43**(16), 8728–8734.

MacGorman, D. R., Apostolakopoulos, I. R., Lund, N. R., Demetriades, N. W. S., Murphy, J. M., & Krehbiel, P. R. 2010. The Timing of Cloud-to-Ground Lightning Relative to Total Lightning Activity. *American Meteorological Society*, **139**, 3871–3886.

Maggio, Christopher R., Marshall, Thomas C., & Stolzenburg, Maribeth. 2009. Estimations of charge transferred and energy released by lightning flashes. *Journal of Geophysical Research*, **114**(D14).

Mailyan, B. G., Nag, A., Murphy, M. J., Briggs, M. S., Dwyer, J. R., Rison, W., *et al.* 2018. Characteristics of Radio Emissions Associated With Terrestrial Gamma-Ray Flashes. *Journal of Geophysical Research: Space Physics*, **123**(7), 5933–5948.

Mailyan, B. G., Nag, A., Dwyer, J. R., Said, R. K., Briggs, M. S., Roberts, O. J., *et al.* 2020. Gamma-Ray and Radio-Frequency Radiation from Thunderstorms Observed from Space and Ground. *Scientific Reports*, **10**(7286).

Marchand, M., Hilburn, K., & Miller, S. D. 2019. Geostationary Lightning Mapper and Earth Networks lightning detection over the contiguous United States and dependence on flash characteristics. *Journal of Geophysical Research: Atmospheres*, **124**(21), 11552–11567.

Marisaldi, M., Fuschino, F., Labanti, C., Galli, M., Longo, F., Monte, Del, E., *et al.* 2010. Detection of terrestrial gamma ray flashes up to 40 MeV by the AGILE Satellite. *Journal of Geophysical Research: Space Physics*, **115**, A00E13.

Marisaldi, M., Fuschino, F., Tavani, M., Dietrich, S., Price, C., Galli, M., *et al.* 2014. Properties of terrestrial gamma ray flashes detected by AGILE MCAL below 30 MeV. *Journal of Geophysical Research: Space Physics*, **119**(2), 1337–1355.

Marisaldi, M., Galli, M., Labanti, C., Østgaard, N., Sarria, D., Cummer, S. A., *et al.* 2019. On the High-Energy Spectral Component and Fine Time Structure of Terrestrial Gamma Ray Flashes. *Journal of Geophysical Research: Atmospheres*, **124**(14), 7484–7497.

Marshall, T. C., Stolzenburg, M., Krehbiel, P. R., Lund, N. R., & Maggio, C. R. 2009. Electrical evolution during the decay stage of New Mexico thunderstorms. *Journal of Geophysical Research*, **114**(D2).

Marshall, Thomas C., & Rust, W. David. 1991. Electric field soundings through thunderstorms. *Journal of Geophysical Research*, **96**(D12), 22297.

Marshall, Thomas C., McCarthy, Michael P., & Rust, W. David. 1995. Electric field magnitudes and lightning initiation in thunderstorms. *Journal of Geophysical Research*, **100**(D4), 7097–7103.

McInnes, L., Healy, J., & Astels, S. 2017. hdbscan: Hierarchical density based clustering. *Journal of Open Source Software*, **2**(11), 205.

Morales Rodriguez, Carlos A., Montanyà, Joan, van der Velde, Oscar A., Fabró, Ferran, & Lopez, Jesus A. 2021. Tropical TGF Paradox: A Perspective From TRMM Precipitation Radar. *Journal of Geophysical Research: Atmospheres*, **126**(14), e2021JD034698.

Moss, G. D., Pasko, V. P., N., Liu, & Veronis, G. 2006. Monte Carlo Model for Analysis of Thermal Runaway Electrons in streamer tips in transient Luminous events and streamer zones of lightning leaders. *Journal of Geophysical Research*, **111**, A02307.

Motley, Shane Michael. 2006 (8). *Total lightning characteristics of ordinary convection.* M.Phil. thesis, Texas A&M University, College Station, TX.

Østgaard, N., Neubert, T., Reglero, V., Ullaland, K., Yang, S., Genov, G., *et al.* 2019. First 10 Months of TGF Observations by ASIM. *Journal of Geophysical Research: Atmospheres*, **124**(24), 14024–14036.

Pallu, M., Celestin, S., Trompier, F., & Klerlein, M. 2021. Estimation of Radiation Doses Delivered by Terrestrial Gamma Ray Flashes Within Leader-Based Production Models. *Journal of Geophysical Research: Atmospheres*, **126**(8), e2020JD033907.

Pawar, S. D., & Kamra, A. K. 2002. Recovery Curves of the Surface Electric Field after Lightning Discharges Occurring between the Positive Charge Pocket and Negative Charge Centre in a Thundercloud. *Geophysical Research Letters*, **29**(23), 23–1–23–4.

Pawar, S. D., & Kamra, A. K. 2004. Evolution of Lightning and the Possible Initiation/Triggering of Lightning Discharges by the Lower Positive Charge Center in an Isolated Thundercloud in the Tropics. *Journal of Geophysical Research: Atmospheres*, **109**(D2).

Petersen, D., Bailey, M., Beasley, W. H., & Hallett, J. 2008. A brief review of the problem of lightning initiation and a hypothesis of initial lightning leader formation. *Journal of Geophysical Research*, **113**(D17).

Price, C. 2008. Lightning Sensors for Observing, Tracking and Nowcasting Severe Weather. *Sensors (Basel)*, **8**(1), 157–170.

Pu, Y., Cummer, S. A., Lyu, F., Briggs, M., Mailyan, B., Stanbro, M., & Roberts, O. 2019. Low Frequency Radio Pulses Produced by Terrestrial Gamma-Ray Flashes. *Geophysical Research Letters*, **46**(12), 6990–6997.

Rakov, Vladimir. 2003. *Lightning : physics and effects*. Cambridge, U.K. New York: Cambridge University Press.

Reynolds, S. E., Brook, M., & Grouley, M. F. 1957. Thunderstorm Charge Separation. *Journal of the Atmospheric Sciences*, **14**(5), 426–436.

Roberts, O. J., Fitzpatrick, G., Stanbro, M., McBreen, S., Briggs, M. S., Holzworth, R. H., *et al.* 2018. The First Fermi-GBM Terrestrial Gamma Ray Flash Catalog. *Journal of Geophysical Research*, **123**, 4381–4401.

Rodger, C. J., Werner, S., Brundell, J. B., Lay, E. H., Thomson, N. R., Holzworth, R. H., & Dowden, R. L. 2006. Detection efficiency of the VLF World-Wide Lightning Location Network (WWLLN) initial case study. *Annales Geophysicae*, **24**(12), 3197–3214.

Rodger, CJ, Brundell, JB, Holzworth, RH, & Lay, EH. 2009. Growing detection efficiency of the world wide lightning location network. *American Institute of Physics*, **1118**(1), 15–20.

Romps, David M., Seeley, Jacob T., Vollaro, David, & Molinari, John. 2014. Projected increase in lightning strikes in the United States due to global warming. *Science*, **346**(6211), 851–854.

Rudlosky, Scott D. 2014. Evaluating ground-based lightning detection networks using TRMM/LIS observations. *23rd International Lightning Detection Conference & 5th International Lightning Meteorology Conference.*

Rudlosky, Scott D. 2015. Evaluating ENTLN Performance Relative to TRMM/LIS. *Journal of Operational Meteorology*, **3**(2), 11–20.

Rust, W. David, & Marshall, Thomas C. 1996. On abandoning the thunderstorm tripole-charge paradigm. *Journal of Geophysical Research: Atmospheres*, **101**(D18), 23499–23504.

Shao, Xuan-Min, Hamlin, Timothy, & Smith, David M. 2010. A closer examination of terrestrial gamma-ray flash-related lightning processes. *Journal of Geophysical Research: Space Physics*, **115**(A6).

Simpson, George C. 1909. XV. On the electricity of rain and its origin in thunderstroms. *Philosophical Transactions of the Royal Society of London. Series A, Containing Papers of a Mathematical or Physical Character*, **209**(441-458), 379–413.

Smith, D. M., Hazelton, B. J., Grefenstette, B. W., Dwyer, J. R., Holzworth, R. H., & Lay, E. H. 2010. Terrestrial Gamma Ray Flashes Correlated to Storm Phase and Tropopause Height. *Journal of Geophysical Research*, **115**, A00E49.

Smith, D. M., Dwyer, J. R., Hazelton, B. J., Grefenstette, B. W., Martinez-McKinney, G. F. M., Zhang, Z. Y., *et al.* 2011. A Terrestrial Gamma Ray Flash Observed from an Aircraft. *Journal of Geophysical Research: Atmospheres*, **116**, D20124.

Smith, D. M., Buzbee, P., Kelley, N. A., Infanger, A., Holzworth, R. H., & Dwyer, J. R. 2016. The rarity of terrestrial gamma-ray flashes: 2. RHESSI stacking analysis. *Journal of Geophysical Research: Atmospheres*, **121**(19), 11,382–11,404.

Smith, D. M., Bowers, G. S., Kamogawa, M., Wang, D., Ushio, T., Ortberg, J., *et al.* 2018. Characterizing Upward Lightning with and without a Terrestrial Gamma-Ray Flash. *Journal of Geophysical Research: Atmospheres*, **121**, 11321–11332.

Smith, David M., Lopez, Liliana I., Lin, R. P., & Barrington-Leigh, Christopher P. 2005. Terrestrial Gamma-Ray Flashes Observed up to 20 MeV. *Science*, **307**(5712), 1085–1088.

Sonnenfeld, Richard, Lapierre, Jeff, Contreras Vidal, Luis, Zhu, Yanan, & Stock, Michael. 2020. EARTH NETWORKS LIGHTNING NETWORK PERFORMANCE. *Earth and Space Science Open Archive*, 5.

Splitt, M. E., Lazarus, S. M., Barnes, D., Dwyer, J. R., Rassoul, H. K., Smith, D. M., Hazelton, B., & Grefenstette, B. 2010. Thunderstorm characteristics associated with RHESSI identified terrestrial gamma ray flashes. *Journal of Geophysical Research: Space Physics*, **115**(A6).

Stanley, M. A., Shao, X.-M., Smith, D. M., Lopez, L. I., Pongratz, M. B., Harlin, J. D., Stock, M., & Regan, A. 2006. A link between terrestrial gamma-ray flashes and intracloud lightning discharges. *Geophysical Research Letters*, **33**, L06803.

Stolzenburg, M., & Marshall, T.C. 2008. Charge Structure and Dynamics in Thunderstorms. *Space Science Reviews*, **137**, 355–372.

Stolzenburg, M., Rust, W. D., Smull, B. F., & Marshall, T. C. 1998. Electrical structure in thunderstorm convective regions: 1. Mesoscale convective systems. *Journal of Geophysical Research: Atmospheres*, **103**(D12), 14059–14078.

Thompson, Kelsey B., Bateman, Monte G., & Carey, Lawrence D. 2014. A Comparison of Two Ground-Based Lightning Detection Networks against the Satellite-Based Lightning Imaging Sensor (LIS). *Journal of Atmospheric and Oceanic Technology*, **31**(10), 2191–2205.

Tsuchiya, H., Enoto, T., Yamada, S., Yuasa, T., Nakazawa, K., Kitaguchi, T., *et al.* 2011. Long-Duration Gamma Ray Emissions for 2007 and 2008 Winter Thunderstorms. *Journal of Geophysical Research: Atmospheres*, **116**(D9).

Turman, B. N. 1977. Detection of lightning superbolts. *Journal of Geophysical Research*, **82**(18), 2566–2568.

Ursi, A., Marisaldi, M., Dietrich, S., Tavani, M., Tiberia, A., & Porcù, F. 2019. Analysis of Thunderstorms Producing Terrestrial Gamma Ray Flashes With the Meteosat Second Generation. *Journal of Geophysical Research: Atmospheres*, **124**(23), 12667–12682.

Ushiro, T., Heckman, S. J., Boccippio, D. J., Christian, H. J., & Kawasaki, Z. 2001. A Survey of Thunderstorm Flash Rates Compared to Cloud Top Height Using TRMM Satellite Data. *Journal of Geophysical Research: Atmospheres*, **106**(D20), 24089–24095.

Wada, Y., Enoto, T., Nakamura, Y., Furuta, Y., Yuasa, T., Nakazawa, K., *et al.* 2019. Gamma-ray glow preceding downward terrestrial gamma-ray flash. *Communications Physics*, **2**(67).

Wada, Y., Enoto, T., Nakamura, Y., Morimoto, T., Sato, M., Ushio, *et al.* 2020. High Peak-Current Lightning Discharges Associated With Downward Terrestrial Gamma-Ray Flashes. *Journal of Geophysical Research: Atmospheres*, **125**(4), e2019JD031730.

Williams, E., Mushtak, V., Rosenfeld, D., Goodman, S., & Boccippio, D. 2005. Thermodynamic conditions favorable to superlative thunderstorm updraft. *Atmospheric Research*, **76**, 288–306.

Williams, Earle R. 1989. The tripole structure of thunderstorms. *Journal of Geophysical Research*, **94**(D11), 13151.

Wilson, C. T. R. 1925. The Acceleration of Beta-particles in Strong Electric Fields such as those of Thunderclouds. *Mathematical Proceedings of the Cambridge Philosophical Society*, **22**(4), 534–538.

Wilson, C.T.R. 1916. On some determinations of the sign and magnitude of electric discharges in lightning flashes. *Proceedings of the Royal Society of London. Series A, Containing Papers of a Mathematical and Physical Character*, **92**(644), 555–574.

Winn, William P., Schwede, G. W., & Moore, C. B. 1974. Measurements of electric fields in thunderclouds. *Journal of Geophysical Research*, **79**(12), 1761–1767.

Wu, X., Kumar, V., Quinlan, J. R., Ghosh, J., Yang, Q., Motoda, H., *et al.* 2008. Top 10 Algorithms in Data Mining. *Knowledge and Information Systems*, **14**, 1–37.

Yoshida, S., Adachi, T., Hayashi, S., Wu, T., & Yoshikawa, E. 2017. Relationship Between Thunderstorm Electrification and Kinetics Revealed by Phased Array Weather Radar. *Journal of Geophysical Research: Atmospheres*, **122**, 3821–3836.

Zhu, Y., Rakov, V.A., Tran, M.D., Stock, M.G., Heckman, S., Liu, C., *et al.* 2017. Evaluation of ENTLN performance characteristics based on the ground truth natural and rocket-triggered lightning data acquired in Florida. *Journal of Geophysical Research: Atmospheres*, **122**(18), 9858–9866.